arXiv:1102.4419v1 [astro-ph.GA] 22 Feb 2011

PROBING TURBULENCE IN THE INTERSTELLAR MEDIUM USING RADIO-INTERFEROMETRIC OBSERVATIONS OF NEUTRAL HYDROGEN

Thesis submitted to the
Indian Institute of Technology, Kharagpur
For the award of the degree

of

Doctor of Philosophy

by

Prasun Dutta

Under the guidance of

Prof. Somnath Bharadwaj

DEPARTMENT OF PHYSICS AND METEOROLOGY
INDIAN INSTITUTE OF TECHNOLOGY, KHARAGPUR
FEBRUARY 2011

© 2011 Prasun Dutta. All rights reserved.

To *My parents, Chotomama, Rupai, Chutki, Babi, Didi and all my friends*

...in the infinite beauty, we all join in one...

APPROVAL OF THE VIVA-VOCE BOARD

Date: 21/2/2011

Certified that the thesis entitled **Probing Turbulence In the Interstellar Medium using Radio-Interferometric Observations of Neutral Hydrogen** submitted by **PRASUN DUTTA** to the Indian Institute of Technology, Kharagpur, for the award of the degree of Doctor of Philosophy has been accepted by the external examiners and that the student has successfully defended the thesis in the viva-voce examination held today.

Signature	Signature	Signature
(Member of the DSC)	(Member of the DSC)	(Member of the DSC)
Signature	Signature	Signature
(Supervisor)	(External Examiner)	(Chairman)

CERTIFICATE

This is to certify that the thesis entitled **Probing Turbulence In the Interstellar Medium using Radio-Interferometric Observations of Neutral Hydrogen**, submitted by **Prasun Dutta** to the Indian Institute of Technology, Kharagpur, is a record of bona fide research work under my supervision and is of consideration for the award of the degree of Doctor of Philosophy of the Institute.

Supervisor

Prof. Somnath Bharadwaj

Date:

DECLARATION

I certify that

a. The work contained in the thesis is original and has been done by myself under the general supervision of my supervisor.

b. The work has not been submitted to any other Institute for any degree or diploma.

c. I have followed the guidelines provided by the Institute in writing the thesis.

d. I have conformed to the norms and guidelines given in the Ethical Code of Conduct of the Institute.

e. Whenever I have used materials (data, theoretical analysis, and text) from other sources, I have given due credit to them by citing them in the text of the thesis and giving their details in the references.

f. Whenever I have quoted written materials from other sources, I have put them under quotation marks and given due credit to the sources by citing them and giving required details in the references.

Signature of the Student

Acknowledgments

It is the collective effort of many individuals, my parents and relatives, teachers, friends, that have poured into a nice A4 size book only to become my thesis. Though this section bears the name "Acknowledgements", I have no words to acknowledge or thank. I will only present here a few of my memorable experiences.

My parents always encouraged me to learn as much as I can and then share the knowledge with everybody. Chotomama taught me photography, but more than that he seeded in me the quest for asking how things work. My teachers Anjan babu, Debasis babu, Sajal babu, Biswanath babu, Ashesh babu, Saibal babu and Tarasankar babu have always encouraged me to pursue higher education. They prepared the base over which I have only tried adding things.

Back home, I shared numerous moments of true joy with my cousins, Didi, Babi, Buronda, Rajada, Tunku di, Sonali di. Many of my time that I have spent with my sisters Chutki and Rupai, are the times that I will always like to go back to. They, being very good students have helped me solve some of my problems too.

If I were ever to do another Ph. D, I would prefer working with Prof. Somnath Bharadwaj again. If I were ever to guide a student, I will just try to emulate how he prepared us. He showed us the art of doing research in a professional way yet with passion and love. He has always clarified all my doubts and then blessed me by showing his magical power of reasoning every aspect starting from the very basics. He has been a true teacher, a friend, philosopher and guide to me always. Working in Collaboration with Jayaram, Ayesha, SPK, Tapomoy and Nirupam has also been encouraging and enjoyable. I will be very happy to continue working with them.

CTS was never felt far from home. Friends here, Prakash, Biswambhar (Bisu), Somnath (Bhaipo), Suman (Mahajan), Tatan, Soma di and Partha da, Sanjit (Dos), Suman (Choto), Abhik (Jethu), Ganesh, Subhasis (Panda), Sudipta, Tapamoy (Mukhanov), all were the part of a big happy family. Supratik da, Ratna di, Anupam da, Biswajit da, Saijad da and Kanan da were like elder brothers and sisters and helped me to overcome

my initial imbalances. The occasional chats with all the members here over a glass of tea at Kalida have been truly refreshing in between work. I have learnt a lot of physics from Prof. Sayan Kar, Prof Sugata Pratik Khastgir, Prof. Arghya Taraphdar, Prof. Anirvan Dasgupta, Prof Krishna Kumar and Prof. Anushree Roy. At times I have interacted with the M Sc students here, Niladri, Anishur, Kamakshya and Upasana. They also had to offer me there share of knowledge. Members of CTS, Ujal da, Venu da, Gopal da and Subhabrata da were always available whenever I needed them.

I will miss the time with SPK. Be it a very scientific discussion amongst us, or a pure"adda" at his residence, the scene was always inspirational. Added to the delightful snacks, tea and coffee from boudi those are the evenings I will always return to.

I am one of the privileged few to have great friends around. Bidesh has been there since my early school days and Prakash shares every moments of mine here at IIT. Sanjit, Suman, Sourav, Surja, Samaresh, Goutam, Tapomoy have never let me walk alone and Subhasis, Somnath (Nagakasi), Kamal, Somnath (bhaipo), Ganesh have been more like my brothers. Nirupam, Sambit, Chandryee di at NCRA, Tapan da, Saranya da, Tuhin at IUCAA and Wasim, Ruta, Yogesh, Kshitij at RRI made my visits over there very pleasant. Starting from our RAS days Wasim and I have discussed and quarreled probably over thousands of hours in understanding different aspects of radio astronomy. However, our friendship surely extends well out of our profession. I must not forget mentioning here of Subhasis, Somnath, Kamal, Tapomoy, Shrobana and Upasana again for wasting their time in proof-reading this thesis.

Finally, I will like to thank IIT Kharagpur, Department of Physics and Meteorology, AJCB hall and all the staff members for making my stay of seven years comfortable and enjoyable.

Signature

List of Symbols

Acronyms

Acronym	Full form
H I	Neutral hydrogen
ISM	Interstellar Medium
SFR	Star Formation Rate
NGC	New General Catalogue
IC	Index Catalogue
SMC	Small Magellanic Cloud
LMC	Large Magellanic Cloud
CMBR	Cosmic Microwave Background Radiation
AIPS	Astrophysical Image Processing System
VLA	Very Large Array
GMRT	Giant Meterwave Radio Telescope
WSRT	Westerbork Synthesis Radio Telescope
FIGGS	Faint Irregular Galaxy GMRT Survey
THINGS	The HI Nearby Galaxy Survey

Symbols

Symbols	Definitions
$\boldsymbol{U}$	Baseline in kilo wavelength
ν	Observing frequency in MHz
$\boldsymbol{\theta}$	Angle in the sky measured from the centre of the galaxy
$\mathcal{V}(\boldsymbol{U},\nu)$ **or** $\mathcal{V}(\boldsymbol{U})$	Visibility
$I(\boldsymbol{\theta},\nu)$	Specific Intensity
$\tilde{I}_\nu$	Smooth part of $I(\boldsymbol{\theta},\nu)$
$\delta I(\boldsymbol{\theta},\nu)$	Fluctuating part of $I(\boldsymbol{\theta},\nu)$
$W(\boldsymbol{\theta},\nu)$ **or** $W(\boldsymbol{\theta})$	Window function
θ_0	Galaxy angular radius
$A(\boldsymbol{\theta},\nu)$	Antenna primary beam
$\mathcal{N}(\boldsymbol{U},\nu)$	Noise at baseline $\boldsymbol{U}$ and frequency ν
$\tilde{\delta I}(\boldsymbol{U},\nu)$	Fourier transform of $\delta I(\boldsymbol{\theta},\nu)$
$\delta_D^2(\boldsymbol{U})$	Two dimensional Dirac delta function
$P_{HI}(\boldsymbol{U},\nu)$	Power spectrum
$\tilde{W}(\boldsymbol{U},\nu)$ **or** $\tilde{W}(\boldsymbol{U})$	Fourier transform of $W(\boldsymbol{\theta},\nu)$ or $W(\boldsymbol{\theta})$
$\mathcal{P}(\boldsymbol{U})$	Power spectrum estimator
U_m	Lowest baseline above which power spectrum is estimated
$1M_\odot$	Solar mass: $1M_\odot = 1.99 \times 10^{30}$ kg

Symbols	Definitions
U_{min}	Minimum value of the baseline above which power spectrum is a power law
U_{max}	Maximum value of the baseline below which power spectrum is a power law
R_{min}	Minimum length-scale above which power spectrum is a power law
R_{max}	Maximum length-scale below which power spectrum is a power law
A	Amplitude of the power law
α	Power law index
$\sigma_{\mathcal{P}}$	Variance in the power spectrum estimator
N_2	Noise covariance
N_g	Number of independent estimates of $\mathcal{P}(U)$ at a given U bin
N_b	Number of visibility pairs at a given U bin
$\hat{h}(\boldsymbol{r})$	Homogeneous and isotropic Gaussian random field
$P(k)$	Three dimensional power spectrum
γ	Power law index of the three dimensional power spectrum
$G(\boldsymbol{r})$	Three dimensional structure of the galaxy
z_h	Scale height of the galaxy
1 pc	parsec: 1 parsec $= 3 \times 10^{16}$ m

List of Tables

List of Figures

Abstract

In this thesis we use radio-interferometric observations to probe the intensity fluctuation power spectrum of the neutral hydrogen (H I) 21-cm emission from the interstellar medium (ISM) of the external galaxies. We develop a visibility based power spectrum estimator to probe the power spectrum directly from the interferometric observations and also estimate the errors in it. A numerical simulation of synthetic observations is also performed to access the efficacy and limitations of this estimator. We use this estimator to evaluate the power spectrum of three individual spiral galaxies, a dwarf galaxy sample and THINGS * spiral galaxies. In each case, the power spectrum is found to follow a power law $P_{\rm HI}(U) = AU^{\alpha}$ over a specific length scale range. The estimated value for the slope α ranges from ~ -1.5 to ~ -2.6 for the sample of dwarf galaxies. We interpret this bi-modality as arising due to 2D turbulence on length scales much larger than the scale-height of the galaxy disk and 3D otherwise. The power law slope also show a weak correlation with the surface density of star formation rate for these galaxies. We found for the external spiral galaxies the power spectrum is a power law up to a length scale of 10 to 16 kpc, indicating turbulence to be operational at these large length scales. We measure the scale-height of the external nearly face-on spiral galaxy NGC 1058 to be $\sim$ 500 pc interpreting a change in the slope observed in it's power spectrum. Power spectrum of the harassed galaxy NGC 4254 is found to be affected by galaxy harassment. For 18 spiral galaxies derived from the THINGS sample we found no correlation between the power law slope and the different dynamical parameters of these galaxies. For most of the dwarf and spiral galaxies, the intensity fluctuation power spectrum is found to be a direct probe of the density fluctuation and not affected by the velocity fluctuations in ISM. We would attempt to understand these new observations in terms of physical models of the ISM in future.

Keywords: Interstellar Medium, Turbulence, Galaxies, Scale-height, Power Spectrum, visibility correlation.

*THINGS: The HI Nearby Galaxy Survey

Contents

1 Introduction

It is now well established (Binney and Merrifield, 1998) that all galaxies have an interstellar medium (ISM) irrespective of their morphological class. This medium carries $10-15\%$ of the baryonic mass of a galaxy and is known to contain rarefied gas (mostly hydrogen and helium), dust (silicate and graphite), relativistic electrons and large scale magnetic fields. The structure of the ISM is different in the spiral and irregular galaxies compared to that in ellipticals. Moreover, for most of the observed galaxies, the gaseous ISM extends well beyond the stellar disk. Most of this gaseous medium is hydrogen ($70\,\%$) and helium ($28\,\%$), whereas there is a trace of the heavier elements ($1.5\,\%$) injected to the ISM during supernovae. Interstellar matter is distributed in discrete clouds of molecular and atomic gas with no preferred cloud scale. The molecular clouds have a temperature of about $100-200$ K compared to the cold atomic gas with temperature $50-100$ K. These denser clouds occupy only $1-2\,\%$ of the interstellar space and constitutes half of its mass. The rest of the ISM in between these clouds consists of warm neutral and ionized gas. These various forms of interstellar matter are highly coupled and is regarded as a single dynamical entity. In the process of star formation, clumps of ISM driven by gravity collapses to give birth to stars, whereas, dying stars in supernovae, ejects a huge amount of gas, dust and metal in the ISM making it highly coupled with the stellar disk of the galaxy.

1.1 A short overview on the ISM turbulence

Over the last few decades the structure and dynamics of the ISM has been extensively studied by observing it in both emission and absorption. The ISM is found to have rich scale invariant structures arranged in clouds of different shapes and sizes. Based on various observations and theoretical understandings it is now believed that the ISM is turbulent. Elmegreen and Scalo (2004) give a review of the progress in observations of ISM turbulence over the last few decades whereas Scalo and Elmegreen (2004) review the theoretical implications and effects of these observations.

Pioneering work in the theory of ISM was done as early as 1951 by von Weizsäcker (1951). He outlined a model for the ISM with a hierarchy of structures formed by the supersonic turbulence stirred at the large length-scales and dissipated at small scales by atomic viscosity. In the following year one of the first statistical models of a continuous and correlated gas distribution was proposed by Chandrasekhar and Münch (1952), who successfully applied it to the extinction fluctuations of Milky Way surface brightness. Observationally, absorption of starlight by the Na and Ca^+ ions revealed clumpy structure of the ISM (Binney and Merrifield, 1998).

Recent observations and numerical modellings, suggest that supersonic turbulent flows play a large role in the processes of star formation (Li et al., 2003). Vázquez-Semadeni et al. (2003) have shown, that first the transient clumpy molecular cloud structures are generated through turbulent fragmentation and then the individual clumps collapse to form proto-stars.

Turbulence generates scale-invariant stochastic fluctuations in the velocity and density field of the ISM. These fluctuations can be traced observing the ISM in emission and absorption lines of gas and metals. Observationally, statistical estimators are used to quantify the nature of these fluctuations as well as the turbulence that generated by

them. Velocity fluctuations are quantified using structure function of order two whereas auto-correlation function or the power spectrum is used to determine the density fluctuations. Most of the knowledge of ISM turbulence is acquired using these statistical measures. Here we briefly discuss a few statistical tools which are widely used to measure and quantify the ISM turbulence.

Auto-correlation function and power spectrum

The stochastic density field generated by fully developed turbulence is statistically homogeneous and isotropic and is believed to follow the Gaussian statistics. The statistical nature of such fluctuations can be completely specified by either the auto-correlation function or the power spectrum. The auto-correlation function $\xi_A(\mid \delta\boldsymbol{r} \mid)$ of any homogeneous and isotropic scalar field A is defined as

$$\xi_A(\mid \delta\boldsymbol{r} \mid) \;=\; \langle A(\boldsymbol{r})\, A(\boldsymbol{r}+\delta\boldsymbol{r})\rangle\,. \tag{1.1}$$

Fourier transform of the auto-correlation function is known as the power spectrum, i.e,

$$P_A(k) = \int d\boldsymbol{r} e^{i\boldsymbol{k}\cdot\boldsymbol{r}} \xi_A(\mid \delta\boldsymbol{r} \mid)\,, \tag{1.2}$$

where $k = \mid \boldsymbol{k} \mid$. For both the above definitions, the angular brackets denote ensemble averages. For a scale-invariant fluctuation both the auto-correlation function as well as the power spectrum are expected to follow power laws, i.e, $P_A(k) \sim k^{\alpha}$. The slope of these power law α is believed to be a good quantifier of the nature of the turbulence generating these structures.

Structure function

The structure function of order p for an observable A is defined as

$$S_p(\mid \delta\boldsymbol{r} \mid) = \langle \mid A(\boldsymbol{r}) - A(\boldsymbol{r}+\delta\boldsymbol{r}) \mid^p \rangle \,. \tag{1.3}$$

For a scale-invariant field, $S_p(\delta r)$ are also expected to be power laws, i.e, $S_p(\delta r) \sim \delta r^{\zeta_p}$. It is to be noted that the structure function of order two is directly related to the auto-correlation function by $S_2(\mid \delta\boldsymbol{r} \mid) = 2(< A^2(\boldsymbol{r}) > - \xi(\mid \delta\boldsymbol{r} \mid))$.

Delta variance

Another common measure of a stochastic field is the delta variance defined as

$$\sigma^2_\Delta(L) \;=\; \left\langle \int_0^{3L/2} d\boldsymbol{x} \left[(A(\boldsymbol{r}+\boldsymbol{x}) - < A >) \, \Theta(\boldsymbol{x}) \right]^2 \right\rangle , \tag{1.4}$$

where the cutoff function Θ is given by

$$\Theta(\boldsymbol{x}) = \pi \left(\frac{2}{L}\right)^2 \times \begin{cases} 1 & \text{if } x < L/2, \\ \\ \frac{1}{8} & \text{if } L/2 < x < 3L/2. \end{cases} \tag{1.5}$$

Power spectra measurements are typically limited by sample variance at large length-scales. Delta variance avoids this problem by using the cutoff function $\Theta(\boldsymbol{x})$.

It is to keep in mind that the estimators discussed above do not provide complete information if the stochastic field they probe has non-Gaussianity. Probes for non Gaussian fluctuations include structure function of higher order, higher order correlation functions, bispectrum, trispectrum etc. However, measuring these from the present observations is very difficult and is not usually addressed.

Most of the known facts about ISM turbulence is inferred by estimating the above quantifiers from mostly spectroscopic observations and then comparing to existing models of turbulence. Here we discuss how some important aspects of ISM turbulence are inferred from various observations.

1.1.1 Observations an inferences

von Hoerner (1951) found that the structure function of velocity fluctuations in the direction of the Orion nebulae is a power law. The slope was found to be $\sim 0.25-0.5$ which indicated a Kolmogorov energy spectrum. However, using a better data Wilson et al. (1959) got a steeper power law with slope ~ 0.6 and inferred in favour of compressible turbulence.

Apart from being scale-invariant, the density field generated by turbulence is also intermittent. Radio scintillation observations showed the clumpy nature of ISM at very small scales down to 10^7 m or lower (Little and Matheson, 1973). These could be understood using a model of magnetic turbulence generated by streaming instabilities (Wentzel, 1968). However, the relation of turbulence at these small length-scales and that observed at parsec length-scales was not very well understood.

During 1980s, a series of observation of spectral line-width at different line of sight revealed power law correlations. Gill and Henriksen (1990) introduced wavelet transformation for the analysis of ^{13}CO centroid velocities in L 1551, and the measured velocity-size slope was 0.7. Hobson (1992) used a clump finding algorithm and various other correlation techniques for HCO^+ and HCN along M 17SW. They found scale-invariant fluctuations for scales < 1 pc. Miesch and Zweibel (1994) used the structure function to determine a slope of 0.43 ± 0.15 for the velocity-size relation.

Comparing delta variance observations with models with and without gravity Ossenkopf et al.

(2001) concluded that self gravity increases power at small scales. The observations of the Polaries flare by Ossenkopf and Mac Low (2002) is compared with the models of delta variance for isothermal MHD turbulence. They found that the turbulence is driven from outside and the dissipation scale is smaller than their resolution scale.

Observing the extinction in the Taurus region, Padoan et al. (2002) found that ζ_p/ζ_3 varies for $p = 1$ to 20 in a similar manner as in a model of supersonic turbulence proposed by Boldyrev et al. (2002). In these models the dissipation of supersonic turbulence occurs in sheets giving $\zeta_p/\zeta_3 = p/9 + 1 - 3^{-p/3}$ assuming She-Leveque scaling (She and Leveque, 1994). Padoan et al. (2003) got a similar result observing ^{13}CO emission lines along Perseus and Taurus.

There is a considerable amount of effort in quantifying the scale-invariant structures present in the ISM using fractal and multi-fractal analysis. Perimeter area dimension are measured for the contour maps of 100 micron dust intensity (Bazell and Desert, 1988), CO emission (Falgarone et al., 1991) etc. The estimated value for the perimeter area dimension was $1.2 - 1.5$ which is consistent with that of a slice from the 3D structures observed in the terrestrial clouds and laboratory turbulence (Sreenivasan, 1991).

Chappell and Scalo (2001) have performed multi-fractal analysis of the column density maps derived from IRAS (The Infrared Astronomical Satellite) 60 μ and 100 μ images. They observed the region to region diversity in the multi-fractal spectra was significantly different from that expected from incompressible turbulence.

These observations not only established that the ISM has clumpy scale-invariant structures generated by turbulence over a large length-scale range, but also provided hints for the characteristics of the ISM turbulence. Though initially some similarity was found with the Kolmogorov energy spectrum, it is now believed that ISM turbulence is quite different. It is a compressible and supersonic fluid turbulence driven at different scales by

different mechanisms and induces scale-invariant multi-fractal structures in the density as well as the velocity field.

1.1.2 Energy sources

There is no wide-scale effective model for ISM turbulence which can explain all the observed features. The physical processes responsible for turbulence also differ enormously across the length-scales.

At smaller scales radio scintillation observations of intermittency can be well explained by sonic reflection of shock waves (Ikeuchi and Spitzer, 1984; Ferriere et al., 1988), cosmic ray streaming and other instabilities (Wentzel, 1969; Hall, 1980), energy cascades from larger scales etc. Lazarian et al. (2004) suggested that moderate turbulence can be maintained in the ionized clouds by variations in the background ionizing UV radiation. Norman and Ferrara (1996) recognized that most Type II SN contribute to cluster winds and super-bubbles at a length-scale range of $100 - 500$ pc.

The gravitational binding energy of a galaxy disk heats the stellar population during swing-amplified shear instabilities (Fuchs and von Linden, 1998) and also heats the gas triggering turbulence (Huber and Pfenniger, 2002). These gas clouds contiguously collapse to feed more turbulence at the smaller scales (Semelin et al., 1999). This kind of gravitational source for turbulence is consistent with the observed power spectra of flocculent spiral arms (Elmegreen et al., 2003). Since gravity acts at all the length-scales, the self gravity can feed turbulence at a wide range of length-scales.

Since ISM extends well beyond the stellar disk, galactic rotation driven turbulence can be effective at the outer regions of the galaxy's disk. Magneto-rotational instability, proposed by Sellwood and Balbus (1999); Kim et al. (2003), explains how galactic rotation pumps energy to the gas motion and hence feeds turbulence. Piontek and Ostriker

(2004) have considered a revised model where they assumed that the reduced dissipation enhances energy input to turbulence by magneto-rotational instability. Rotational energy also generates spiral shocks where the fast-moving inter-spiral medium hits the slower dense gas in the density wave arms (Roberts, 1969) making the ISM turbulent at the outer edges of the disk.

These physical mechanisms though could explain the observed fluctuations or shapes of the spectral lines at different length-scales, their interplay in generating wide scale coherent structures is not very well understood.

1.1.3 Simulations

Simulation play an effective role in understanding various physical models, particularly nonlinear processes such as turbulence. Observationally, only a static picture of ISM can be probed since the dynamic time scales involved are large. Using numerical hydrodynamic and magneto-hydrodynamic simulations it is possible to understand the effect of different mechanisms that drives ISM turbulence. Here we briefly discuss the different studies performed in this direction.

Bania and Lyon (1980) performed the first ever simulation of ISM turbulence. However, the lack of computational facilities limited them to a very small length-scale range. Higher resolution studies of non-gravitating and non-magnetogenic compressible turbulence was first performed by Porter et al. (1999, 2002). Their models were dominated by filaments, sheets and clusters in the compressible part of the flow and can explain the observed morphology of diffuse and small molecular clouds.

The first nonmagnetic simulations which included gravity were performed by Leorat et al. (1990) on a 128^3 grid, whereas Zhou (1993) did the first non-gravitating compressible simulation to include magnetic field. These earlier works were expanded by considering

different aspects of ISM like magnetic and gravitational fields, realistic heating and cooling mechanisms, stellar energy injections and galactic rotation (Vazquez-Semadeni et al., 1995, 1996). These simulations were meant to reproduce the ISM dynamics at the length-scale range of ~ 1 pc. In recent times higher resolution simulations (Kaneda et al., 2003) observed a constant energy flux over a large length-scale range with significant departure from Kolmogorov energy spectrum.

Despite the efforts simulation of ISM turbulence remained challenging due to the huge range of length-scales involved and high Reynolds number. It is important to include a wide range of length scales along with different models of energy inputs in the simulations to understand the interplay and cascading of the energy driving the ISM turbulence. Considering viscosity as the damping mechanism, Reynolds number (Re) for the ISM is estimated as high as 10^5 to 10^7. The number of degrees of freedom for three dimensional incompressible turbulence scales like $Re^{9/4}$. Hence simulating turbulence with $Re \sim 10^5$ requires a dynamic range of 10^5 which is far beyond the reach of present day computers.

1.2 Radio-interferometric observation as a probe of the ISM turbulence

In the previous section we have discussed the observation of ISM using different atomic and molecular lines which suggest turbulence. However, these elements, like dust, Ca^+, Na, CO etc., constitute a very small part of the interstellar matter both by mass and volume. These also are not very evenly distributed over the galaxy's disk. Almost 70 % of the gas in ISM is dominated by the atomic (H I) and ionized (H II) hydrogen which is spread all over the galaxy's disk making it a better tracer of the ISM dynamics.

21-cm radiation

The hyperfine structure transition radiation (21-cm radiation) of the neutral atomic hydrogen in the ground state (H I) is an excellent probe of the column density fluctuations in the ISM. This spectral line has a frequency of 1420 MHz, which falls in the radio band of the electromagnetic spectrum. The associated transition probability being very small, this line is considered as forbidden for laboratory experiments. However, at astrophysical scales it is possible to observe this radiation using very sensitive radio telescopes. The ISM has relatively small optical depth at these frequencies and the observed intensity fluctuations in the sky $I(\boldsymbol{\theta}, \nu)$ directly probes the column density fluctuations $N_{HI}(\boldsymbol{\theta}, \nu)$ in ISM, i.e,

$$I(\boldsymbol{\theta}, \nu) = \frac{3}{16\pi} h\nu \, A_{21} \, N_{HI}(\boldsymbol{\theta}) \phi(\nu) \tag{1.6}$$

Here, $\boldsymbol{\theta}$ is a vector in the sky, ν is the observing frequency and A_{21} is the corresponding Einstein coefficient. $\phi(\nu)$ gives the shape of the H I spectral line.

Radio-interferometric observations

Most of our understanding regarding the ISM is based on the observations in our Galaxy, the Milky Way. This is because the single dish radio telescopes lack the necessary resolution to resolve the structures in the external galaxies. Radio-interferometers like the VLA (Very Large Array*), GMRT (Giant Meterwave Radio Telescope†), WSRT (Westerbork Synthesis Radio Telescope‡) on the other hand provides higher resolution. These are capable of probing ISM structures and dynamics at smaller length-scales in our Galaxy and also provides means of observing turbulence at larger length-scales in external galaxies. In this section we briefly discuss the different efforts made in probing

*Very Large Array, NRAO, New Mexico
†Giant Meterwave Radio Telescope, NCRA, TIFR, India
‡Westerbork Synthesis Radio Telescope, Netherlands Foundation for Radio Astronomy

turbulence using radio-interferometric observations.

Unlike conventional optical, infrared or ultraviolet telescopes, radio interferometers do not measure the sky intensity, rather they measures the visibilities which are the Fourier transform of the sky brightness fluctuations. These visibilities can then be used to construct column density maps or the image of the observed field of view (Perley et al., 1989). Using these column density maps the auto-correlation functions can be estimated. However, these technique has limited utility due to the the presence of correlated noise at the image-plane generated because of limited baseline coverages (see **Appendix A**).

Crovisier and Dickey (1983) measured the power spectrum of H I emission from our galaxy squaring the directly observed visibilities (from radio-interferometric observations using WSRT) and subtracting the noise bias estimated from the line-free channels. They found that the power spectrum is roughly a power law with a slope of ~ -3 up to the largest of 10 pc they could probe. Using similar techniques, Green (1993) estimated the power spectrum of the H I emission of our galaxy from observations with DRAO (Dominion Radio Astrophysical Observatory[§]) synthesis radio telescopes. He found that the power spectrum is a power law with slope $-2.2 - 3.0$ up to a length-scale of 15 pc.

Deshpande et al. (2000) used a high dynamic range estimator to measure the power spectrum of the optical depth map created by observing H I in the Perseus spiral arm of our Galaxy in absorption towards Cassiopeia A. They found that the power spectrum can be well fitted by a power law with slope -2.75 for the length-scale ranges $0.10 - 3.0$ pc. Based on their observation they concluded that the ISM exhibits non-Kolmogorovian turbulence at these length-scales.

Fourier transform power spectra of the Large and Small Magellanic Clouds (LMC, SMC) are also found to obey power laws (Elmegreen et al., 2001; Burkhart et al., 2010) for a length-scale range of $20 - 200$ pc. Other techniques adopted by different authors to

[§]Dominion Radio Astrophysical Observatory : National Research Council, Canada

probe the ISM turbulence include velocity channel analysis or velocity coordinate spectrum (Lazarian, 1995), fractal dimensional analysis (Stutzki et al., 1998) and spectral correlation function (Rosolowsky et al., 1999) etc. These methods were limited either by the correlated noise induced by incomplete baseline coverages of radio-interferometric observations or by the noise bias in the power spectrum. They lack the necessary sensitivity to probe the faint emissions from the nearby dwarf or external galaxies.

1.3 Motivations and objectives

ISM of the Milky way is studied at length-scales ranging from 10^7 m to ~ 10 pc and is found to have scale invariant power spectrum with slope -2.0 to -3.0 indicating turbulence is operational. For the nearby galaxies (LMC, SMC), a similar power spectrum is observed till a length-scale of ~ 200 pc. The proposed driving mechanisms of these observed turbulence in our galaxy includes galactic rotation and self gravity which operates at even larger length-scales compared to the galaxies disk. It is necessary to probe the ISM of the external faint dwarf and nearby large spiral galaxies to investigate the existence of turbulence at large length-scales.

Conventionally, star formation in galaxies was known to be governed by the interplay of the gravity and magnetic pressure modulated by the ambipolar diffusion. However, recent observations and numerical modelings suggest that supersonic turbulent flow rather than the static magnetic field has larger role to play in this process (Li et al., 2003). Star formation is now believed to be a two phase process (Vázquez-Semadeni et al., 2003); first the generation of the transient clumpy molecular cloud structures by turbulent fragmentation and then the collapse of the individual clumps to form the proto-stars. The fragmentation governed by turbulence in the ISM leads to cloud structures which are reflected in the fluctuations of the H I 21-cm intensity. Hence, these fragmentation can

be traced estimating the power spectrum of the H I 21-cm intensity fluctuations. Dwarf galaxies often have irregular morphologies and peculiar large scale kinematics. This also makes them interesting to study the ISM turbulence beside investigating the galaxy formation scenario. Observations of the nearby faint dwarf galaxies with sufficient spatial resolution offers us a good opportunity to understand the early stages of the star as well as the galaxy formation.

Observationally it is difficult to estimate the power spectrum of the external galaxies because of the instrumental noise. A visibility based estimator was used by Hobson and Maisinger (2002) to estimate the Cosmic Microwave Background Radiation (CMBR) angular power spectrum. Bharadwaj and Ali (2005) have introduced a visibility based power spectrum estimator which can be used to probe the intensity fluctuations of H I 21-cm line using radio-interferometric observations. A modified form of this estimator is used by Begum et al. (2006a) to estimate the power spectrum of the nearby dwarf galaxy DDO 210. The power spectrum was found to be power law with slope ~ -2.8 for a length-scale range till 500 pc suggesting the presence of turbulence in the ISM of the dwarf galaxies.

Using a similar estimator from radio-interferometric observations of H I, it is possible to probe the ISM in external dwarfs and spirals and investigate the existence and nature of turbulence at kpc length-scales. The work presented in this thesis aims to use these observations to estimate the power spectrum of H I column density fluctuations in a large sample of galaxies. Earlier studies indicate that these fluctuations, which typically have a scale-invariant power spectrum, are possibly the outcome of turbulence in the ISM. The results of our study are expected to shed light on the nature of ISM turbulence.

The specific objectives of this thesis are highlighted below:

- Visibilities are the quantities directly measured in radio-interferometric observa-

tions, and there are several advantages if these be used to directly estimate the power spectrum. This is particularly important for the H I emission from faint external galaxies where the signal is weak and buried in noise. It is thus necessary to have a well quantified technique for visibility based power spectrum estimation.

- Simulations play an important role in assessing the efficacy and limitations of any technique. It is very important to apply the power spectrum estimation technique to simulated galaxies in order to asses the dynamical range and errors in the estimate.

- Having established a technique, it is then appropriate to apply this to estimate the power spectrum of the ISM of a large sample of dwarf and spiral galaxies.

- Finally, it is desirable to have some understanding of the measured power spectra in terms of the underlying ISM turbulence and the processes driving it.

1.4 Outline of the thesis

An outline of the rest of the thesis is as follows.

Throughout our different investigations presented in this thesis we use archival radio-interferometric data observed using the GMRT or the VLA. The directly observed quantity in these observations is visibility, which is the Fourier transform of the sky intensity fluctuations. In **Chapter 2** we discuss a visibility based power spectrum estimator. The application of such an estimator to the H I 21-cm observation of the ISM and the error estimation are also discussed.

We present the power spectrum analysis of the nearly face-on spiral galaxies NGC 628 and NGC 1058 and a harassed galaxy NGC 4254 of the Virgo cluster in **Chapter 3**. In **Chapter 4** we perform numerical simulations to study the efficacy and limitations of the

power spectrum estimator and access the dynamic range of length-scales for which it can be used. We present the result of our power spectrum analysis of a sample of 7 nearby external dwarf galaxies, and a sample of 18 external spiral galaxies from the THINGS[¶] survey in **Chapter 5** and **6** respectively. Finally, in **Chapter 7**, we summarize the main results of the thesis and discuss about the future scopes.

[¶]**THINGS** : **T**he **HI** **N**earby **G**alaxy **S**urvey, Walter et al. (2008)

2 Visibility based power spectrum estimator*

2.1 Introduction

Turbulence generates scale-invariant structures in the ISM density field. These structures can be quantified through the power spectrum of H I 21-cm radiation. The power spectrum is expected to be a power law for scale-invariant fluctuations. In this chapter we discuss a visibility based estimator which can be used to probe the H I intensity fluctuation power spectrum of external faint dwarf or spiral galaxies using radio-interferometric observations. We also present the error estimation and limitations in this estimator.

2.2 Visibility-visibility correlation

The specific intensity of H I emission from a galaxy at the phase centre of the observation can be modeled as

$$I(\boldsymbol{\theta},\nu) \;=\; W_\nu(\boldsymbol{\theta})\left[\bar{I}_\nu \;+\; \delta I(\boldsymbol{\theta},\nu)\right] \;, \tag{2.1}$$

*A part of the work presented in this chapter is originally published in the paper titled "A study of interstellar medium of dwarf galaxies using H I power spectrum analysis" by Dutta et al. (2009a).

were $\boldsymbol{\theta}$ is the angle on the sky measured in radians from the center of the galaxy. We assume that the galaxy subtends a small angle so that $\boldsymbol{\theta}$ may be treated as a two dimensional (2D) planar vector on the sky. The H I specific intensity is modeled as the sum of a smooth component and a fluctuating component. Typically, $I(\boldsymbol{\theta}, \nu)$ is maximum at the center and declines with increasing $\mid \boldsymbol{\theta} \mid$. We model this through a window function $W_\nu(\boldsymbol{\theta})$ which is defined so that $W_\nu(0) = 1$ at the center and has values $1 \geq W_\nu(\boldsymbol{\theta}) \geq 0$ elsewhere. This multiplied by $\bar{I}_\nu$ gives the smooth component of the specific intensity. For a face-on galaxy, the window function $W_\nu(\boldsymbol{\theta})$ corresponds to the galaxy's radial profile.

In our analysis we consider two different models for the window function of a galaxy of angular radius θ_0. In the "top-hat" model it is assumed that the specific intensity has a constant value within a circular disk of radius θ_0, and it abruptly falls to 0 outside. The window function, in this case, is a Heaviside step function

$$W_\nu(\boldsymbol{\theta}) = \Theta(\theta_0 - \theta) \tag{2.2}$$

In the "exponential" model the window function has the form

$$W_\nu(\boldsymbol{\theta}) = \exp\left(-\frac{\sqrt{12}\theta}{\theta_0}\right) , \tag{2.3}$$

where it falls exponentially away from the center. Note that for both the models we have assumed the radial profile to be isotropic compared to the centre of the galaxy.

It is also possible to use $W_\nu(\boldsymbol{\theta})$ to define a normalized window function $W_\nu^N(\boldsymbol{\theta})$ such that $\int d\boldsymbol{\theta}\, W_\nu^N(\boldsymbol{\theta}) = 1$. The second moment of θ defined as $\int d\boldsymbol{\theta} \mid \boldsymbol{\theta}^2 \mid W_\nu^N(\boldsymbol{\theta})$ provides a good estimate of the angular extent of the window function. Here we have used the condition that this should have the same value $\theta_0^2/2$ for all models of the window function,

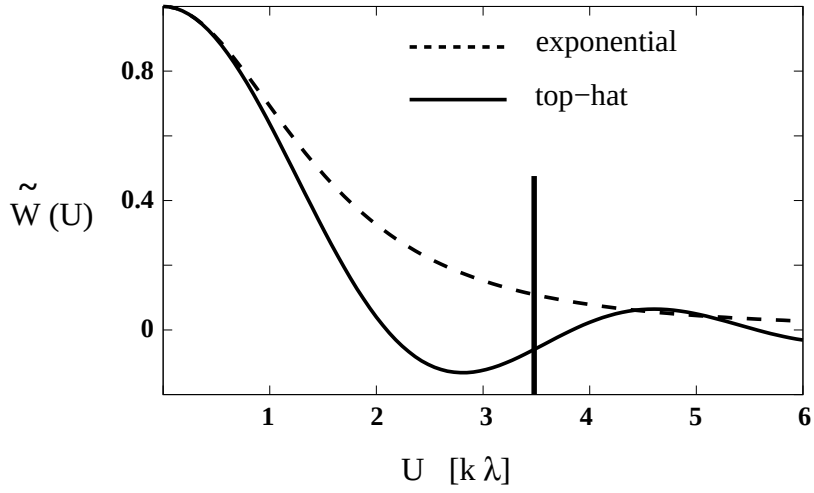

Figure 2.1: $\tilde{W}(\boldsymbol{U})$ for top-hat and exponential window functions for $\theta_0 = 1'$. The vertical line marks θ_0^{-1}. Note that the FWHM (Full Width at Half Maxima) of the two window functions are nearly the same and both window functions have a very small value for $U > \theta_0^{-1}$.

to determine the width of the exponential window function in terms of θ_0. Throughout we have assumed $\theta_0 \ll 1$ radian.

We express the fluctuating component of the specific intensity as $W_\nu(\boldsymbol{\theta})\,\delta I_\nu(\boldsymbol{\theta})$. Here $\delta I_\nu(\boldsymbol{\theta})$ is a stochastic fluctuation which is assumed to be statistically homogeneous and isotropic. The H I emission traces these fluctuations modulated by the window function which quantifies the large-scale H I distribution. In this thesis we use radio-interferometric observations to quantify the statistical properties of the fluctuations $\delta I_\nu(\boldsymbol{\theta})$. These fluctuations are believed to be the outcome of turbulence in the ISM.

The visibility $\mathcal{V}(\boldsymbol{U}, \nu)$ is the quantity that is directly observed in the radio-interferometric observations[†]. It is the Fourier transform of the product of the antenna primary beam pattern $A(\boldsymbol{\theta}, \nu)$ and the specific intensity distribution of the galaxy.

$$\mathcal{V}(\boldsymbol{U}, \nu) \;=\; \int d\boldsymbol{\theta}\; e^{-i2\pi \boldsymbol{U}\cdot\boldsymbol{\theta}} A(\boldsymbol{\theta}, \nu)\, I(\boldsymbol{\theta}, \nu). \tag{2.4}$$

[†]We assume the $2D$ approximation of the visibility here. Interested readers are referred to the **Appendix B**.

Here $\boldsymbol{U}$ refers to a baseline, the antenna separation measured in units of the observing wavelength λ. It is common practice to express $\boldsymbol{U}$ in units of kilo wavelength (kλ). Throughout this paper we follow the usual radio-interferometric convention and express $\boldsymbol{U}$ in units of kilo wavelengths (kλ).

The angular extent of the galaxies that we consider here is much smaller than the primary beam, and it's effect may be ignored. We then have

$$\mathcal{V}(\boldsymbol{U},\nu) \;=\; \tilde{W}(\boldsymbol{U},\nu)\bar{I}(\nu) + \tilde{W}(\boldsymbol{U},\nu) \otimes \tilde{\delta I}(\boldsymbol{U},\nu) + \mathcal{N}(\boldsymbol{U},\nu) \tag{2.5}$$

where the tilde $\tilde{}$ denotes the Fourier transform of the corresponding quantity and $\otimes$ denotes a convolution. In addition to the signal, each visibility also contains a system noise contribution $\mathcal{N}(\boldsymbol{U},\nu)$ which we have introduced in **Eqn. (2.5)**. The noise in each visibility is a Gaussian random variable and the noise in the visibilities at two different baselines $\boldsymbol{U}$ and $\boldsymbol{U}^{'}$ is uncorrelated. We will discuss the property of the noise term $\mathcal{N}(\boldsymbol{U},\nu)$ in detail in a following section.

The Fourier transform of the normalized window functions are

$$\tilde{W}(\boldsymbol{U},\nu) = 2\;\frac{J_1(2\pi\theta_0 U)}{2\pi\theta_0 U} \tag{2.6}$$

and

$$\tilde{W}(\boldsymbol{U},\nu) = \frac{1}{\left[1+\pi^2\theta_0^2 U^2/3\right]^{3/2}} \tag{2.7}$$

for the top-hat and exponential models respectively. Here $J_1(x)$ is the Bessel function of order 1. These functions, shown in **Figure 2.1**, have the property that they peak around $U = 0$ and fall off rapidly for $U \gg \theta_0^{-1}$. This is a generic property of the window function, not restricted to just these two models. At baselines $U \gg \theta_0^{-1}$ we may safely neglect the first term in **Eqn. (2.5)** whereby

$$\mathcal{V}(\boldsymbol{U},\nu) = \tilde{W}(\boldsymbol{U}) \otimes \tilde{\delta I}(\boldsymbol{U},\nu) + \mathcal{N}(\boldsymbol{U},\nu) \tag{2.8}$$

We use the power spectrum of H I intensity fluctuations $P_{HI}(U)$ defined as

$$\langle \tilde{\delta I}(\boldsymbol{U},\nu) \tilde{\delta I}^{*}(\boldsymbol{U}',\nu) \rangle = \delta_D^2(\boldsymbol{U}-\boldsymbol{U}')\, P_{HI}(U,\nu) \tag{2.9}$$

to quantify the statistical properties of the intensity fluctuations. Here, $\delta_D^2(\boldsymbol{U}-\boldsymbol{U}')$ is a two dimensional Dirac delta function. The angular brackets denote an ensemble average over different realizations of the stochastic fluctuation. In reality, it is not possible to evaluate this ensemble average because a galaxy presents us with only a single realization. In practice we evaluate an angular average over different directions of $\boldsymbol{U}$. This is expected to provide an estimate of the ensemble average for a statistically isotropic fluctuation. Note that, the power spectrum thus defined can in general be a function of the observation frequency. However, for the observation of the ISM turbulence, the power spectrum is expected to remain constant within the frequency range of observation. We will explicitly check this assumption in a later chapter and will find deviation to it for the ISM in a particular galaxy. However, for the time being for most of the galaxies, it is safe to assume that the power spectrum is independent of ν. We will drop the ν dependence henceforth.

The square of the visibilities can, in principle, be used to estimate $P_{HI}(U)$

$$\langle\ \mathcal{V}(\boldsymbol{U},\nu)\mathcal{V}^{*}(\boldsymbol{U},\nu)\ \rangle\ = \left|\tilde{W}(\boldsymbol{U},\nu)\right|^2 \otimes\ P_{HI}(\boldsymbol{U}) + \langle |\ \mathcal{N}(\boldsymbol{U},\nu)\ |^2 \rangle \tag{2.10}$$

and this has been used in several earlier studies (Crovisier and Dickey, 1983; Green, 1993; Lazarian, 1995). This technique has limited utility to observations where the H I signal in each visibility exceeds the noise. This is because the noise variance in the

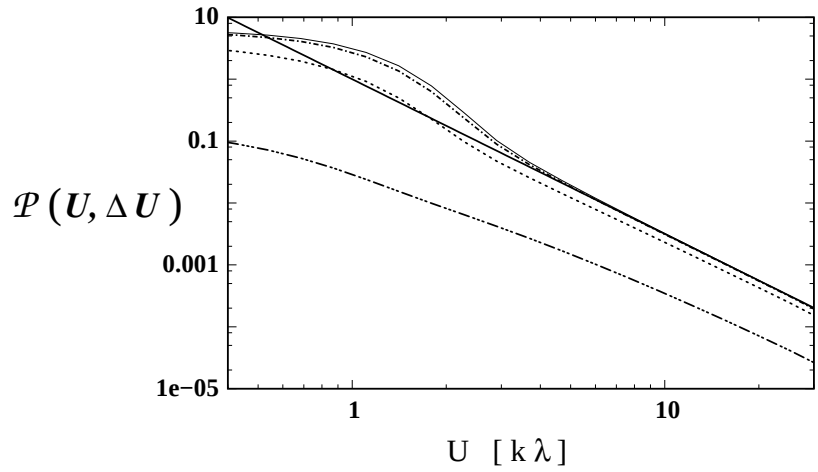

Figure 2.2: This shows the convolution (**Eqn. (2.11)**) of a power law $P_{HI}(U) = U^{-2.5}$ with the product of two exponential window functions (**Eqn. (2.7)**) with $\theta_0 = 1'$ ($(\pi\theta_0)^{-1} \approx 1\,\mathrm{k}\lambda$). The bold solid curve shows the original power law and the thin solid curve shows $\mathcal{P}(\boldsymbol{U}, \Delta\boldsymbol{U})$ for $\Delta\boldsymbol{U} = 0$. The dashed curves are for $\mid \Delta\boldsymbol{U} \mid = 0.2, 1.0$ and $3.0\,\mathrm{k}\lambda$ respectively from top to bottom. The direction of $\Delta\boldsymbol{U}$ is parallel to that of $\boldsymbol{U}$. Note that $\mathcal{P}(\boldsymbol{U}, 0.2) \approx \mathcal{P}(\boldsymbol{U}, 0)$ and the correlation between two different visibilities is small for $\mid \Delta\boldsymbol{U} \mid > (\pi\theta_0)^{-1}$.

last term $\langle \mid \mathcal{N}(\boldsymbol{U}, \nu) \mid^2 \rangle$ introduces a positive bias in estimating the power spectrum. The noise bias can be of orders of magnitude larger than the power spectrum for the faint external galaxies considered here. In principle, it may be separately estimated using line-free channels and subtracted. In practice this is extremely difficult owing to uncertainties in the bandpass response which restrict the noise statistics to be estimated with the required accuracy. Attempts to subtract out the noise-bias have shown that it is not possible to do this at the level of accuracy required to detect the H I power spectrum (Begum, 2006).

The problem of noise bias can be avoided by correlating visibilities at two different baselines for which the noise is expected to be uncorrelated. We define the power

spectrum estimator as

$$\begin{aligned}\mathcal{P}(\boldsymbol{U},\Delta\boldsymbol{U}) &= \langle\ \mathcal{V}(\boldsymbol{U},\nu)\mathcal{V}^{*}(\boldsymbol{U}+\Delta\boldsymbol{U},\nu)\ \rangle \\ &= \int d\boldsymbol{U}'\,\tilde{W}(\boldsymbol{U}-\boldsymbol{U}',\nu)\,\tilde{W}^{*}(\boldsymbol{U}+\Delta\boldsymbol{U}-\boldsymbol{U}',\nu)\ P_{HI}(\boldsymbol{U}'). \quad (2.11)\end{aligned}$$

Since $\tilde{W}(\boldsymbol{U},\nu)$ falls off rapidly for $U \gg \theta_0^{-1}$ (**Figure 2.1**), the window functions $\tilde{W}(\boldsymbol{U}-\boldsymbol{U}',\nu)$ and $W^{*}(\boldsymbol{U}+\Delta\boldsymbol{U}-\boldsymbol{U}',\nu)$ in **Eqn. (2.11)** have a substantial overlap only if $|\Delta\boldsymbol{U}| < (\pi\theta_0)^{-1}$. Visibilities at two different baselines will be correlated only if $|\Delta\boldsymbol{U}| < (\pi\theta_0)^{-1}$, and not beyond (**Figure 2.2**). In our analysis we restrict the difference in baselines to $|\Delta\boldsymbol{U}| \ll (\pi\theta_0)^{-1}$ so that $\tilde{W}(\boldsymbol{U}+\Delta\boldsymbol{U}-\boldsymbol{U}^{'},\nu) \approx \tilde{W}(\boldsymbol{U}-\boldsymbol{U}^{'})$ and the estimator $\mathcal{P}(\boldsymbol{U},\Delta\boldsymbol{U})$ no longer depends on $\Delta\boldsymbol{U}$ (**Figure 2.2**). We then use the visibility correlation estimator

$$\begin{aligned}\mathcal{P}(\boldsymbol{U}) &= \langle\ \mathcal{V}(\boldsymbol{U},\nu)\mathcal{V}^{*}(\boldsymbol{U}+\Delta\boldsymbol{U},\nu)\ \rangle \\ &= \int d\boldsymbol{U}'\ |\ \tilde{W}(\boldsymbol{U}-\boldsymbol{U}',\nu)\ |^{2}\ P_{HI}(\boldsymbol{U}')\,. \quad (2.12)\end{aligned}$$

The measured visibility correlation $\mathcal{P}(\boldsymbol{U})$ will, in general, be complex. The real part is the power spectrum of H I intensity fluctuations convolved with the square of the window function. A further simplification is possible at large baselines $U \gg \theta_0^{-1}$, provided $|\ \tilde{W}(U,\nu)\ |^2$ decays much faster than the variations in $\mathrm{P_{HI}}(U)$. We then have

$$\mathcal{P}(\boldsymbol{U}) = C\,P_{HI}(\boldsymbol{U}) \quad (2.13)$$

where $C = \int |\ \tilde{W}(U,\nu)\ |^2\ \ d\boldsymbol{U}$ is a constant.

We use the real part of the estimator $\mathcal{P}(U)$ to estimate the power spectrum $P_{HI}(U)$. Our interpretation is restricted to the U range $U \gg (\pi\theta_0)^{-1}$ where the convolution in

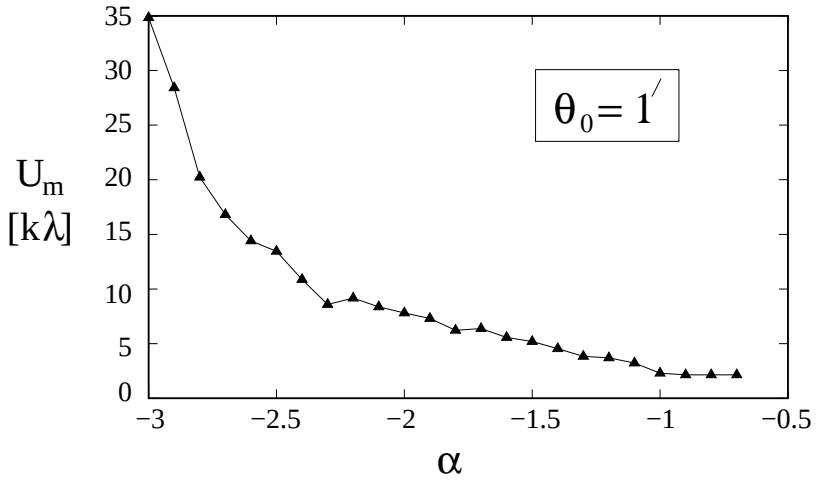

Figure 2.3: This shows how U_m changes with α for an exponential window function with $\theta_0 = 1'$. Note that the discontinuities seen in the plot appear to be genuine features and not numerical artifacts, though the cause of these features is not clear at present. We find that a 4^{th} order polynomial $U_m(\alpha) = (a + b * \alpha + c * \alpha^2 + d * \alpha^3 + e * \alpha^4)/\theta_0$ provides a good fit to the above curve with the parameter values as $a = 35.6$, $b = 104.5$, $c = 112.5$, $d = 48.9$, and $e = 7.7$. We use this as a template for estimating U_m in the real observations.

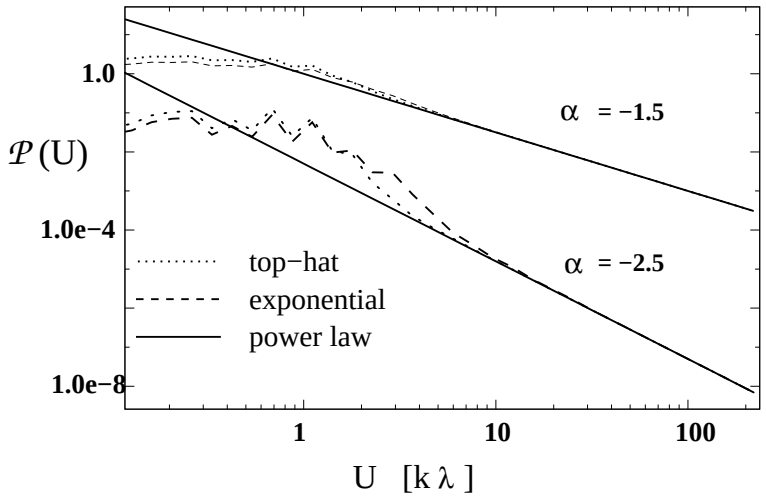

Figure 2.4: Effect of window function modifies the power spectrum differently for different power law exponents.

Eqn. (2.12) does not affect the shape of the power spectrum and **Eqn. (2.13)** is a valid approximation. Since for this case the estimator is independent of $\Delta \boldsymbol{U}$ and hence we write it as $\mathcal{P}(\boldsymbol{U})$. In order to estimate the U range where this approximation is valid we have numerically evaluated **Eqn. (2.11)** assuming $P_{HI}(U)$ to be a power law $P_{HI}(U) = AU^{\alpha}$. **Figure 2.4** shows the results for both the top-hat and the exponential models with $\theta_0 = 1'$ ($\theta_0^{-1} = 3.4\,\mathrm{k}\lambda$) and $\alpha = -1.5$ and -2.5 which roughly spans the range of slopes usually observed for different galaxies. Using U_m to denote the value (in kλ) where the deviation from the original power law is 10%, we find that for the top-hat and exponential models respectively U_m has values $(3.1, 5.3)$ for $\alpha = -1.5$ and $(4.8, 13.0)$ for $\alpha = -2.5$. Note that U_m depends on two parameters, namely α and θ_0. **Figure 2.3** shows how U_m changes with α for the exponential model with $\theta_0 = 1'$. For other values of θ_0 we scale the value of U_m in **Figure 2.3** using $U_m \propto \theta_0^{-1}$. For a given power law index, the estimator $\mathcal{P}(U)$ gives a direct estimate of the power spectrum for $U \geq U_m$.

2.3 Method of analysis

We use radio-interferometric spectroscopic multichannel data observed using GMRT or VLA for power spectrum analysis. In this section we discuss the method of estimating the power spectrum and its errors in practice.

2.3.1 Visibility correlation

The starting point of each analysis is the radio-interferometric spectroscopic multichannel raw *uv* fits data. We reduced the raw data in the usual way using standard tasks in classic AIPS[‡]. For each observations, bad visibility points were edited out, after which the data was calibrated. The calibrated data is then inspected for H I emission and the

[‡]NRAO Astrophysical Image Processing System, a commonly used software for radio data processing.

line-channels are identified. A continuum image is then made averaging all the line-free channels. In the next step, this model continuum is subtracted from the visibility data in the uv plane using the AIPS task UVSUB. The resulting continuum subtracted data was used for the subsequent analysis. Such a typical spectroscopic data has n emission channels. To determine if the H I power spectrum changes with the width of the frequency channel, we combine N successive channels to obtain a data set with n/N channels. The power spectrum is evaluated in each of this combined channels and then averaged over them for a particular U value. We use a range of N values for the power spectrum analysis.

We measure $\mathcal{P}(U)$ by multiplying every visibility $V(\boldsymbol{U}, \nu)$ with all other visibilities $V(\boldsymbol{U} + \Delta\boldsymbol{U}, \nu)$ within a disk $\mid \Delta\boldsymbol{U} \mid \leq U_D$ and then average over different $\boldsymbol{U}$ directions. We will discuss the considerations for choosing the value of U_D shortly. Note that correlation of a visibility with itself is excluded. To increase the signal to noise ratio we further average the correlations in logarithmic bins of U and over all frequency channels with H I emission. To choose a particular value of U_D, we perform this analysis varying $\mid \Delta\boldsymbol{U} \mid$ from $1/\pi\theta_0$ to lesser values. Note that, for larger values of U_D, we find that the imaginary part of the estimator $\mathcal{P}^I$ becomes comparable to $\mathcal{P}$, while for smaller values of $\mid \Delta\boldsymbol{U} \mid$, the amplitude of $\mathcal{P}^I$ decreases. For a particular observation we identify a value of $\mid \Delta\boldsymbol{U} \mid$, for which the ratio $\mathcal{P}/\mathcal{P}^I > 10$ and the amplitude of $\mathcal{P}$ is maximum. We use this value as U_D for the subsequent analysis.

The measured visibility correlation estimator $\mathcal{P}(U)$ [**Eqn. (2.12)**] is the convolution of the actual H I power spectrum with a window function. We do not attempt to estimate this window function to deconvolve the power spectrum. Our approach is to estimate a baseline U_m, such that for $U \geq U_m$ the effect of the convolution can be ignored. $\mathcal{P}(U)$ is proportional to the H I power spectrum [**Eqn. (2.13)**] at baselines $U \geq U_m$. We estimate the H I power spectrum using only this range ($U \geq U_m$).

Assuming an exponential window function [**Eqn. (2.3)**], the value of U_m depends on the parameters θ_0 and α. Note that we do not attempt to actually fit an exponential to the observed overall H I distribution and thereby determine θ_0. The galaxies are typically oriented randomly compared to the line of sight direction assuming different inclination angles. This offers the window functions with elliptical shapes in the sky plane, not circular disks as assumed in **Section 2.2**. For each of the individual galaxies we generate column density maps. We determine the extent of the major axis and the minor axis of the galaxy window function from these maps at a column density value of 10^{21} atoms cm^{-2}. We use the smaller of the two angular extents as θ_0 in our analysis. As $U_m \propto \theta_0^{-1}$, choosing the smaller value gives a conservative estimate of U_m. We also estimate $\mathcal{P}(U)$ combining the visibilities of the line-free channels. The upper limit U_u where we have a reliable estimate of the H I power spectrum is determined by the requirement that the real part of $\mathcal{P}(U)$ estimated from the line-channels should be more than its imaginary part and also that estimated from the line-free channels.

2.3.2 Error estimation

The variance $\sigma_{\mathcal{P}}$ of the visibility correlation estimator $\mathcal{P}(U)$ is given by (see **Appendix C**, also Ali et al. (2008))

$$\sigma_{\mathcal{P}}^2 = \frac{\mathcal{P}(U)^2}{N_g} + \frac{N_2^2}{2N_b}, \tag{2.14}$$

where N_g is the number of independent estimates of $\mathcal{P}(U)$ in a given U-bin, N_b is the total number of visibility pairs in the bin and N_2 is the noise variance. The first term in **Eqn. (C13)** is a contribution from the sample variance where the second term incorporates the noise contribution. We evaluate N_2 estimating the variance in the visibility values. Since in a particular interferometric observation, the uv space can be

sparsely sampled, we grid the uv plane. We chose the grid size such that each grid have same area as a circle of radius U_D. We determine the fraction of grids filled with visibility values in each annular bin (f_G). We use $\frac{2\pi U \delta U}{\pi U_D^2} f_G$ as an estimate for N_g. Here, δU is the width of a bin at U from origin in the uv plane. With these parameters the variance in the visibility correlation estimator is given by

$$\sigma_{\mathcal{P}} = \sqrt{\frac{\mathcal{P}(U) U_D^2}{2U\delta U} f_G + \frac{N_2^2}{N_b}} \tag{2.15}$$

Note that the first term under the square-root sign in the above equation dominates for smaller values of U, since there both U and δU are small. The second term, however, dominates at large baselines where the uv plane is very sparsely sampled.

2.3.3 Fitting a power law to the power spectrum

We check if the estimated power spectrum follow a power law over a length-scale range and evaluate the slope of this power law. The procedure that we adopt to determine the best fit power law to the H I power spectrum is as follows. We first visually identify a baseline U_m beyond which ($U \geq U_m$) the visibility correlation estimator appears to be a power law in U. The largest baseline U_{max} till which the estimator can be used is limited by the requirement that the real part of $\mathcal{P}(U)$ estimated from the line-channels is greater than its imaginary part as well as the real part of the $\mathcal{P}(U)$ estimated from the line-free channels. We use the range $U_m \leq U \leq U_{max}$ to fit a power law $\mathcal{P}(U) = A\ U^{\alpha}$ through a χ^2 minimization. The best fit α obtained by this fitting procedure is used to get a revised estimate for U_m [see **Figure 2.3**] and the power law fitting is repeated with this new value of U_m. We iterate this procedure a few times till it converges. To test whether the impact of the window function is actually small, we convolve the best fit power law with $\mid \tilde{W}(U,\nu) \mid^2$ assuming an Exponential window. The convolved

power spectra are visually inspected to asses the deviations from the power law. The goodness of fit to the data was also estimated by calculating χ^2 for the convolved power spectrum. We accept the final fit only after ensuring that the effect of the convolution can actually be ignored. We note the value of the best fit power law index α and the range of U values ($U_{min} - U_{max}$) for the fit. We also determine the values $R_{max} = D/U_{min}$ and $R_{min} = D/U_{max}$, where D is the distance to the galaxy. These provide the range of length-scales at the galaxy's disk over which the power-law fit holds. We can then conclusively state that over those length-scales in the galaxy the power spectrum assumes power law and the ISM is turbulent.

2.4 Discussions and Conclusions

We discuss the major points of this chapter here and conclude.

- In this chapter we have presented a method of estimating the power spectrum of H I intensity fluctuation from radio-interferometric observations using the visibility correlation. The effect of noise bias is avoided correlating the visibilities at nearby baselines. This method holds the key in measuring turbulence in the external galaxies.

- We have discussed an operating formula for estimating the error bars in the visibility correlation estimator we presented. This estimates of the error incorporates the effect of sample variance as well as the statistical errors and signifies the quality of the power spectrum measurement.

- For a turbulent ISM, the power spectrum of the H I intensity fluctuation is expected to be a power law. We have discussed the procedure to obtain the best fit power law slope α from the power spectrum estimates. However, since we do not

exclusively evaluate the shape of the window function here, our method can not be used to measure the intensity of these fluctuations.

Armed with this technique, in the following chapters we will use this estimator for external dwarf and spiral galaxies and investigate the relation of turbulence with some of their dynamical and morphological parameters. In a different investigation we have also used the same estimator to evaluate the power spectrum of the supernovae remnant and opacity fluctuation power spectrum of our galaxy. However, these works are not relevant in the objective of the present thesis. Interested readers may look at Roy et al. (2009) and Roy et al. (2010) for further information.

3 Power Spectrum Analysis of Three Spiral Galaxies*

3.1 Introduction

Power spectrum analysis is extensively used for studying the ISM in our galaxy (Crovisier and Dicke 1983; Green, 1993; Deshpande et al., 2000; Faison and Goss, 2001; Braun and Kanekar, 2005). Being observations from inside the Galaxy, these are restricted to length scales of $\sim$ 10 AU to 10 pc, where a power law power spectrum with a slope of ~ -2.8 is seen. This is believed to be the outcome of ISM turbulence. The power spectra of LMC and SMC are also studied (Stanimirovic et al., 1999; Elmegreen et al., 2001; Stanimirović and Lazarian, 2001), where the ISM is probed at relatively larger length-scales ($\sim$ 200 pc). The power spectrum of the nearby dwarf galaxies are also found to be power laws of similar slope as observed for our Galaxy.

Recently Begum et al. (2006a) have used the power spectrum estimator defined in **Chapter 2** to probe the ISM of the external dwarf galaxy DDO 210. The power

*The works presented in this chapter are derived from the following three original publications:
(1) "H I power spectrum of the spiral galaxy NGC 628" by Dutta et al. (2008),
(2) "The scale-height of NGC 1058 measured from its H I power spectrum." by Dutta et al. (2009b),
(3) "Turbulence in the harassed galaxy NGC 4254" by Dutta et al. (2010a).

Galaxy	Major ($'$)	Minor ($'$)	D (M pc)	i_{HI} ($^\circ$)	Reff
NGC 628	15.0	11.0	8.0	13	1
NGC 1058	13.0	11.0	10.0	11	2
NGC 4254	8.0	6.5	16.7	42	3

Table 3.1: Some relevant parameters of the 3 galaxies for which we do the power spectrum analysis in this chapter. The refferences are as follows: 1- Kamphuis and Briggs (1992), 2- Petric and Rupen (2007), 3- Phookun et al. (1993),

spectrum is found to be a power law indicating the presence of turbulence. Further, they found that the slope of the power spectrum is ~ -2.7, which is similar to what was observed for our Galaxy, LMC or SMC previously. Since DDO 210 is a relatively nearby faint dwarf galaxy, they have managed to probe a length-scale of 80 to 500 pc, which is also similar to what was probed for our Galaxy.

Observing nearby spiral galaxies using radio interferometers like GMRT or VLA, it is possible to probe the ISM at larger length-scales. Such observations can directly estimate the operating length-scale range of the ISM turbulence. In this chapter we present the power spectrum analysis of 3 external spiral galaxies namely NGC 628, NGC 1058 and NGC 4254 (**Table 3.1**). First two of these galaxies are nearly face on spirals whereas the galaxy NGC 4254 resides in a cluster environment and is believed to be a harassed galaxy. The objective of this chapter will be to investigate the ISM intensity fluctuation power spectrum at larger length-scales than it is hitherto probed. Moreover, the power spectrum of NGC 4254 can reveal the nature of ISM for the galaxies residing and interacting in a cluster environment.

3.2 Evidence of turbulence at large length-scales : NGC 628

NGC 628 (M 74) is a nearly face-on SA(s)c spiral galaxy with an inclination angle in the range 6° to 13° (Kamphuis and Briggs, 1992). It has a very large H I disk extending out to more than 3 times the Holmberg diameter. Elmegreen et al. (2006) have found a scale-free size and luminosity distribution of star forming regions in this galaxy, indicating turbulence to be functional here. The distance to this galaxy is uncertain with previous estimates ranging from 6.5 Mpc to 10 Mpc. Briggs et al. 1980 and Kamphuis and Briggs 1992 have used a Hubble flow distance of $\sim$ 10 Mpc. On the other hand, Sharina et al. (1996) estimated a distance of 7.8 ± 0.9 Mpc from the brightest blue star in the galaxy. This distance estimate matches with an independent photometric distance estimate by Sohn and Davidge (1996). In a recent study Vinkó et al. (2004) inferred the distance to be 6.7 ± 4.5 Mpc by applying the expanding photosphere method to the hyper novae SN 2002ap. Here we adopt the photometric distance of 8 Mpc for NGC 628. At this distance $1''$ corresponds to 38.8 pc.

3.2.1 A brief description of the data used

We have used archival H I data of NGC 628 from the Very Large Array (VLA). The observations had been carried out on August 1^{st} and November 14^{th}, 1993 respectively in the C and D configurations of the VLA, as a part of the AAO163 observing program. We performed the data analysis following the method described in **Section 2.3**. The multi-configuration data were downloaded from the VLA archive and reduced in the usual way using standard tasks in classic AIPS[†]. For each VLA configuration, bad visibility

[†]NRAO Astrophysical Image Processing System, a commonly used software for radio data processing.

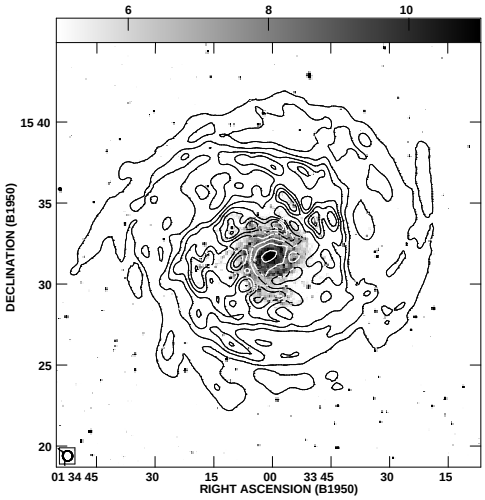

Figure 3.1: The $38'' \times 36''$ resolution integrated H I column density map of NGC 628 (contours) overlayed on the optical DSS image (grey scale). The contour levels are 0.24, 1.96, 3.68, 5.41, 7.13, 8.85, 10.57 and 12.29 $\times 10^{20}$ cm^{-2}.

points were edited out, after which the data were calibrated. The calibrated data for both configurations was combined using the AIPS task DBCON. The H I emission from NGC 628 spans 64 central channels (i.e, $n = 64$) of the 256 channel spectral cube (with channel width 1.29 km s^{-1}). A continuum image was made using the average of all the line-free channels. The continuum from the galaxy was subtracted from the data in the *uv* plane using the AIPS task UVSUB. The resulting continuum subtracted data was used for the subsequent analysis. **Figure 3.1** shows a total H I column density (Moment 0) map of NGC 628 from an image made from this data. The H I disc of the galaxy is nearly face-on. The angular extent of the H I distribution in **Figure 3.1** is roughly $11' \times 15'$. Using deep VLA D array mosaic observations, Kamphuis and Briggs (1992) had detected a $\sim 38' \times 31'$ faint diffuse H I envelope around NGC 628. This extended envelope is not detected in the current data set; the emission that we do detect is instead restricted to the main H I disc of NGC 628. The results we discuss below are hence also

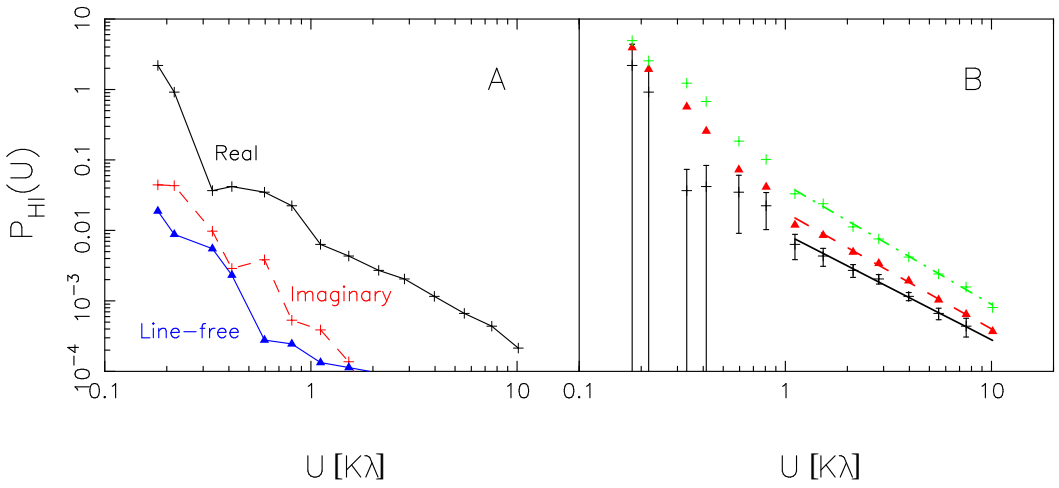

Figure 3.2: A) Real and imaginary parts of the observed value of the H I power spectrum estimator $\mathcal{P}(U)$ for $N = 64$ *ie.* all frequency channels with H I emission were collapsed into a single channel. The real part is also shown using 64 line-free channels collapsed into a single channel. B) Best fit power law to $\mathcal{P}(U)$. The channel width is varied ($N = 1, 32, 64$; top to bottom), 1 σ error-bars are shown only for $N = 64$.

relevant only to the gas in the main H I disc around NGC 628.

3.2.2 Results and discussion

Figure 3.2.1A shows the real and imaginary parts of the observed value of the estimator $\mathcal{P}(U)$ for the 64 channels which have H I emission. As expected from the theoretical considerations mentioned earlier, the imaginary part is well suppressed compared to the real part. To test for a possible contribution from residual continuum, we also show the real part of $\mathcal{P}(U)$ using 64 line-free channels. This is found to be much smaller than the signal for the channels with H I emission. We find that a power law $A\ U^{\alpha}$ with slope $\alpha = -1.6 \pm 0.2$ provides a good fit to the the observed $\mathcal{P}(U)$ over the U range $U_{min} = 1.0\,\mathrm{K}\,\lambda$ to $U_{max} = 10.0\,\mathrm{K}\,\lambda$ (**Figure 3.2.1B**) which corresponds to spatial scales of $R_{min} = 800\mathrm{pc}$ to $R_{max} = 8\,\mathrm{kpc}$.

Both H I density fluctuations as well as spatial fluctuations in the velocity of the

N	Δv (km s^{-1})	U_{min} (k λ)	U_{max} (k λ)	R_{min} (k pc)	R_{max} (k pc)	α
1	1.3	1.0	10.0	0.8	8.0	-1.7 ± 0.2
32	42.3	1.0	10.0	0.8	8.0	-1.6 ± 0.2
64	82.5	1.0	10.0	0.8	8.0	-1.6 ± 0.2

Table 3.2: NGC 628 power spectrum are well fitted by a power law of $P_{HI} = AU^{\alpha}$. This table summarises the result for different channel widths. Note that the slope of the power spectrum does not changes with the width of the velocity channel.

H I gas contribute to fluctuations in the H I specific intensity. Considering a turbulent ISM, Lazarian and Pogosyan (2000) have shown that it is possible to disentangle these two contributions by studying the behavior of the H I power spectrum as the thickness of the frequency channel is varied. If the observed H I power spectrum is due to the gas velocities, the slope of the power spectrum is predicted to change as the frequency channel thickness is increased. We have tested this by determining the H I power spectrum for different values of the channel width in the range $1.29\,\mathrm{km\,s^{-1}}$ to $82.6\,\mathrm{km\,s^{-1}}$ (**Figure 3.2.1B**) and did not find any change in the slope of the H I power spectrum (**Table 3.2**). As the thickest channel that we have used is considerably wider than the typical H I velocity dispersion of $7 - 10\,\mathrm{kms^{-1}}$ seen in spiral galaxies (Shostak and van der Kruit, 1984), we conclude that the observed H I power spectrum of NGC 628 is purely due to density fluctuations. Our finding is similar to that of Begum et al. (2006a) who noticed no change of the slope with channel width for the dwarf galaxy DDO 210. Further, Elmegreen et al. (2001) also reported a similar behavior for LMC.

Earlier studies of the Milky-Way, and also of the dwarf galaxies LMC, SMC and DDO 210 (Crovisier and Dickey, 1983; Green, 1993; Stanimirovic et al., 1999; Deshpande et al., 2000; Elmegreen et al., 2001; Begum et al., 2006a) have all found a power law H I power

spectrum with slope ~ -3. On the contrary, we find a slope -1.6 ± 0.2 for NGC 628. This is a little more than one in excess of the earlier values. However, when comparing these values it should be noted that the earlier works have all measured the H I power spectrum at much smaller length-scales in the range 10 to 500 pc [MW (1 pc - 20 pc), SMC (4 pc - 30 pc), LMC (60 pc - 200 pc), DDO 210 (80 pc - 500 pc)] whereas the current measurement probes much larger length-scales from 800 pc to 8.0 kpc. The typical H I scale-heights within the Milky-Way (Lockman et al., 1984; Wouterloot et al., 1990) and external galaxies (e.g. Narayan and Jog 2002) are well within 1.5 kpc. This implies that on the largest length-scales which we have probed, the turbulence is definitely confined to the plane of the galaxy's disk and is therefore two dimensional (2D). Elmegreen et al. (2001) have found that the HI power spectrum of LMC flattens at large length-scales, which was interpreted as a transition from three dimensional to two dimensional turbulence. Based on these we conclude that the slope is different in our observation because it probes 2D turbulence, whereas the earlier observations were on length-scales smaller than the scale-height where we can expect three dimensional (3D) turbulence. To the best of our knowledge our results are the first observational determination of the HI power spectrum of an external spiral galaxy at such large length-scales which are comparable to the radius of the galaxy's disk.

Westpfahl et al. (1999) have performed a fractal analysis using the perimeter-area dimension of intensity contours in HI images of several galaxies in the M 81 group. Of particular interest is the galaxy M 81, a spiral galaxy for which the perimeter-area dimension was found to be $\sim$ 1.5 at a length-scale $\sim$ 10 kpc. This observation is consistent with a power law power spectrum of slope -1.6 ± 0.2 provided the assumption that the local dimension has the same value as the perimeter-area dimension is valid.

It is difficult to probe the H I scale-height of external face-on galaxies. Padoan et al. (2001) presented a method to probe the scale-height from a change in the slope of the

Spectral Correlation Function (SCF) [Rosolowsky et al. (1999)], and applied it to H I data for the LMC to estimate the scale-height to be $\sim$ 180 pc. Elmegreen et al. (2001) suggested that one could use a change in the slope of the power spectrum of the density fluctuations to measure the scale-height of face on gas disks. Applying this method to H I data for the LMC they measured scale-height of 100 pc. To the best of our knowledge, prior to this work, there hava been no observational constraint on the H I scale-height of NGC 628. Since the scale-height is definitely less than 8 kpc and the power spectrum is found to have the same slope from 800 pc to 8 kpc, we conclude that the scale-height must be less than 800 pc. Kregel et al. (2004) present H I images of a large sample of edge on intermediate to late type spirals; from their data the ratio of the H I disk height to the radius of the H I disk (at a column density of 1 $M_{\odot}$pc-2) is $\sim 0.06 \pm 0.015$. From **Fig. 3.1** the disk of NGC 628 has a diameter of $\sim$ 28 kpc at this column density. From the average thickness to radius ratio for edge on galaxies, one would expect NGC 628 to have a scale-height of $\sim$ 840 pc, which is consistent with our observation.

3.3 Estimating scale-height of a face on galaxy : NGC 1058

NGC 1058 is an almost face-on, type Sc, spiral galaxy with an inclination angle in the range 4° to 11° (Petric and Rupen, 2007). The distance to this galaxy is uncertain with previous estimates ranging from 10.0 Mpc (Boroson, 1981) to 14.5 Mpc ((Sandage and Tammann, 1974)). Throughout this paper we adopt a distance of 10 Mpc for NGC 1058. At this distance 1″ corresponds to 48.5 pc.

In this section we present a measurement of the power spectrum of H I intensity fluctuations of NGC 1058. The observed power spectrum shows a break with a steeper

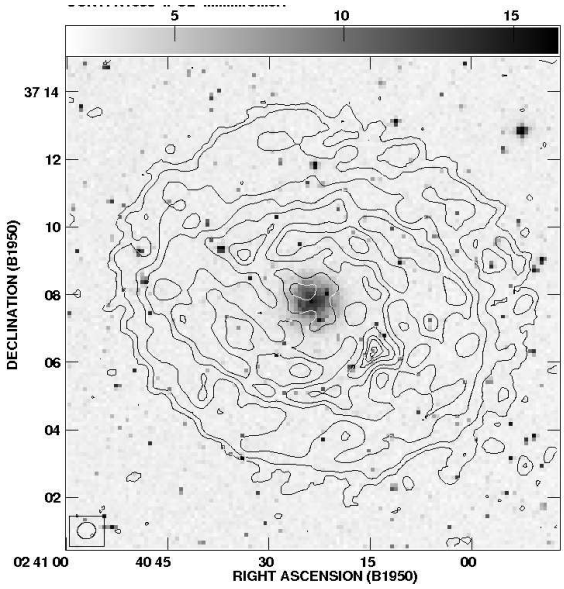

Figure 3.3: The $13.6'' \times 13.6''$ resolution integrated H I column density map of NGC 1058 (contours). The contour levels are 3., 10., 30., 50., 70., 100., 120., 130., and 140. $\times 10^{20}$ cm^{-2}.

slope at length-scales smaller than the break. We use this to estimate the scale-height of NGC 1058

3.3.1 A brief description of the data used

We have used archival H I data of NGC 1058 from the Very Large Array (VLA). The observations had been carried out on 14^{th} June 1993 in the C configurations of the VLA. The data was downloaded from the VLA archive and reduced in the usual way using standard tasks in classic AIPS[‡]. We adopted the data analysis procedure discussed in **Section 2.3** for reducing the raw data and for the power spectrum analysis. The H I emission from NGC 1058 spans 24 central channels (i.e, channel 53 to channel 76) of the 127 channel spectral cube. We have used only the central 16 channels (i.e, channel 57 to channel 72) with relatively higher H I emission. The frequency width of

[‡]NRAO Astrophysical Image Processing System, a commonly used software for radio data processing.

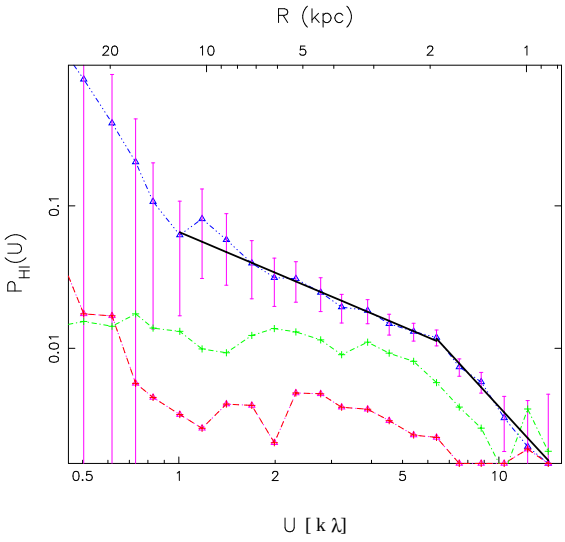

Figure 3.4: Real (blue) and imaginary (green) parts of the observed value of the H I power spectrum estimator $\mathcal{P}(U)$ for $N = 16$. 1 σ error-bars are shown only for the real part. The real part of the $\mathcal{P}(U)$ from line-free channels (red) is also shown.

each channel corresponds to $2.58\,\mathrm{kms}^{-1}$. **Figure 3.3** shows a total H I column density (Moment 0) map of NGC 1058 from an image made using the continuum subtracted data. The angular extent of the H I distribution in **Figure 3.3** is measured to be $11' \times 13'$ at a column density of $10^{19}\,\mathrm{atoms\,cm}^{-2}$, which is ~ 4 times it's Holmberg diameter (Persic and Rephaeli, 2007).

3.3.2 Results and discussion

Figure 3.3.1 shows the real and imaginary parts of the observed value of the estimator $\mathcal{P}(U)$ for the 64 channels which have H I emission. As expected, the imaginary part and the real part of $\mathcal{P}(U)$ estimated using line-free channels is well suppressed compared to the real part from the line channels indicating that for these channels the observed $\mathcal{P}(U)$ may be directly interpreted as the H I power spectrum at U values that are considerably larger than $(\pi\theta_0)^{-1} = 0.1\,\mathrm{k}\lambda$.

U_{min} (k λ)	U_{max} (k λ)	R_{min} (k pc)	R_{max} (k pc)	N	Δv (km s^{-1})	α
6.5	16.0	0.6	1.5	1	2.68	-2.5 ± 0.6
				8	21.44	-2.2 ± 0.6
				16	42.88	-2.2 ± 0.5
1.5	6.5	1.5	10.0	1	2.68	-1.0 ± 0.2
				8	21.44	-0.9 ± 0.2
				16	42.88	-0.8 ± 0.2

Table 3.3: NGC 1058 power spectrum are well fitted by two power laws of $P_{HI} = AU^{\alpha}$ in two different length scales. This table summerises the result for different channel width.

The power spectrum is well fitted by two different power laws $P(U) = AU^{\alpha}$, one with $\alpha = -1.0 \pm 0.2$ for $U = 1.0\,\mathrm{k}\lambda$ to $6.5\,\mathrm{k}\lambda$ (large length-scales) and another with $\alpha = -2.5 \pm 0.6$ for $U = 6.5\,\mathrm{k}\lambda$ to $16.0\,\mathrm{k}\lambda$ (small length-scales). The results are tabulated in **Table 3.3**. We also find that the H I power spectrum of NGC 1058 does not exhibit a statistically significant change with increase of the channel thickness (**Table 3.3**), indicating that the observed power spectrum is due to H I density fluctuations.

The slope $\alpha = -1.0 \pm 0.2$ gives a good fit to the power spectrum measured at length-scales $1.5 - 10.0$ kpc. The length-scale 10 kpc is definitely larger than the typical H I scale-heights within the Milky-Way (Lockman et al., 1984; Wouterloot et al., 1990) and in external spiral galaxies (e.g. Narayan and Jog 2002). Considering the H I disk of NGC 1058, it is reasonable to conclude that the slope $\alpha = -1.0 \pm 0.2$ is that of 2D turbulence in the plane of the galaxy's disk. On the other hand we have a slope of $\alpha = -2.5 \pm 0.6$ at the small length scales 600 pc to 1.5 kpc. We expect the scale-height of the galaxy's H I disk to be larger than 600 pc (Kregel et al., 2004). The slope $\alpha = -2.5 \pm 0.6$ may thus be interpreted as being that of 3D turbulence on length-scales smaller than the thickness of the disk. We interpret the wavelength of 1.5 kpc where

we observe the transition from 3D to 2D turbulence in terms of the scale-height of the galaxy's H I disk.

To our knowledge this is the first observational determination of the scale-height of a nearly face on spiral galaxy through its H I power spectrum. Further, the length scales at which this break in the power spectrum is seen is measured to an accuracy of the width of the bins in baseline (U) for calculating the power spectrum. Based on that we can also put 1 σ errors to our estimate, whereby we have the scale-height 1.5 ± 0.3 kpc. Since the disk of NGC 1058 has a diameter of 35 kpc (**Figure 3.3**) at the column density of 1 $M_\odot$ pc^{-2}), following Kregel et al. (2004) we expect it's scale-height to be 1.05 ± 0.26 kpc, consistent with our result. Note that, H I scale-height is known to increase with the distance from the centre and our value is an average over the entire disk.

It is interesting to note that a break in the power spectrum, like the one seen here for NGC 1058, has also been observed in the shell-type supernovae remnant Cassiopeia A (Roy et al., 2009). The slope of the power spectrum changes from -2.22 ± 0.03 at $1.6 - 10\,\mathrm{k}\lambda$ (large length-scales) to -3.23 ± 0.09 at $11 - 30\,\mathrm{k}\lambda$ (short length-scales). This change in the slope is interpreted as a transition from 2D to 3D magnetohydrodynamic turbulence. The transition occurs at a length-scale of 50 pc which corresponds to the thickness of the shell.

3.4 Power spectrum of the harassed galaxy NGC 4254

Galaxy harassment (frequent high speed galaxy encounters, Moore et al. 1996) is believed to be an important process in driving the morphological transformation of spiral galaxies to ellipticals inside clusters. Typically, the first encounters convert a normal spiral galaxy to a disturbed spiral with dramatic features drawn out from the dynamically

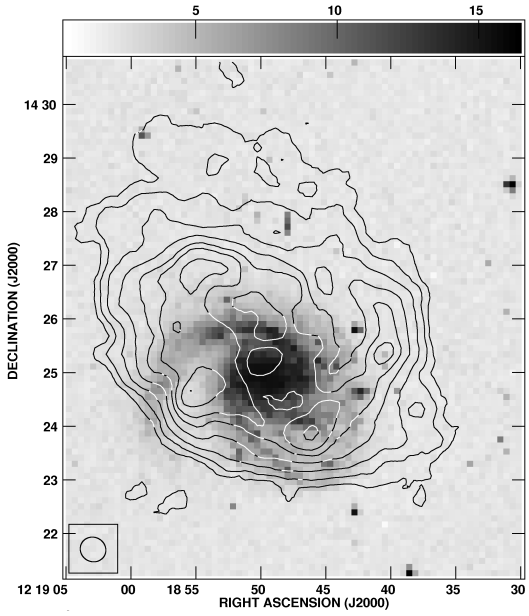

Figure 3.5: The $6.5'' \times 8.0''$ resolution integrated H I column density map of NGC 4254 (contours) is overlayed with the optical image of the galaxy (density). The contour levels are 3., 5., 10., 20., 25., 35., 40. and 45. $\times 10^{20}$ atoms cm^{-2}.

cold gas. The spiral galaxy NGC 4254, located in the nearby Virgo cluster, is found to have a tail (Minchin et al., 2005) with neutral hydrogen (H I) mass 2.2×10^8 $M_\odot$ within a distance of 120 kpc from the galaxy. This gaseous tail, without any stellar counterpart, is believed to be produced by an act of galaxy harassment (Haynes et al., 2007). Each act of harassment has the potential to induce a burst of star formation and to change the internal properties of the galaxy, including the properties of the ISM. In this section, we study the effect of the harassment on the large scale structure of the ISM. We use the power spectrum of H I intensity fluctuations to quantify these structures.

NGC 4254 is a lopsided spiral galaxy (morphological type SA(s)c), with an inclination of $\sim 42^\circ$ (Phookun et al., 1993). The galaxy is located at a distance of 1 Mpc from the core of Virgo cluster and is believed to be falling into the cluster with a relative velocity of 1300 km s^{-1} (Vollmer et al., 2005). The distance to this galaxy is estimated to be 16.7 Mpc (Mei et al., 2007); at this distance $1''$ corresponds to 81 pc.

3.4.1 A brief description of the data used

We have used archival H I data of NGC 4254 from the Very Large Array (VLA). The observations had been carried out on $4^{th} - 5^{th}$ of March, 1992 using the C configuration of the VLA (Phookun et al., 1993). The data was downloaded from the VLA archive and reduced in the usual way using standard tasks in classic AIPS[§]. As usual, we adopted the data analysis procedure discussed in **Section 2.3** for reducing the raw data and power spectrum analysis. The H I emission from NGC 4254 spans over 30 central channels i.e, (18 to 47) from 1401.7 MHz (2253 km s^{-1}) to 1416.4 MHz (2562 km s^{-1}) of the 63 channel spectral cube. A frequency width of 48.8 k Hz for each channel in the data cube corresponds to the velocity resolution of 10.32 km s^{-1}. **Figure 3.5** shows a integrated H I column density (Moment 0) map of NGC 4254 made from the continuum subtracted data. The angular extent of the H I distribution in **Figure 3.5** is measured to be $6.5' \times 8.0'$ at a column density of 10^{19} atoms cm^{-2}, which is comparable to it's optical diameter (de Vaucouleurs et al., 1991).

3.4.2 Results and discussion

Figure 3.4.1 shows the real and imaginary parts of the observed value of the estimator $\mathcal{P}(U)$ evaluated using 16 channels from 27 to 42 with relatively H I emission. The imaginary part is well suppressed compared to the real part. We also estimate $\mathcal{P}(U)$ using the line-free channels to test for any contribution from the residual continuum. This is found to be much smaller than the signal (**Figure 3.4.1**) indicating that the continuum has been adequately subtracted out.

The power law $A\,U^{\alpha}$, with $\alpha = -1.7 \pm 0.2$ is found to give a good fit to the H I power spectrum for the U range 2.0 kλ to 10.0 kλ (**Table 3.4**). Corresponding largest length-

[§]NRAO Astrophysical Image Processing System, a commonly used software for radio data processing.

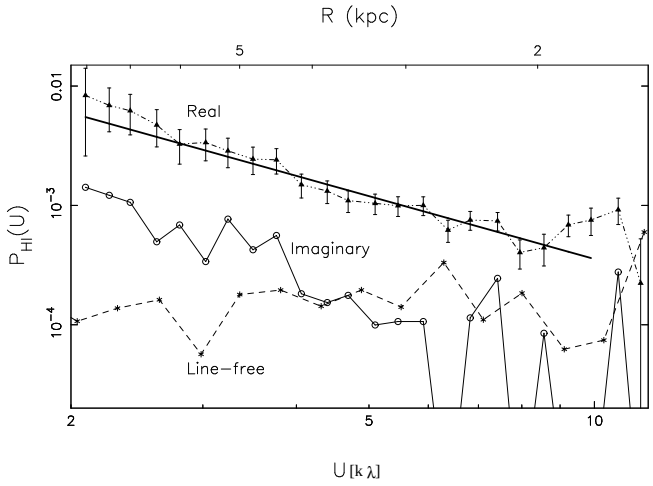

Figure 3.6: Real and imaginary parts of the observed value of the H I power spectrum estimator for channels 27-42 with $N = 16$. 1 σ error-bars are shown only for the real part. The real part of the estimator from line-free channels is also shown.

scale (8.4 kpc) is definitely larger than the typical H I scale-heights of the galaxies. It is thus quite reasonable to conclude that the slope $\alpha = -1.7 \pm 0.2$ is of 2D turbulence in the plane of the galaxy's disk. The fact that we do not observe the transition to 3D turbulence allows us to place an upper limit on the galaxy's scale-height as 2.6 kpc.

Galaxy harassment is expected to have different effects on the inner and outer parts of the galaxy. While gas is stripped from the outer parts, the inner part looses angular momentum and gradually collapses to the center through repeated galaxy encounters.

Data	Channels	U_{min} (k λ)	U_{max} (k λ)	α
16 central channels	$27 - 42$	2.5	10.0	-1.7 ± 0.2
A	$23 - 30$	2.0	10.0	-2.0 ± 0.3
B	$31 - 38$	2.5	10.0	-1.5 ± 0.2
C	$39 - 46$	2.0	10.0	-2.0 ± 0.3

Table 3.4: Results of the power spectrum analysis of NGC 4254 for different data cubes spanning over different velocity ranges.

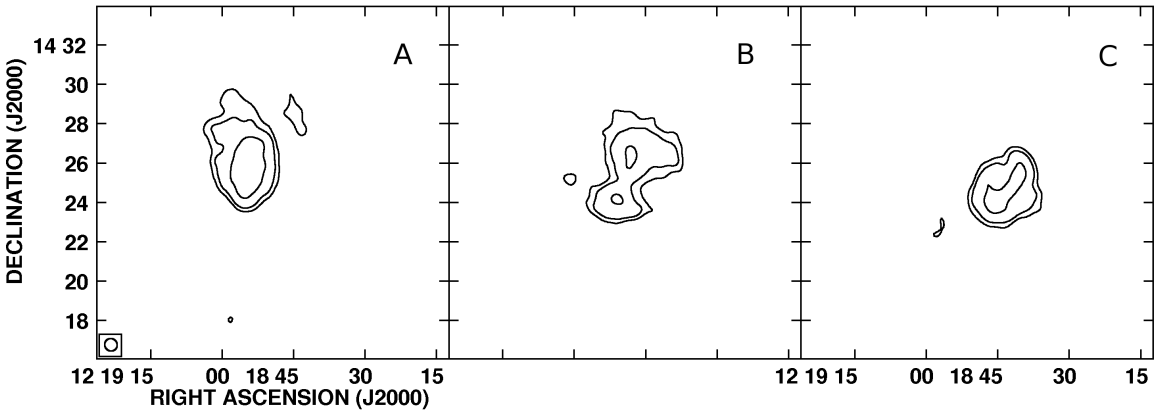

Figure 3.7: Integrated H I column density maps of the galaxy NGC 4254 using data cubes A, B and C. Note the diagonal movement of the centroid of emission from North east (A) to South west (C). The contour levels are 5., 8. and 12. $\times 10^{20}$ atoms cm^{-2}.

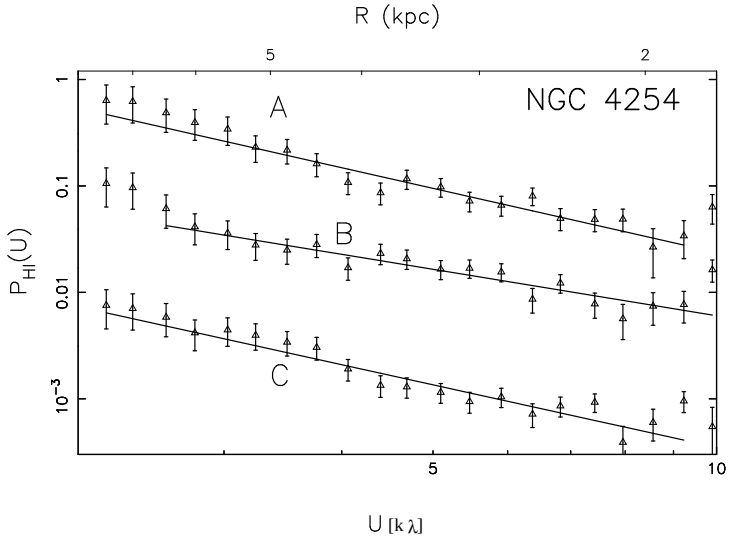

Figure 3.8: H I power spectrum for data cubes A, B and C plotted with arbitrary offsets to prevent them from overlapping.

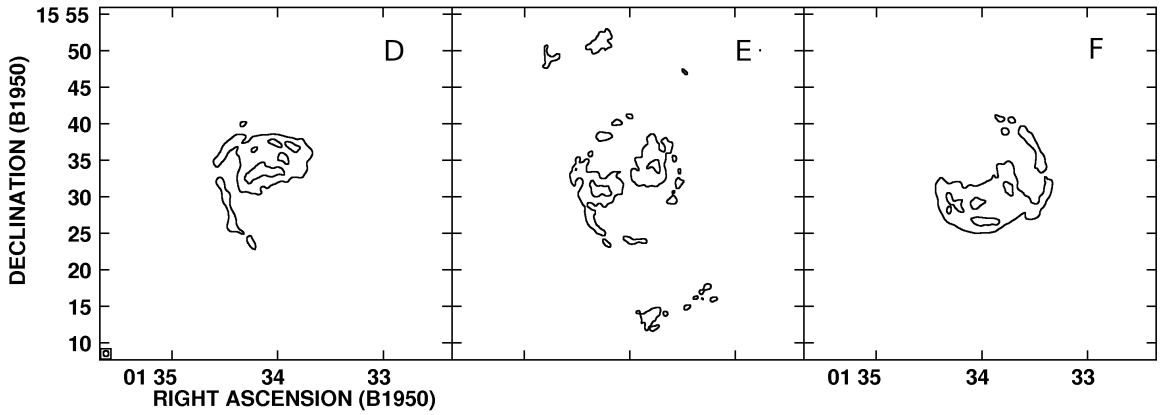

Figure 3.9: Integrated H I column density maps of the galaxy NGC 628 using data cubes D, E and F. Note the diagonal movement of the centroid of emission from North east (D) to South west (F). The contour levels are 6., 12. and 18. $\times 10^{20}$ atoms cm^{-2}.

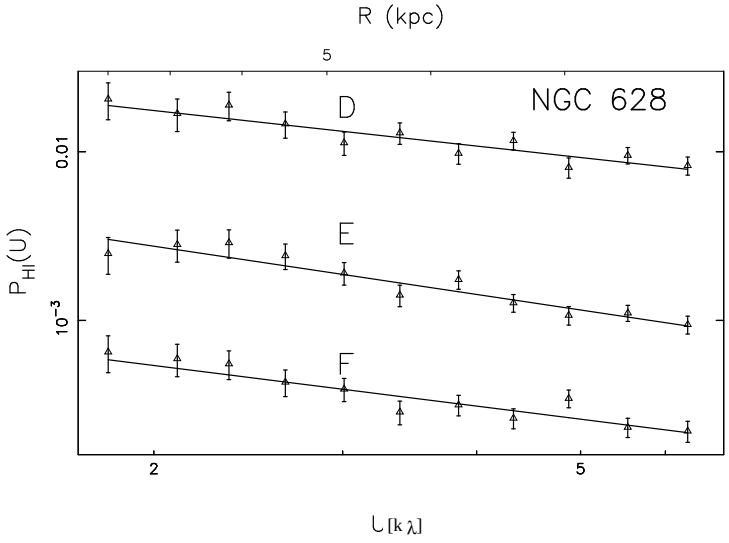

Figure 3.10: Power spectra of the H I emission for the galaxy NGC 628 is shown for D (channels 108-119), E (channels 120-131) and F (channels 132-143) with arbitrary offsets to prevent them from overlapping.

We can selectively study different parts of NGC 4254, whose rotation axis is tilted at 42° to the line of sight, by considering different velocity channels. Our analysis till now has used only the central 16 channels, we now use the central 24 channels $(23 - 46)$ for the subsequent analysis. We construct 3 different data cubes namely A, B and C containing channels $23 - 30$, $31 - 38$ and $39 - 46$ respectively. We can now separately probe the North east, Central and South west parts of the galaxy (**Figure 3.7**) using these three data cubes. For each data cube, we evaluate the H I power spectrum using individual channels and then average over the channels in the respective cubes. We estimate U_m separately for A, B and C and the best fit power law is obtained for $U \geq U_m$ only. We find that for each data cube the H I power spectrum is well fitted by a power law (**Figure 3.8**), the details being shown in **Table 3.4**. We find that the slope α is -2.0 ± 0.3 for A and C which probe the outer parts of the disk while it is -1.5 ± 0.2 in B which probes the central region. To verify if this change in slope is generic to all galaxies, we also consider the H I power spectrum of the spiral galaxies NGC 628 and NGC 1058 which are not undergoing galaxy harassment. **Figure 3.9** shows the regions of the spiral galaxy NGC 628 corresponding to each of the channel range 108-119 (D), 120-131 (E) and 132-143 (F). We find that the power spectra of these three data cubes (**Figure 3.10**) all have the same slope ~ -1.6, which is also similar to the slope of the central part of NGC 4254. The results are similar for NGC 1058 and hence we do not explicitly show these here. Based on this we conclude that the difference in slope between the inner and outer parts of NGC 4254 is not a generic feature of the spiral galaxies rather is a consequence of the galaxy harassment. This suggests that not only does galaxy harassment affect the global morphology of the galaxy, it also affects the fine scale structure in the ISM as reflected by H I power spectrum.

We note that NGC 4254 has an inclination of 42°, on the other hand NGC 628 and NGC 1058 are more face-on galaxies (inclination $\sim 10°$). In our analysis we selectively

study different parts of a galaxy by considering different velocity channel ranges. However, since face-on galaxies do not have much range in radial velocity from the rotation curve, the spatial extent of H I in NGC 628 and NGC 1058 will not be very different for the three velocity channel ranges, which is unlike the case for NGC 4254. Hence, it is likely that we failed to find a change of slope in NGC 628 and NGC 1058 because of this effect of inclination. However, as seen in **Figure 3.9** for NGC 628, all three data cubes D, E and F have a significant contribution of H I from the outer region of NGC 628, leading us to believe that the power spectrum has a slope of ~ 1.6 in the outer parts of NGC 628. This is similar to the value of slope seen in the central parts of NGC 4254 and significantly different from the slope in the outer parts of NGC 4254. Hence it indicates an impact of harassment in NGC 4254. Further analysis of spiral galaxies with large inclination angles would possibly be able to resolve this issue.

We currently do not have an understanding of how galaxy harassment caused a steepening of the H I power spectrum in the outer parts of the galaxy. Theoretical modeling and the analysis of other Virgo cluster spiral galaxies are needed for further progress in this direction.

3.5 Summary and conclusions

We have presented the result of power spectrum analysis of the external spiral galaxies NGC 628, NGC 1058 and NGC 4254 in this chapter. Here we summarize the main points of this analysis.

- For all the three galaxis we have studied here, the power spectrum is well fitted by a power law indicating the presence of turbulence in the ISM. The slope of the power law is found to be ~ -1.7 for NGC 628 and NGC 4254 and ~ -1.1 for NGC 1058 at large length scales. We have interpreted this as a result of the 2D

turbulence in the scale of the galaxy's disk.

- Our present observation also suggests that the spiral galaxies exhibit scale-invariant density fluctuations that extend to length-scales of ~ 10 kpc which is comparable to the diameter of the H I disk. While a large variety of possible energy sources like proto-stellar winds, supernovae, shocks, etc. have been proposed to drive turbulence seen at the smaller scales (Elmegreen and Scalo, 2004), it is still to be seen whether these are effective on length-scales as large as 10 kpc.

- We have successfully estimated the scale-height of the galaxy NGC 1058. This, to the best of our knowledge, is the first determination of the scale-height of any external face-on spiral galaxy. However, for the two other galaxies we could not detect any change in slope of the power spectrum and hence could only put limits to their scale-height.

- For all three galaxies in our sample we could not detect any change in the slope of the power spectrum with increasing thickness of the velocity channels. This definitely shows that for these galaxies velocity does not noticeably modify the power spectrum. The result presented in Lazarian and Pogosyan (2000) shows a possible modification of the power spectrum of the ISM intensity fluctuation of our Galaxy.

- We observe that the outer part of the galaxy NGC 4254 has a different power law slope compared to the inner part. This difference, we propose, is because of galaxy harassment. We do not find any such difference in slope for the other two galaxies presented in this chapter. However, since this is a single observation of a harassed galaxy, it is not possible to conclusively report this as a generic feature of galaxy harassment. A systematic study of the other harassed galaxies in the

nearby Coma or Virgo cluster may provide us more interesting information about the ISM turbulence in such environments.

Since it is now evident that the external spiral galaxies also have turbulent ISM, we may now proceed in estimating the power spectrum of a spiral galaxy sample. This will help us understand the nature of turbulence, its origin and the energy input to it. In **Chapter 6** we will consider such a sample and investigate how the turbulence is correlated with other dynamical and morphological properties of the spiral galaxies.

4 Simulating Galaxy Observations*

We have presented a visibility based power spectrum estimator in **Chapter 2** which we have used to perform power spectrum analysis of three external spiral galaxies and the results are presented in **Chapter 3**. The observed bi-modality in the value of the best fit power law slope α of these spiral galaxies with the same from Milkyway or nearby galaxies have been explained in terms of 3D and 2D turbulence at small and large scales respectively. The power spectrum of the galaxy NGC 1058 is found to be a broken power law showing a transition from 3D to 2D turbulence. The break was seen at a wavelength of 1.5 kpc which we interpreted as the scale-height of the galaxy. However, the actual length-scales associated with the scale-height could not be definitively estimated.

In this chapter we perform numerical simulations to asses the impact of the overall galaxy structure on our estimates of the power spectrum of H I intensity fluctuations. We are particularly interested in the effect of galaxy's radial and transverse profile, inclination angle and the large scale density field in the power spectrum estimator we have been using.

*The work presented in this chapter is originally published in the paper titled "A study of interstellar medium of dwarf galaxies using H I power spectrum analysis" by Dutta et al. (2009a).

4.1 Simulation

The starting point of our simulation is a three dimensional (3D) 512^3 mesh, labeled using coordinates $\boldsymbol{r}$, on which we generate a statistically homogeneous and isotropic Gaussian random field $\hat{h}(\boldsymbol{r})$ with power spectrum $P(k) = Ck^{\gamma}$. We have used $\gamma = -2.5$ throughout our simulations, the results can be easily generalized to other γ values. The 3D power spectrum is shown in **Figure 4.1**. For reference we also show the two dimensional (2D) power spectrum of $\hat{h}(\boldsymbol{r})$ evaluated on a 512^2 planar section of the cubic mesh. As expected, the 2D power spectrum also is a power law with $P(k) \propto k^{\gamma+1}$. In all cases we have generated five independent realizations of the Gaussian random field, and averaged the power spectrum over these to reduce the statistical uncertainties.

In our simulations we use the Gaussian random field $\hat{h}(\boldsymbol{r})$ as a model for the 3D H I density fluctuations that would arise from homogeneous and isotropic 3D turbulence. The $\hat{h}(\boldsymbol{r})$ values on a 2D section through the cube serves as a model for the H I density fluctuations in the limiting situation where we ignore the thickness of the galaxy and treat it as a 2D disk. Note that the resulting $\hat{h}(\boldsymbol{r})$ is a statistically homogeneous and isotropic Gaussian random field on the 2D section. We use this to represent the density fluctuations that would arise from homogeneous and isotropic 2D turbulence.

We next embed a galaxy in the middle of the 3D cube. The overall, large scale 3D structure of the galaxy is introduced through a function $G(\boldsymbol{r})$ so that the H I density at any position is $G(\boldsymbol{r})[h_0 + \hat{h}(\boldsymbol{r})]$. Here $G(\boldsymbol{r})h_0$ is the smoothly varying component of the galaxy's H I density and $G(\boldsymbol{r})\hat{h}(\boldsymbol{r})$ is its fluctuating component. It is assumed that the observer's line of sight is along the z axis. The H I density $G(\boldsymbol{r})[h_0 + \hat{h}(\boldsymbol{r})]$ is projected on the $x-y$ plane. We interpret the projected values as the H I specific intensity $I(\boldsymbol{\theta}, \nu)$ in the plane of the sky [**Eqn. (2.1)**]. The 512^2 mesh in the $x-y$ plane of our simulation corresponds to $4' \times 4'$ on the sky.

To understand the effect of different parameters such as the shape of the window function, the inclination angle etc. on the power spectrum estimation we consider two models for the galaxy's H I density.

4.1.1 Case I : Without a radial profile

We first consider a face-on galaxy, and use $G(\boldsymbol{r}) = \exp(-z^2/z_h^2)$. This incorporates only the finite thickness of the disk which is characterized by the scale-height z_h and ignores the galaxy's radial profile in the plane of the disk. Note that, for $z < z_h$ this function closely matches the function $\mathrm{sech}(-z^2/z_h^2)$ which is also used to model the scale-height profile (Binney and Merrifield, 1998). For the scale-height, we have used the values $z_h = 4$ and 32 mesh units which we refer to as the "thin' and "thick" disk respectively.

Results

Figure 4.1 shows the power spectrum of the simulated H I specific intensity $I(\boldsymbol{\theta}, \nu)$ for both the thin and thick disk. We find that the H I power spectrum of the thin disk has a slope -2.5, same as the 3D power spectrum, at large U. There is a break at $U \sim 35\,\mathrm{k}\lambda$ which corresponds to $1/\pi z_h$, and the slope is ~ -1.9 at smaller U. We interpret this change in the slope in terms of a transition from 3D fluctuations on scales smaller than the disk thickness (large U) to 2D fluctuations on scales larger than disk thickness (small U). We expect the slope to approach -1.5, the 2D slope, at very small U. Note that in our simulation it is not possible to evaluate the slope at very small U values where the sample variance is rather large. We find that the H I power spectrum of the thick disk is well fit by a single power law $P_{HI}(U) = AU^{-2.5}$ which has the 3D slope. In this case we expect the break corresponding to the transition from 3D to 2D at $U \sim 4\mathrm{k}\lambda$. This break lies in the sample variance dominated region which explains

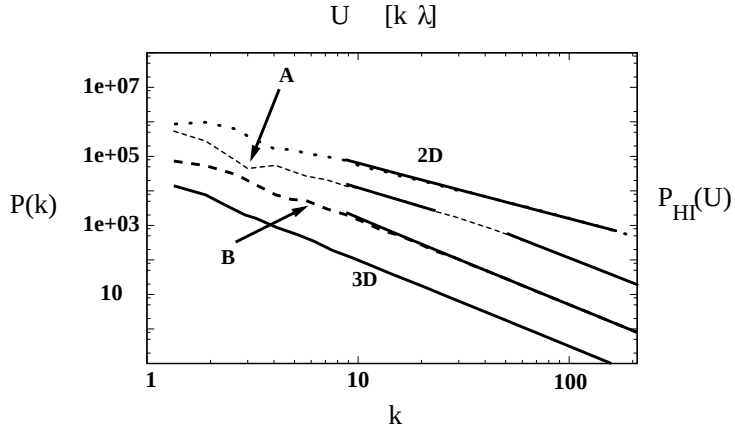

Figure 4.1: The 3D and 2D power spectrum $P(k)$. The simulated H I power spectrum $P_{HI|}(U)$ for the thin (A) and thick (B) disk without the radial profile are also shown. The $P(k)$ and k values (left and bottom axes) have been arbitrarily scaled to match the $P_{HI}(U)$ and U axes (top and right). The power-law fits are shown by solid lines. The different curves have been plotted with arbitrary offsets to make them distinguishable.

why we do not detect it.

4.1.2 Case II : With a radial profile

We next incorporate the galaxy's radial profile using

$$G(\boldsymbol{r}) = \exp\left[-\frac{\sqrt{12}\theta}{\theta_0}\right] \exp(-z^2/z_h^2), \tag{4.1}$$

where $\theta = \sqrt{x^2 + y^2}$ is the radial coordinate in the plane of the disk. Here θ coincides with the angle in the sky measured from the center of the galaxy. We have used $\theta_0 = 1'$ which corresponds to 128 mesh units . Note that the radial profile used in the simulation is exactly the same as the window function $W(\boldsymbol{\theta})$ of the exponential model introduced in **Chapter 2**. The relative amplitude of h_0 and $\hat{h}(\boldsymbol{r})$ is a free parameter which decides the respective contributions from the smooth and the fluctuating H I components. Using

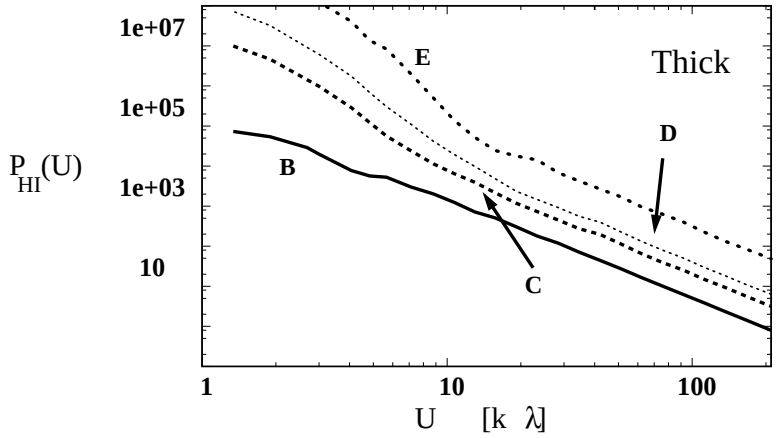

Figure 4.2: The simulated H I power spectrum for the face-on thick disk with (B) no radial profile and (C), (D) with radial profile using $\theta = 0.35, 0.7$ respectively. (E) is same as (C) with the disk tilted at 60°. The different curves have been plotted with arbitrary offsets to make them distinguishable.

the ratio $R = \sqrt{\langle \hat{h}^2 \rangle}/h_0$ of the root mean square value of $\hat{h}(\boldsymbol{r})$ to h_0 to quantify this, we have carried out simulations for $R = 0.35$ and 0.7. We have also carried out simulations where the disk is tilted, and the normal to the disk make an angle of 60° to the line of sight.

Results

The simulated H I power spectra are shown in **Figures 4.2** and **4.3** for the thick and thin disks respectively. We find that for a face-on disk with $\theta_0 = 1'$, for both the thick and thin disks, the results of our simulations are in good agreement with our analytic estimate presented in the **Section 2.2**, which predicts that the effect of the galaxy's radial profile is contained within a limited baseline range $U \leq U_m$, which comes out to be $U \leq U_m \sim 3.5\ \theta_0^{-1}$, for $\alpha = -2.5$ (**Figure 2.3**). The H I power spectrum is insensitive

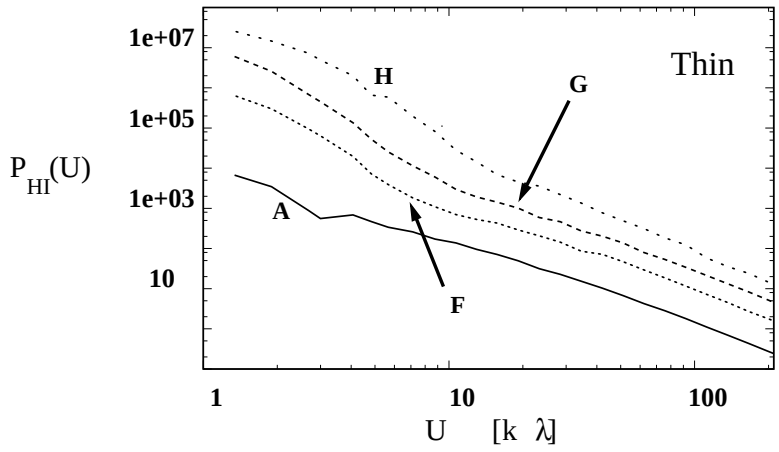

Figure 4.3: The simulated H I power spectrum for the face-on thin disk with (A) no radial profile and (F), (G) with radial profile using $\theta = 0.35, 0.7$ respectively. (H) is same as (F) with the disk tilted at 60°. The different curves have been plotted with arbitrary offsets to make them distinguishable.

to the galaxy's radial profile at $U > U_m$, and the shape of the power spectrum is the same whether we include the galaxy's radial profile or not. We find that the value of U_m is not very sensitive to changes in R, the ratio of the fluctuating component to the smooth component. For a disk of the same size, the value of U_m increases when the disk is tilted. The image of the disk tilted by 60° has an anisotropic window function $W(\boldsymbol{\theta})$ with angular radius $1'$ and $0.5'$ along the major and minor axes respectively. We find that for a tilted disk, the value of U_m is determined by the smaller of the two angular diameters, $0.5'$ in this case.

4.2 Scale-height estimation

In **Chapter 3** we have observed a break in the power spectrum of the galaxy NGC 1058 at a baseline of 6.5 k λ (or at a wavelength of 1.5 kpc) and interpreted it as arising due to a transition from 3D to 2D turbulence. The results of our simulation suggests that a break in the power spectrum at a baseline U corresponds to an angular scale of

$z_h = 1/\pi U$ and a length-scale of $D/\pi U$ at the plane of the sky (D is the distance to the galaxy). Following this for an adopted distance of 10 Mpc to the galaxy NGC 1058, its scale-height is 490 ± 90 pc. We have also observed that the galaxy NGC 628 exhibit 2D turbulence up to a baseline of 1.0 k λ with a single power law of slope ~ -1.6. This imposes an upper limit of 320 pc on its scale-height. Note that the scale-height of 320 pc for NGC 628 differs from what is presented in Dutta et al. (2008) because of the extra factor of π indicated by our simulations. We do not attempt to set a bound for the scale-height of the galaxy NGC 4254 here, since it has a considerably large inclination angle. Finally, we note that we have not considered the fact that the scale-height varies with the distance from the centre of the galaxy's disk. Hence our estimate gives an average value of the disk scale-height.

4.3 Summary and conclusions

We discuss the main findings of this chapter here.

- We find that if the H I distribution is a thin disk, the power spectrum is well fitted using a broken power law with the change in scope at a length-scale corresponding to the line of sight thickness of the disk. We interpret this as a geometrical effect arising because of a transition from 3D to 2D fluctuation. Since the spiral galaxies have disk like geometry, a break in the power spectrum at a U value greater than U_m is indicative of a transition from 3D to 2D at the length-scale corresponding to the scale-height $z_h = D/\pi U$.

- Our simulations demonstrate that for baselines $U > U_m$ the galaxy's radial profile has no effect on the power spectrum of H I fluctuations. In other words, the power spectrum would be unchanged if the same fluctuations were present in an uniform

disk with no radial profile.

- We find that the inclination angle of the Galaxy further restricts the usable range of baselines for the power spectrum estimation. Our simulation shows that the semi-minor axis of the projected image of the galaxy has to be used to determine the U_m value over which the power spectrum can be estimated.

Finally, we note that we have ignored velocity fluctuations and the galaxy's rotation throughout our simulations. This would rearrange the H I emission amongst the different frequency channels. Our simulation corresponds to the situation where there is just a single frequency channel whose width encompasses the entire HI emission, and the velocities have no effect in this situation.

5 Power Spectrum as a Probe of Dwarf Galaxy Properties*

5.1 Introduction

This chapter presents the results of our analysis of a sample of 7 nearby gas rich faint ($M_B > -13.0$ mag) dwarfs. The corresponding H I radio-interferometric data used here is from GMRT. The observation parameters and other details are given in the **Table 5.1**. Note that the galaxy GR 8 is known to have peculiar kinematics (Begum and Chengalur, 2003) whereas the spiral dwarf galaxy NGC 3741 has an extended H I disk (Begum et al., 2005). These were included in our sample to see the effect of the peculiar dynamics and morphology of the ISM in the power spectrum.

5.2 Notes on the individual galaxies

We briefly discuss some of the relevant properties of the galaxies in our sample. A few of the galaxy parameters are also summarized in **Table 5.2** which contains - Column

*The work presented in this chapter is originally published in the paper titled "A study of interstellar medium of dwarf galaxies using H I power spectrum analysis" by Dutta et al. (2009a).

Galaxy	α(J2000) (h m s)	δ(J2000) ($^\circ\,'\,''$)	Date of observation	Time on source	References
DD0 210	20 46 53.00	−12 50 57	13-15 July 02	16 hrs	2,5
NGC 3741	11 36 06.40	+45 17 07	22 Jul & 26 Aug 04	8 hrs	3,5
UGC 4459	08 34 06.50	+66 10 45	15,23,24 Nov 02	14 hrs	4,5
GR 8	12 58 40.40	+14 13 03	16-18 Nov 02	16 hrs	1,5
AND IV	00 42 32.30	+40 34 19	1 Jan, 07		6
KK 230	14 07 10.70	+35 03 37	May 8, 6 Jun, 26 Nov 01	18 hrs	4,5
KDG 52	08 32 56.00	+71 01 46	21-23, 27 Jun 02	18 hrs	4,5

Table 5.1: Some observation parameters of the galaxies in our sample. References are as follows: 1- Begum and Chengalur (2003), 2- Begum and Chengalur (2004), 3- Begum et al. (2005), 4- Begum et al. (2006b), 5- Begum et al. (2008a), 6- Chengalur et al. 2009 (in preparation)

(1): Name of the galaxy; (2) and (3): major and minor axis in arc min calculated at a column density of 10^{19} atoms cm^{-2}; (4): distance in Mpc; (5): H I inclination angle; (6): Log[SFR] in $M_\odot yr^{-1}$ measured from Hα emission; (7): H I velocity dispersion in km s^{-1}; (8): total dynamical mass in $10^8\,M_\odot$; (9): references.

DDO 210

DDO 210 is the faintest ($M_B \sim -10.9$) relatively close (at a distance 950 ± 50 kpc; Lee et al. 1999) gas-rich member of the Local Group. The H I disc of the galaxy is nearly face-on. On large scales, the H I distribution is not axisymmetric; the integrated H I column density contours are elongated towards the east and south. No Hα emission was detected indicating a lack of on-going star formation in this galaxy.

NGC 3741

NGC 3741 is a nearby dwarf irregular galaxy ($M_B \sim -13.13$) with a gas disk that extends to ~ 8.8 times the Holmberg radius (Begum et al. 2005, 2008b). The galaxy is

Galaxy	Major ($'$)	Minor ($'$)	D (M pc)	i_{HI} ($^\circ$)	log(SFR) ($M_\odot$ yr^{-1})	σ_v (km s^{-1})	M_{dy} (10^8 $M_\odot$)	Ref.
DD0 210	5.0	4.5	1.0	26.0	> -5.4	6.5(1.0)	0.34	2,5
NGC 3741	27.0	12.0	3.0	68.0	-2.47	~ 8.0	40.3	3,5
UGC 4459	4.5	3.6	2.1	30.0	-2.04	9.0(1.6)	1.40	4,5
GR 8	4.2	4.0	2.1	27.0	-2.46	9.0(0.8)	0.78	1,5
AND IV	15.0	8.5	6.7	55.0	-3.0	~ 8.0	32.5	5,6
KK 230	3.0	2.0	1.9	50.0	> -5.53	7.5(0.5)	-	4,5
KDG 52	3.5	3.0	3.55	23.0	> -5.1	9.0(1.0)	-	4,5

Table 5.2: Some relevant morphological and dynamical parameters of the galaxies in our sample. The references are as follows: 1- Begum and Chengalur (2003), 2- Begum and Chengalur (2004), 3- Begum et al. (2005), 4- Begum et al. (2006b), 5- Begum et al. (2008a), 6- Chengalur et al. 2009 (in preparation)

fairly edge-on with kinematics inclination varying from $\sim 58^\circ - 70^\circ$. NGC 3741 appears to have a H I bar and is dark matter dominated with a dark to luminous mass ratio of $\sim$ 149. Further, this galaxy is undergoing significant star formation in the center. An interplay between the neutral ISM and star formation in this galaxy is studied in detail by Begum et al. (2008b). The rotation curve flattens beyond $300''$ to a value ~ 50 km s^{-1} (Gentile et al., 2007). They find that the ISM in this galaxy shows radial motion of $\sim 5 - 13$ km s^{-1}. Karachentsev et al. (2004) have estimated the distance to this galaxy as 3.0 ± 0.3 Mpc using the tip of the red giant branch (TRGB) method.

UGC 4459

The faint dwarf ($M_B \sim -13.37$) galaxy UGC 4459 is a member of the M 81 group of galaxies. It is fairly isolated from its nearest neighbor UGC 4483 at a projected distance of 3.6° ($\sim$ 223 kpc) and a velocity difference 135 km s^{-1}. UGC 4459 is a relatively metal poor galaxy, with 12 + log(O/H) $\sim$ 7.62 (Kunth and Östlin, 2000). The optical appearance of this galaxy is dominated by bright blue clumps, which emits copious

amount of Hα, indicating high star formation. The velocity field of UGC 4459 shows a large scale gradient across the galaxy with an average of $\sim$ 4.5 km s^{-1} kpc^{-1}, though this gradient is not consistent with that expected from a systematic rotating disk. This galaxy has a TRGB distance of 3.56 Mpc (Karachentsev et al., 2004).

GR 8

This is a faint ($M_B \sim -12.1$) dwarf irregular galaxy with very unusual H I kinematics (Begum and Chengalur, 2003). The H I distribution in the galaxy is very clumpy, and shows substantial diffuse, extended gas. The high density H I clumps in the galaxy are associated with optical knots. In optical, it has a patchy appearance with the emission dominated by bright blue knots which are sites of active star formation (Hodge, 1967). Both radial and circular motions are present in this galaxy. It also possesses a faint extended emission in Hα. The distance to this galaxy is estimated to be 2.10 Mpc (Karachentsev et al., 2004).

AND IV

This is a dwarf irregular galaxy with a moderate surface brightness ($\bar{\mu}_V \sim 24$) and a very blue color ($V - I \leq 0.6$) (Ferguson et al., 2000). It is at a projected distance of $40'$ from the center of M 31 (Merrett et al., 2006) and has a very low ongoing star formation rate (SFR) of $\sim 0.001 M_{\odot}\mathrm{yr}^{-1}$. Its H I disk extends to ~ 6 times the Holmberg diameter and also shows large scale, purely gaseous spiral arms [Chengalur et al. 2008 (in preparation)]. The distance to this galaxy is estimated to be 6.7 ± 1.5 Mpc (Ferguson et al., 2000).

KK 230

KK 230, the faintest($M_B \sim -9.55$) dwarf irregular galaxy in our sample, lies at the periphery of the Canes Venatici I cloud of galaxies (Karachentsev et al., 2004). The velocity field shows a gradient in the direction roughly perpendicular to the H I and optical major axis with a magnitude of ~ 6 km s^{-1} kpc^{-1} (Begum et al., 2006b). There is no measurable ongoing star formation in this galaxy as inferred from the absence of any detectable Hα emission. Karachentsev et al. (2004) has found a tidal index of -1.0 indicating the galaxy to be fairly isolated. They have estimated the TRGB distance to be 1.9 Mpc.

KDG 52

KDG 52 (also called M 81DwA), another member of the M81 group, is a faint dwarf galaxy ($M_B \sim -11.49$) with a clumpy H I distribution in a broken ring surrounding the optical emission (Begum et al., 2006b). The H I hole is not exactly centered around the optical emission. This galaxy does not have any detectable ongoing star formation. The distance to this galaxy is estimated to be 3.55 Mpc (Karachentsev et al., 2004) derived from the TRGB method.

5.3 Results and discussions

We adopt the data analysis procedure discussed in **Section 2.3**. All the data are reduced in the usual way using standard tasks in classic AIPS [†]. For each galaxy, after calibration, the frequency channels with H I emission are identified and a continuum image is made by combining the line-free channels. The continuum is hence subtracted from the data

[†]NRAO Astrophysical Image Processing System, a commonly used software for radio data processing.

in the *uv* plane using the AIPS task UVSUB. The number of channels with H I emission (n) is different for each galaxy. To determine if the H I power spectrum changes with the width of the frequency channel, N successive channels are combined to obtain n/N channels. Power spectrum analysis is performed for different values of N in the range $1 \leq N \leq n$. The analysis is initially carried out for $N = 1$ and unless mentioned otherwise the results refer to this value.

Figure 5.1 and **5.2** show the results of our analysis. The results are also summarized in **Table 6.2**. We have detected the H I power spectrum of the galaxies DDO 210, NGC 3741, UGC 4459, GR 8 and AND IV. For these galaxies we find a range of baselines U, where the real part of $\mathcal{P}(U)$ estimated from the channels with H I emission is larger than the imaginary part estimated from the same channels as well as the real part estimated from the line-free channels. This is not true for KK 230 and KDG 52 (and also for AND IV with $N = n$), for these galaxies all three curves (**Figure 5.2**) lie within the 1 σ errors bars with very small offset and the interpretation is not straightforward. For the subsequent analysis we use only the real part of $\mathcal{P}(U)$ estimated from the channels with H I emission and interpret it as power spectrum.

We find that a power law $\mathcal{P}(U) = A\,U^{\alpha}$ provides a good fit at a baseline range U_{min} to U_{max} with a reasonable χ^2/ν for DDO 210, NGC 3741, UGC 4459, GR 8 and AND IV. The presence of a scale-invariant, power law power spectrum indicates that turbulence is operational in the ISM of these galaxies. The range of length-scales for the power law fit differs from galaxy to galaxy and in total it covers 100 pc to 6.2 kpc. The details are summarized in **Table 6.2**.

Both H I density fluctuations as well as spatial fluctuations in the velocity of the H I gas contribute to fluctuations in the H I specific intensity. To test if the power spectrum has any contribution from the gas velocity fluctuations, we have repeated the

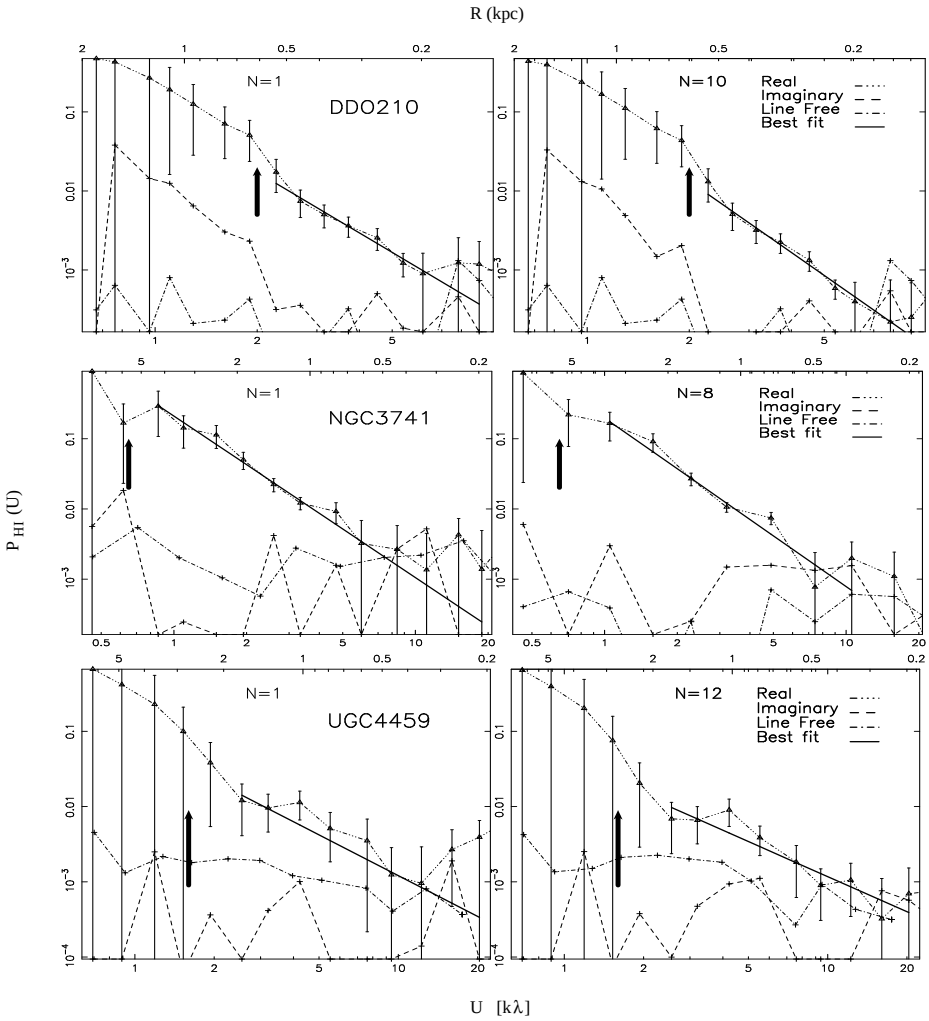

Figure 5.1: Power spectrum of the galaxies DDO 210, NGC 3741 and UGC 4459. The real and imaginary parts of $\mathcal{P}(U)$ estimated after averaging N channels with H I emission, and the real part from N line-free channels are shown together for $N = 1$ (left panel) and $N = n$ (right panel). The error-bars are for the real part from channels with H I emission. The best fit power law is shown in bold. In each case U_m is marked with a bold-faced arrow and the fit is restricted to $U > U_m$ where the effect of the convolution with the window function can be ignored.

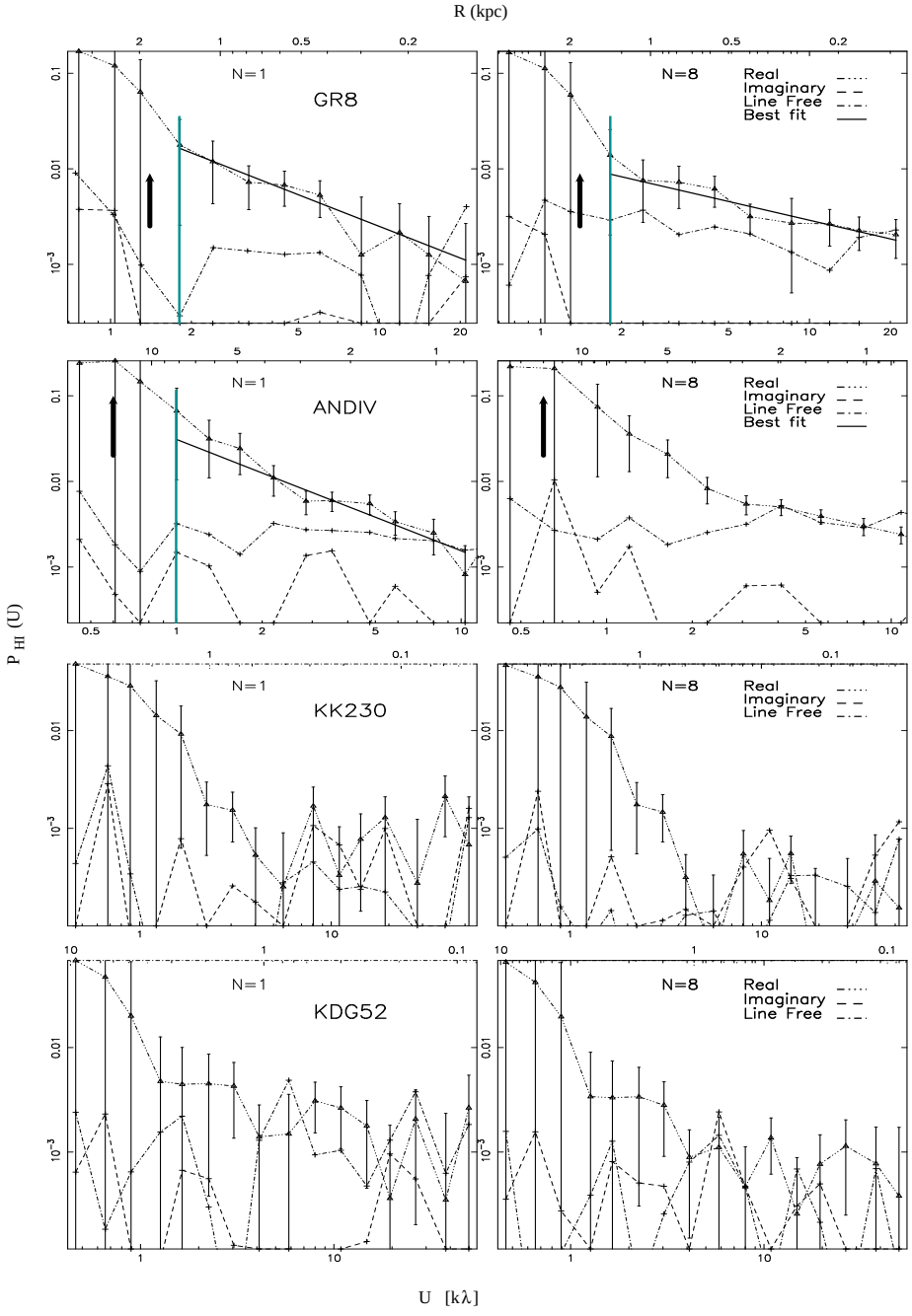

Figure 5.2: Power spectrum of the galaxies GR 8, AND IV, KK 230 and M81DWA. The real and imaginary parts of $\mathcal{P}(U)$ estimated after averaging N channels with H I emission, and the real part from N line-free channels are shown together for $N = 1$ (left panel) and $N = n$ (right panel). The error-bars are for the real part from channels with H I emission. The best fit power law is shown in bold only where such a fit is possible. For those, U_m is marked with a bold-faced arrow and the fit is restricted to $U > U_m$ where the effect of the convolution with the window function can be ignored.

Galaxy	N	Δv (km s^{-1})	U_{min} (k λ)	U_{max} (k λ)	R_{min} (k pc)	R_{max} (k pc)	α	ζ_2
DD0 210	1	1.65	3.7	13.0	0.06	0.27	-2.3 ± 0.6	0.0 ± 1.2
NGC 3741	1	1.65	1.6	16.0	0.19	1.90	-2.2 ± 0.4	0.0 ± 0.8
UGC 4459	1	1.65	3.1	22.0	0.18	1.16	-1.8 ± 0.6	0.0 ± 1.2
GR 8	1	1.65	1.6	23.0	0.10	1.30	-1.1 ± 0.4	0.0 ± 0.8
AND IV	1	1.65	0.6	6.7	0.56	6.20	-1.3 ± 0.3	0.0 ± 0.6
DD0 210	10	16.5	3.7	13.0	0.06	0.27	-2.1 ± 0.6	0.0 ± 1.2
NGC 3741	8	13.2	1.6	16.0	0.19	1.90	-2.5 ± 0.4	0.0 ± 0.8
UGC 4459	12	19.8	3.1	22.0	0.18	1.16	-1.7 ± 0.4	0.0 ± 1.2
GR 8	8	13.2	1.6	23.0	0.10	1.30	-0.7 ± 0.3	0.0 ± 0.8
AND IV	16	26.4	–	–	–	–	–	0.0 ± 0.6

Table 5.3: The results for the 5 galaxies in our sample. Columns 1-9 give (1) Name of the galaxy, (2) N: the number of channels averaged over, (3) ΔV: the corresponding velocity width, (4) and (5) U_{min} and U_{max}: the baseline range for which the power spectrum is determined, (6) and (7) R_{min} and R_{max}: corresponding range of length scales in the galaxies disk, (8) α: the best fit slope for the HI power spectrum, (7) ζ_2: possible limits for the spectral slope of the velocity structure function.

power spectrum analysis increasing the channel thickness N from $N = 1$ to $N = n$. In addition to $N = 1$, **Figures 5.1** and **5.2**, and **Table 6.2** also show the results for $N = n$ where the channel thickness spans the entire frequency range that has significant H I emission. We do not find a significant change in the slope of the power spectrum for any of the galaxies. Since for all the galaxies the thickest channel is considerably larger than the velocity dispersion, we conclude that the H I power spectrum is purely due to density fluctuations and not gas velocities. The fact that the slope does not change with channel thickness can be used to constrain the value of the slope of the velocity structure function ζ_2 (see Lazarian and Pogosyan 2000). The ζ_2 values are tabulated in **Table 6.2**.

The galaxies in our sample have slope α ranging from -2.6 to -1.1. The two galaxies DDO 210 and NGC 3741 have slope ~ -2.5, while the slope is ~ -1.5 for UGC 4459 and AND IV, and -1.1 for GR 8. We have proposed a possible explanation for this dichotomy in the values of α in **Section 2.3**. This was based on the fact that DDO 210, where the power spectrum was measured across length-scales $100-500$ pc, had a slope of -2.6 while NGC 628, a nearly face-on galaxy where the power spectrum was measured across length-scales $0.8 - 8$ kpc had a slope of -1.6. We have interpreted the former as three dimensional (3D) turbulence operational at small scales whereas the latter was interpreted as two dimensional (2D) turbulence in the plane of the galactic disk. In **Chapter 4** we have performed numerical simulations which tend to support this interpretation. Continuing with this implies that we have also measured 3D turbulence in NGC 3741, and 2D turbulence in UGC 4459, GR 8 and AND IV. Our dwarf galaxy sample contains 3 nearly face-on galaxies with $i_{\rm HI} < 30^\circ$, namely DDO 210, UGC 4459 and GR 8. DDO 210 has 3D turbulence across the baselines $2.0 - 10.0$ kλ. The absence of a break in the power spectrum places a lower limit of 160 pc on the scale-height. The galaxies UGC 4459 and GR 8 exhibit 2D turbulence for the entire U range (**Table 6.2**)

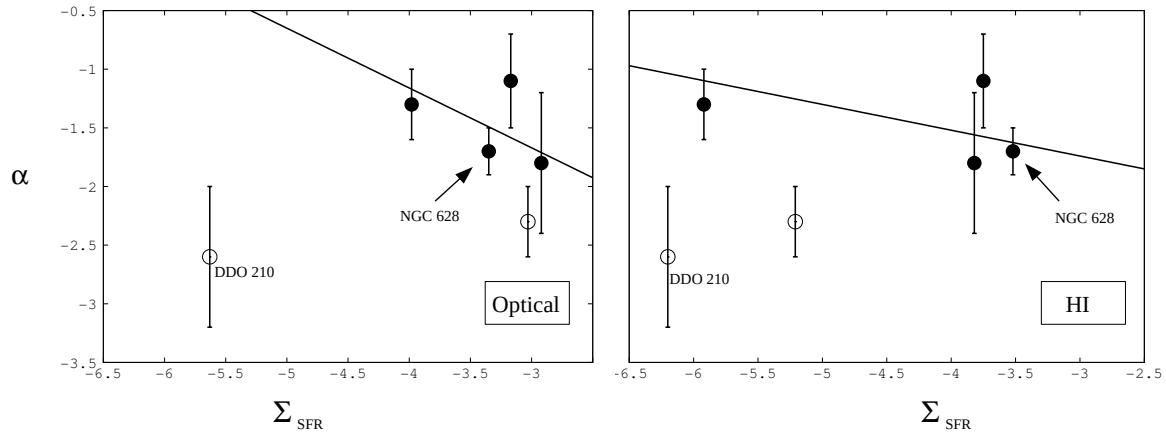

Figure 5.3: The slope α of the H I power spectrum plotted against $\Sigma_{\rm SFR}$, the SFR per unit area. The area has been determined from optical images and H I images in the left and right panels respectively. The galaxies with 3D and 2D turbulence are shown using empty and filled circles respectively. Note that the SFR for DDO 210, marked in the figure, is only an upper limit. We also include the data for NGC 628, a spiral galaxy. It is marked with an arrow. The straight lines show the linear correlation that we find (discussed in the text) between the slope of the H I power spectrum and the SFR per unit area.

in the measured H I power spectrum. This imposes the upper limit of 51 pc and 30 pc respectively on the scale-height.

The energy input from star formation is believed to be a major driving force for the turbulence in the ISM (Elmegreen and Scalo, 2004). Also first stage of the star formation process is known to be driven by the ISM turbulence. Hence, it is very interesting to check whether the slope of the power spectrum of intensity fluctuations in these galaxies has any correlation with the SFR. Any correlation, if present, will provide an insight into the relation between the star formation and ISM turbulence. In a recent study Willett et al. (2005) calculates the SFR per unit area for 9 irregular galaxies and investigates the correlation with the V-band and Hα power spectra. The length-scales they probe are $10 - 400$ pc. In Hα they find that the power spectra becomes steeper as the SFR per unit area increases. However they do not find any correlation in the

V-band. In this paper we probe length-scales 100 pc to 3.5 kpc. We test for a possible correlation between the slope of the power spectrum and the SFR per unit area and per unit H I mass for the 5 dwarf galaxies in our sample (**Figure 5.3**). We also include the spiral galaxy NGC 628. We report results using the area estimated from both, the H I disk and the optical disk. The data for the SFR, angular extent, inclination in H I and H I mass for these galaxies are from Begum et al. (2005) and Begum et al. (2008a). The SFR is determined from Hα emission, and the angular extent in H I is determined from the column density maps at the value of 10^{19} atoms cm^{-2}. For the angular extent and inclination of the optical disk we use the parameters from Begum et al. (2006b) and Sharina et al. (2008). The linear correlation coefficient is found to have values 0.35 and 0.34 for the H I and optical disks respectively, indicating the absence of any correlation between the slope of the power spectrum and the SFR per unit area. We have similar result for SFR per unit H I mass for these 5 galaxies.

Turbulence can also possibly be related to different parameters of the galaxy. We test for correlations between the slope of the H I power spectrum and the following parameters: total H I mass, H I mass to light ratio, total dynamical mass, total baryonic mass, gas fraction, baryon fraction. We use the estimates of these observable quantities from Begum et al. (2008a). In all the cases the linear correlation coefficient is found to lie between -0.5 and 0.5, indicating the absence of correlation.

In the above analysis we have considered galaxies with both 3D and 2D turbulence taken together, which in turn can suppress the correlations. Hence, we further investigated the correlations by considering the 3 galaxies in our sample with 2D turbulence. In this case the correlation coefficient comes out to be -0.70 and -0.74 for SFR per unit area of optical and H I disks respectively. This indicates a strong correlation and the result is similar to that of Willett et al. (2005), namely that the surface density of star formation rate is larger for galaxies with steeper H I power spectrum. These findings

indicate a possible link between star formation and the nature of turbulence in the ISM. However, it would not be realistic to speculate on a possible cause and effect relation between these two. It is quite possible that the observed correlation is an outcome of extraneous factors which influence both.

5.4 Summary and conclusions

In this chapter we have performed and presented the power spectrum analysis of 7 faint dwarf galaxies. For 5 of these galaxies we can conclusively estimate the power spectrum. Below we summarize the main points of this chapter.

- ISM of the dwarf galaxies have a scale-invariant power spectrum consistent with turbulence. Power law power spectrum of slope -1.1 to -2.6 provides good model to these power spectrum.

- We have observed dichotomy in the slope of the power spectrum which we have explained by 3D and 2D turbulence. Based on this we could also provide limits to the scale-height of these galaxies.

- We have investigated possible correlation between the power spectrum slope and the dynamical parameters of the galaxies. Our null result suggests that these parameters does not influence turbulence in the dwarf galaxies.

- We have found a correlation between the SFR per unit area (of the optical disk and the H I disk) with the power spectrum slope for the galaxies with 2D turbulence in our sample. This is a possible indication of the relation between the star formation and turbulence in the ISM. However, the Hα emission is not a good tracer of SFR in low mass galaxies due to stochastic star formation (Karachentsev and Kaisin,

2007; Lee et al., 2007). Also, the length-scales across which the power spectrum has been estimated for the dwarf galaxies in our sample are substantially larger than the optical disk where star formation occurs. These points must be taken into consideration while interpreting our results.

Finally, we note that the total number of galaxies in our analysis is rather small for a statistical conclusion. A larger galaxy sample is required for a better understanding of the generic features, if any, of turbulence in the ISM of faint dwarf galaxies. We considered the possibility of performing the power spectrum analysis of a larger sample derived from the FIGGS [‡]. We tried to estimate the power spectrum of the galaxies DDO 43, DDO 125, DDO 189, UGC 7605 and UGC 8508. We found that the FIGGS data are noise limited for these galaxies which suggests the necessity of deeper observations.

[‡]Faint Irregular Galaxies GMRT Survey (Begum et al., 2008a)

6 Power Spectrum Analysis of the THINGS Galaxies

6.1 Introduction

In **Chapter 3** we have performed power spectrum analysis of three spiral galaxies and have found that the power spectrum shows the existence of scale-invariant structures in the ISM at a wide range of length-scales starting from $\sim$ 10 kpc to lower. It will be interesting to probe ISM of a sample of spiral galaxies to investigate the nature of turbulence therein and possible relation of turbulence with the other dynamical properties of the galaxy. This requires systematic observations of a hand full of nearby spiral galaxies with good spatial resolution.

THINGS, The H I Nearby Galaxy Survey, is a survey using H I 21-cm emission of 34 nearby galaxies obtained using the VLA (Walter et al., 2008). The main aim of this survey is to investigate the nature of the ISM, galaxy morphology, star formation and mass distribution etc. across the Hubble sequence. THINGS provides homogeneous, high quality 21-cm data cubes, with high spatial ($\sim$ 6) and velocity ($\leq$ 5.2 km s^{-1}) resolution, for a representative sample of local spiral and dwarf galaxies. de Blok et al. (2008) have

presented high resolution rotation curve for the galaxies in the THINGS sample. Star formation rate and efficiency of the THIGNS galaxies are also very extensively studied (Bigiel et al., 2008; Leroy et al., 2008). This is an ideal data set for a comparative study of turbulence in the neutral ISM of spiral galaxies. In this chapter we present the result of power spectrum analysis of a sample of 18 spiral galaxies drawn from the THINGS survey.

6.2 Data and analysis

Here we restrict our analysis to the spiral galaxies in the THINGS sample with minor axis greater than $6'$. **Table 6.1** gives different parameters of the galaxy sample analyzed here. The values for the parameters like the distance to the galaxy, SFR and the total H I mass is taken from Walter et al. (2008), whereas values for the inclination angle are taken from de Blok et al. (2008). de Blok et al. (2008) also present rotation curves for the 13 galaxies in our sample. We use these rotation curves to estimate the dynamical mass for those galaxies. For the rest of the galaxies the dynamical mass values are taken from Bottinelli and Gouguenheim (1973); Huchtmeier and Witzel (1979); Huchtmeier and Seiradakis (1985); Kamphuis and Briggs (1992); Sofue (1996) and then rescaled for the adopted distances noted in **Table 6.1**. We have estimated the H I velocity dispersion using a method described in **Section 6.3**. Note that, although the galaxy NGC 4826 fits our selection criteria, we have not used it in our analysis. It has a very bright H I core which makes the window function complicated and the power spectrum estimation is not straight forward.

The observations and data reduction of the THINGS galaxies are discussed in Walter et al. (2008)*. For our analysis, we start with the calibrated *uv* data prior to continuum sub-

*We are indebted to Fabian Walter for providing us with calibrated H I data from the THINGS survey.

Galaxy	Major ($'$)	Minor ($'$)	D (Mpc)	i_{HI} ($^\circ$)	SFR ($M_\odot$ yr^{-1})	M_{HI} (10^8 $M_\odot$)	M_{dy} (10^{11} $M_\odot$)	σ_v (km s^{-1})
NGC 628	22.0	20.0	7.3	15.0	1.2	38.8	6.3	7.2
NGC 925	16.0	10.0	9.2	50.0	1.1	45.8	1.7	9.4
NGC 2403	25.0	22.0	3.2	55.0	0.9	25.8	3.1	9.6
NGC 2841	22.0	26.0	14.1	69.0	0.2	85.8	31.2	21.6
NGC 2903	25.0	15.0	8.9	66.0	–	43.5	4.3	15.8
NGC 3031	38.0	24.0	3.6	59.0	1.1	36.4	5.2	12.9
NGC 3184	17.0	14.0	11.1	29.0	1.4	30.7	6.4	9.1
NGC 3198	22.0	7.5	13.8	72.0	0.9	101.7	8.1	11.6
NGC 3521	22.0	7.5	10.7	69.0	8.4	80.2	12.2	29.8
NGC 3621	25.0	15.0	6.6	62.0	2.1	70.7	12.8	22.6
NGC 4736	18.0	12.0	4.7	44.0	0.4	4.0	1.2	11.4
NGC 5055	30.0	25.0	10.1	51.0	2.4	91.0	12.8	12.0
NGC 5194	16.0	12.0	8.0	30.0	6.1	25.4	2.7	14.4
NGC 5236	30.0	24.0	4.5	31.0	2.5	17.0	2.6	10.9
NGC 5457	30.0	25.0	7.4	30.0	2.5	141.7	5.9	15.6
NGC 6946	35.0	25.0	5.9	35.0	4.8	41.6	7.3	9.3
NGC 7793	12.0	9.0	3.9	43.0	0.5	8.9	0.7	9.9
IC 2574	14.0	8.0	4.0	51.0	0.1	14.8	0.5	9.9

Table 6.1: Some parameters of the galaxies used for the power spectrum analysis. Columns 1-9 gives 1) Name of the galaxy, 2) and 3) Major and Minor axis at a column density of 10^{19} atoms cm^{-3}, 4) Distance to the galaxy, 5) average HI inclination angle, 6) Star Formation Rate, 7) HI mass, 8) Dynamical mass, 9) average velocity dispersion. evaluated from the Moment II map. These values are obtained from the following refferences: Walter et al. (2008), de Blok et al. (2008), Bottinelli and Gouguenheim (1973), Huchtmeier and Witzel (1979), Huchtmeier and Seiradakis (1985), Kamphuis and Briggs (1992), Sofue (1996).

traction. In the standard THINGS pipeline, the continuum is subtracted by fitting a linear polynomial to each visibility (i.e. AIPS task UVLIN), whereas for our analysis it is important that the strong continuum sources be modelled and then subtracted from the visibilities. For each galaxy, the frequency channels with H I emission are identified and a continuum image is made by combining all the line-free channels. This continuum is then subtracted from the data in the *uv* plane using the AIPS task UVSUB. The resulting continuum-subtracted data are used subsequently. We follow the pipeline discussed in **Section 2.3** for the rest of the analysis.

6.3 Result and discussion

For each galaxy, we have identified a baseline range (U_{min} to U_{max}) over which the real part of $\mathcal{P}(U)$ estimated from the channels with H I emission is large compared to both its imaginary part and the real part of $\mathcal{P}(U)$ estimated from the line-free channels. A power law of the form $A\,U^{\alpha}$ is found to provide a good fit to the observed power spectra. **Figure 6.1**, **6.2** and **6.3** shows the result of our power spectrum analysis. The results are also summarized in **Table 6.2**, where Column (2) to (7) gives the value for the velocity channel thickness, range of baseline for the fit, corresponding range of length-scales and the power law index α respectively for $N = n$ (see **Section 2.3**). Column (8) gives the power law index α for $N = 1$. Unless otherwise stated we will use the values of α with $N = n$ for further analysis. The presence of a scale-invariant, power law power spectrum indicates that turbulence is operational in the ISM of these galaxies.

For the galaxies NGC 2841, NGC 3031 and NGC 3521, the angular extent, θ_0, is comparable to the telescope field of view and hence two observations with two different pointing centers (North and South) were used. We refer these two different directions using N or S after the galaxy's name. For NGC 3031S, the power spectrum could be

Galaxy		$\Delta\ v$ ($km\ s^{-1}$)	U_{min} (k λ)	U_{max} (k λ)	R_{min} (kpc)	R_{max} (kpc)	α ($n = N$)	α ($n = 1$)
NGC 628		41.6	1.0	10.0	0.8	7.5	-1.6 ± 0.1	-1.6 ± 0.1
NGC 925		41.6	1.0	10.0	0.9	9.2	-1.0 ± 0.2	-1.0 ± 0.2
NGC 2403	*	83.2	0.7	7.0	0.6	4.0	-1.1 ± 0.1	-2.1 ± 0.3
NGC 2841N		83.2	1.0	10.0	1.4	14.0	-1.7 ± 0.2	-1.7 ± 0.1
NGC 2841S		83.2	1.0	10.0	1.4	14.0	-1.5 ± 0.2	-1.5 ± 0.1
NGC 2903		83.2	0.8	8.0	1.1	11.1	-1.5 ± 0.2	-1.5 ± 0.1
NGC 3031N		41.6	2.0	10.0	0.4	1.8	-0.7 ± 0.1	-0.7 ± 0.1
NGC 3184		41.6	0.7	7.0	1.6	15.8	-1.3 ± 0.2	-1.3 ± 0.1
NGC 3198	*	83.2	1.6	10.0	1.4	8.6	-0.4 ± 0.3	-1.6 ± 0.3
NGC 3521N		83.2	1.0	17.0	0.6	10.7	-1.8 ± 0.1	-1.8 ± 0.1
NGC 3521S		83.2	1.0	17.0	0.6	10.7	-1.6 ± 0.2	-1.6 ± 0.2
NGC 3621	*	83.2	1.0	12.0	0.6	6.6	-0.8 ± 0.2	-1.9 ± 0.2
NGC 4736	*	83.2	0.6	10.0	0.5	7.8	-0.3 ± 0.2	-0.9 ± 0.2
NGC 5055		83.2	1.0	10.0	1.0	10.0	-1.6 ± 0.1	-1.6 ± 0.1
NGC 5194		83.2	1.0	8.0	1.0	8.0	-1.7 ± 0.2	-1.7 ± 0.2
NGC 5236		83.2	0.6	6.0	0.8	7.5	-1.9 ± 0.2	-1.9 ± 0.2
NGC 5457		83.2	0.6	12.0	0.6	12.3	-2.2 ± 0.1	-2.2 ± 0.1
NGC 6946		20.8	1.5	10.0	0.3	4.0	-1.6 ± 0.1	-1.6 ± 0.1
NGC 7793		41.6	0.6	6.0	0.6	6.5	-1.7 ± 0.2	-1.7 ± 0.1
IC 2574		41.6	1.8	10.0	0.4	3.3	-1.7 ± 0.3	-2.0 ± 0.2

Table 6.2: Result of the power spectrum analysis with $N = n$ and $N = 1$. Column 1 to 8 gives 1) name of the galaxy, 2) width of the channel used to estimate the power spectrum, 3) and 4) the range of U value for which the power spectrum is evaluated, 5) and 6) correspoindin length scales and 7) the power law index α with $1 - \sigma$ error for $N = n$ and Column 8) gives the power law index α with $1 - \sigma$ error for $N = n$. We found the power law index α changes with channel thickness for the galaxies marked by (*) in the table. The values for the U_{max}, U_{min}, R_{max} and R_{min} are given for $N = n$ only

.

estimated over a very limited baseline range and hence we do not consider it here.

The length-scales over which we could fit the power law (**Table 6.2**) covers in total a range from 300 pc to 15.8 kpc across the entire sample. The power spectrum of the galaxy NGC 5457 is found to be a power law for the length-scale range of 0.6 kpc to 12.0 kpc which is the largest dynamical range obtained for an individual galaxy in our analysis. Note that, NGC 3184 exhibits a power law power spectrum up to a length-scale of $\sim$ 16 kpc, where the same for the galaxy NGC 2841 is 14 kpc. These could be understood as the existence of turbulence in the ISM of the spiral galaxies at a scale comparable to the radius of the galaxy's disk.

Figure 6.4 shows a histogram of the distribution of the estimated power law index α. The histogram is sharply peaked in the range $\alpha = -1.8$ to -1.5. The mean and the standard deviations are -1.4 and 0.5 respectively. We do not find a break in the power spectrum of any of the galaxies in our sample. For all the galaxies in our sample, the largest length-scales over which the power law is estimated are larger than the typical scale-height of galaxies. Following the results of our simulation discussed in the **Chapter 4**, we conclude that we are dealing with 2D turbulence for all these galaxies.

The galaxies in our sample have a wide range of inclination angles 'i', ranging from 7° for NGC 628 to 74° for NGC 2841. To investigate whether the spread in the value of α seen here is an effect of the difference in i, we evaluate the linear correlation between the power law index α and the inclination angle of the galaxy (**Figure 6.5**). The resultant linear correlation coefficient of 0.25 is a clear indication that the dispersion in the values of α is not due to the inclination angles.

At small scales, a major driving force of the ISM turbulence is the energy input from star formation processes. For a sample of irregular galaxies Willett et al. (2005) finds that on scales of $10 - 400$ pc the power law index of the Hα power spectra becomes

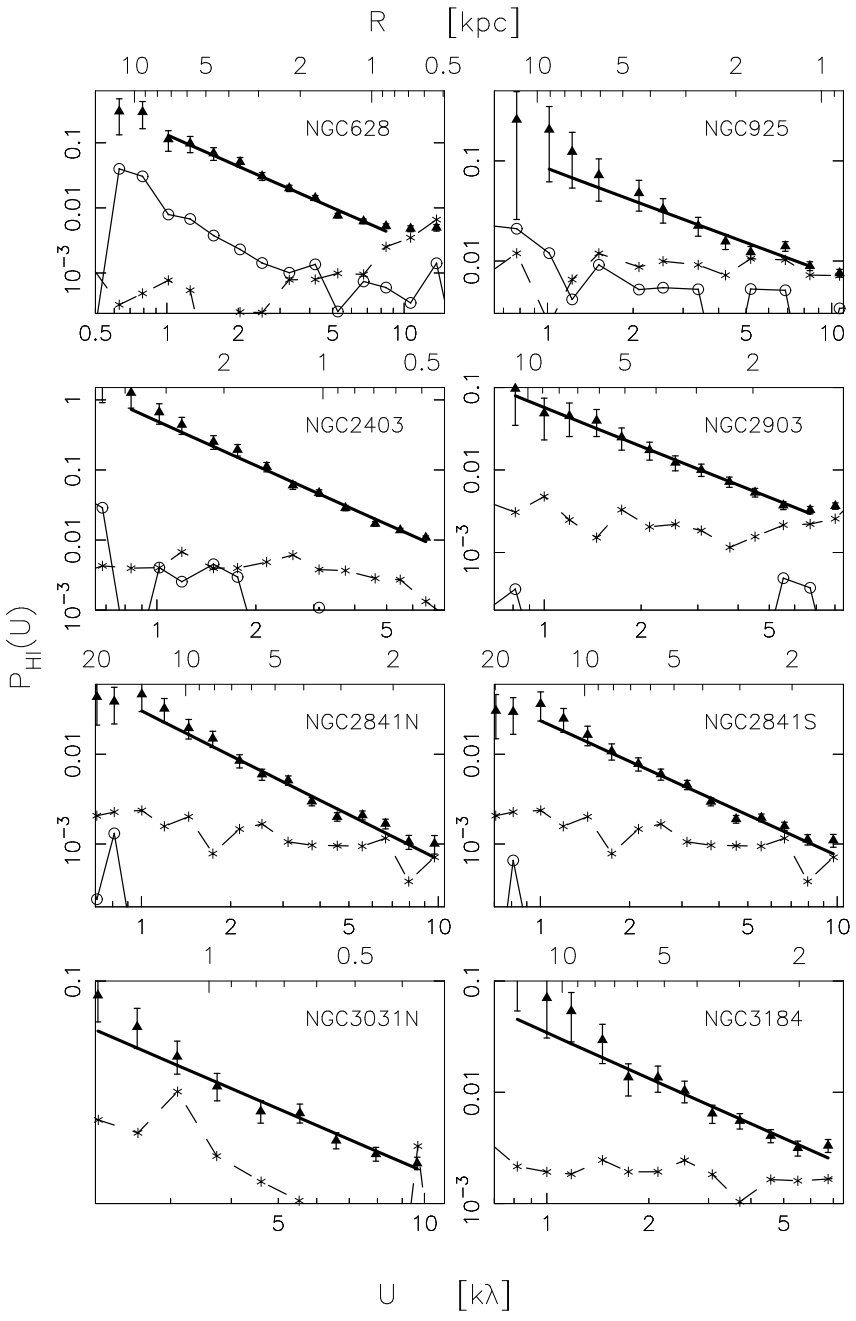

Figure 6.1: The real (triangle) and imaginary (circle) part of the estimator evaluated using the channels with HI emission is plotted with the 1 σ error bars in a log log scale against the baseline values for the galaxies NGC 628, NGC 925, NGC 2403, NGC 2903, NGC 2841, NGC 3031 and NGC 3184. The real part evaluated with the line-free channels (star) is also shown. The best fit power law is given by the bold solid line. Note that in the U range the power spectrum is deduced, the real part of the estimator has a higher value compared to the imaginary part or the real part of it from the line free channels.

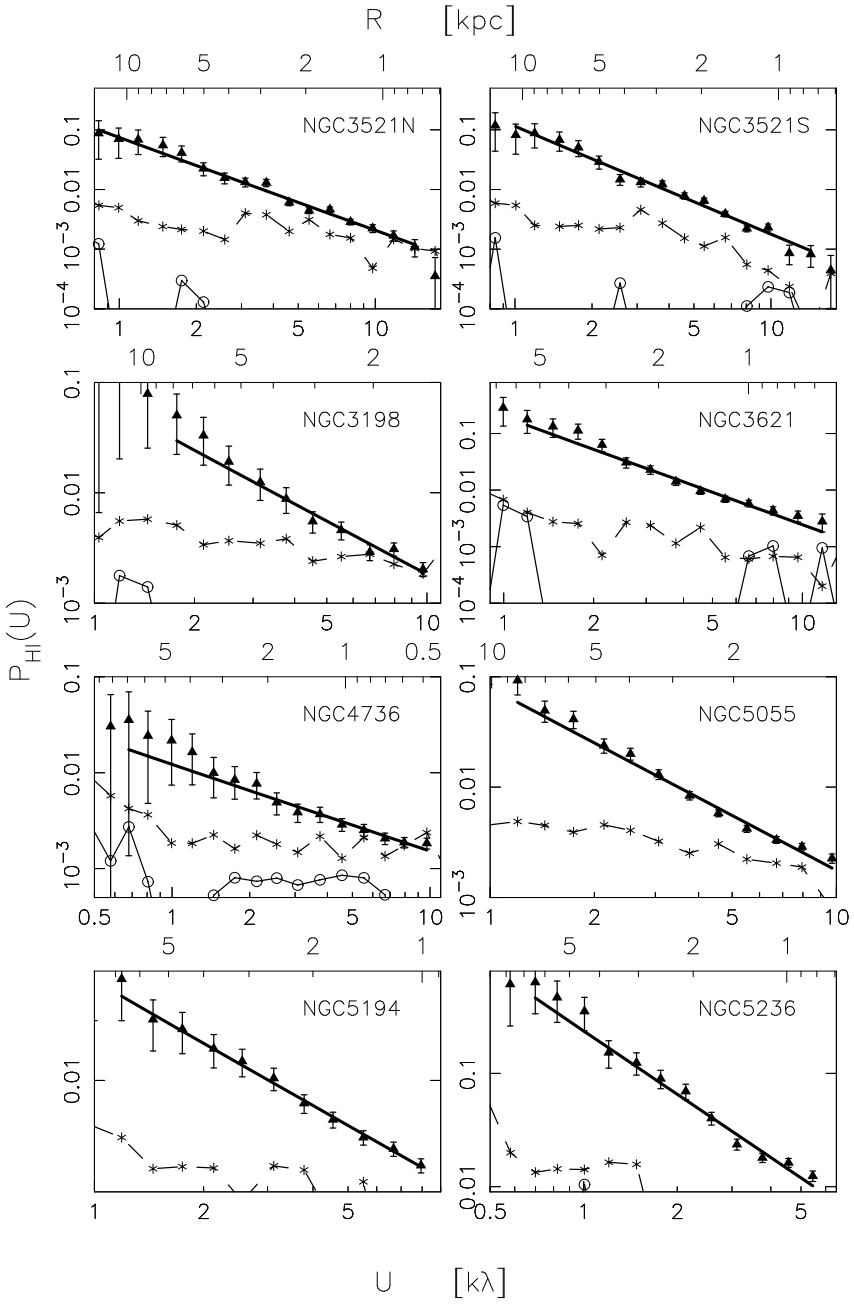

Figure 6.2: The real (triangle) and imaginary (circle) part of the estimator evaluated using the channels with HI emission is plotted with the 1 σ error bars in log-log scale against the baseline values for the galaxies NGC 3521, NGC 3198, NGC 3621, NGC 4736, NGC 5055, NGC 5194 and NGC 5236. The real part evaluated with the line-free channels (star) is also shown. The best fit power law is given by the bold solid line. Note that in the U range the power spectrum is deduced, the real part of the estimator has a higher value compared to the imaginary part as well as the real part of it from the line free channels.

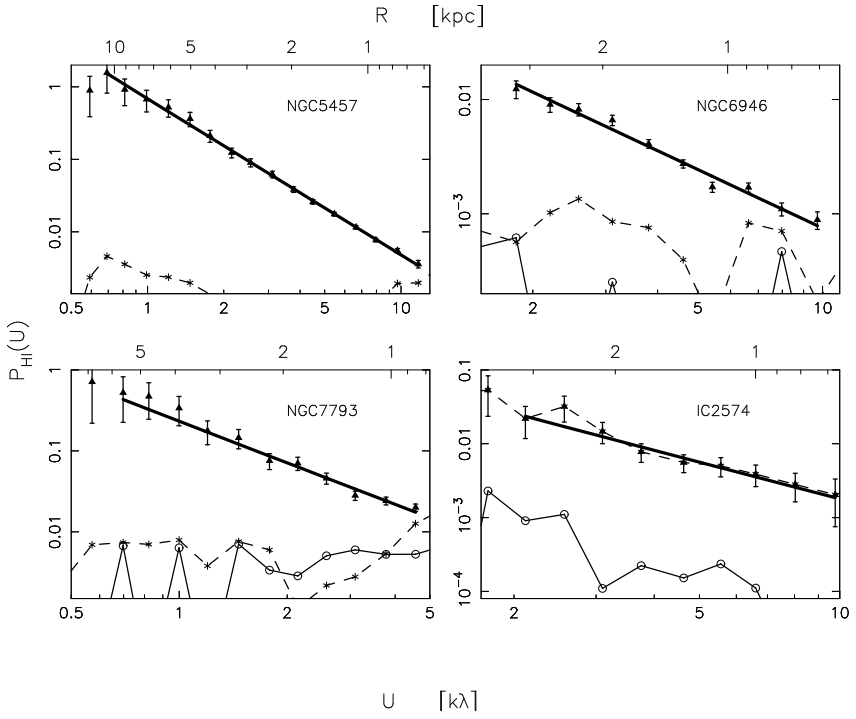

Figure 6.3: The real (triangle) and imaginary (circle) part of the estimator evaluated using the channels with HI emission is plotted with the 1 σ error bars in log-log scale against the baseline values for the galaxies NGC 5457, NGC 6946, NGC 7793 and IC 2574. The real part evaluated with the line free channels (star) is also shown. The best fit power law is given by the bold solid line. Note that in the U range the power spectrum is deduced, the real part of the estimator has a higher value compared to the imaginary part as well as the real part of it from the line free channels.

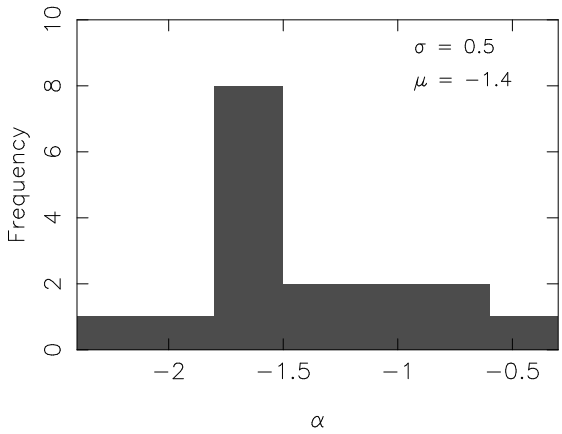

Figure 6.4: Shaded regions shows the histogram of the distribution of the power law index α. Note that the histogram has 7 bins for 18 data points. Sample mean μ and sample standard deviation σ is also shown.

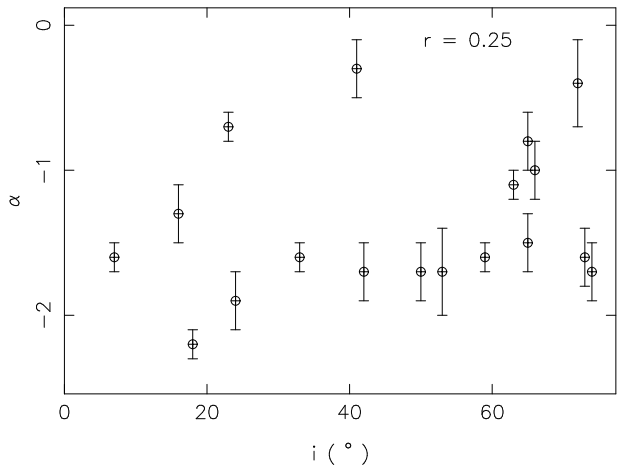

Figure 6.5: Scatter plot of the average inclination angle i with power law index α. The 1 σ error bars of α are also shown. The value of the linear correlation coefficient r is given at the top right corner.

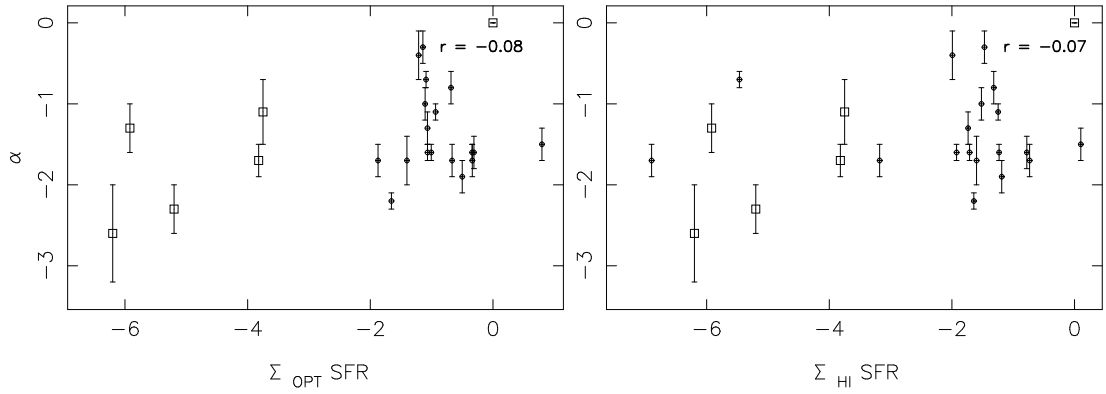

Figure 6.6: Scatter plot of the surface density of the star formation rate (**Table 6.1**) with power law index α. The 1 σ error bars of α are also shown. The left and right pannels shows the SFR per unit area of the optical and HI disk of the galaxy respectively. The value of the Linear Correlation Coefficient r is given at the top right corner of the each panel.

steeper as the SFR per unit area increases. In **Chapter 5** we have reported a weak correlation between the SFR and the power law index of the H I intensity fluctuations in dwarf galaxies. We have calculated the linear correlation coefficient of α with the SFR per unit area of the optical disk as well as the SFR per unit area of the H I disk. The result, shown in **Figure 6.6**, suggests that on large-scales at least, there is no correlation between the SFR and the power law spectral index.

We next investigate the linear correlation of the power law index α with the large scale dynamical parameters of the galaxies namely the H I mass (M_{HI}) and the dynamical mass (M_{dy}). We use the values of the maximum rotational velocity (V_{max}) and the maximum radius (r_{max}) from the rotation curves presented in de Blok et al. (2008) to evaluate the dynamical mass enclosed within that radius, viz. ($M_{dy} = V_{max}^2 r_{max}/G$). Note that de Blok et al. (2008) have given rotation curves for only 13 galaxies in our sample. For the other 5 galaxies, namely NGC 68, NGC 3184, NGC 5194, NGC 5236 and NGC 5457, we have taken the M_{dy} estimates from earlier references, viz. (Bottinelli and Gouguenheim, 1973; Huchtmeier and Witzel, 1979; Huchtmeier and Seiradakis, 1985; Kamphuis and Briggs,

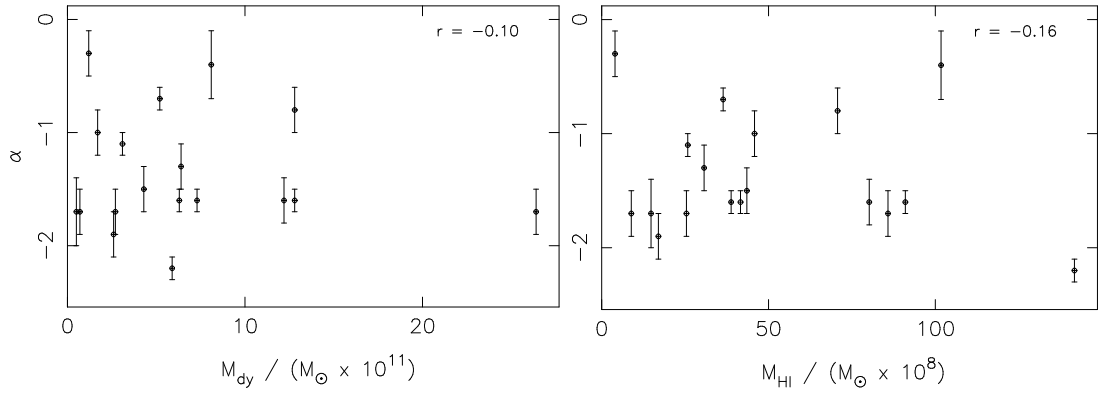

Figure 6.7: Scatter plot of the dynamical mass M_{dy} and the total HI mass M_{HI} with power law index α. The 1 σ error bars of α are also shown. The value of the Linear correlation coefficient r is given at the top right corner.

1992; Sofue, 1996). The M_{HI} values are taken from Walter et al. (2008). **Figure 6.7** shows the scatter plot of α with M_{dy} (left) and M_{HI} (right) respectively. Our analysis shows that α is not correlated with the dynamical mass or the total H I mass.

ISM turbulence can also be driven by the kinetic energy of the H I gas. In this case, one would expect that the H I velocity dispersion (σ_v) would be correlated with α. We use **Eqn. (7)** in Walter et al. (2008) to define the average H I velocity dispersion. In estimating σ_v, we perform a 8 pixel smoothing on the THINGS archival Robust Weight velocity dispersion (MOMENT 2) maps [†] and then resample it to a resolution of 6″. The overall velocity dispersion of the galaxies in the sample is evaluated using the values in individual pixels of the resampled map (**Table 6.1**, Column (9). **Figure 6.8** shows the scatter plot of the σ_v values with α. We find no correlation between α and σ_v.

In summary, the slope α is not correlated with any of the galaxy parameters that we have considered. While $\sim$ 40% of the α values are in the narrow range -1.8 to -1.5, the remaining galaxies have α values spread over the broad range -2.2 to -0.3. It is unclear if this arises from statistical fluctuations in the distribution of α, or if there is a physical mechanism underlying this spread.

[†]http://www.mpia-hd.mpg.de/THINGS/Data.html

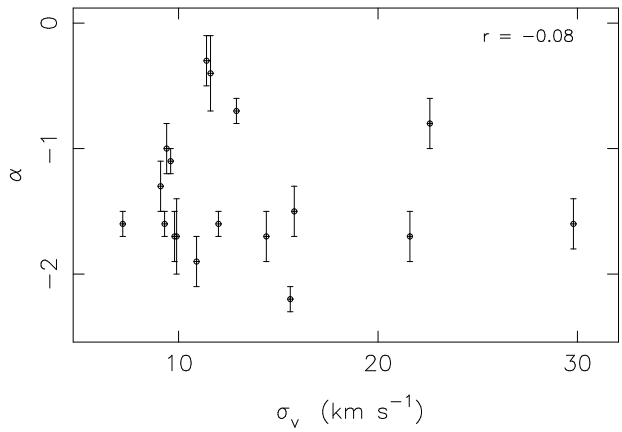

Figure 6.8: Scatter plot of the average velocity dispersion σ_v with power law index α. The 1 σ error bars of α are also shown. The value of the Linear correlation coefficient r is given at the top right corner.

Both H I density fluctuations as well as spatial fluctuations in the velocity of the H I gas could contribute to observed fluctuations in the H I specific intensity. Lazarian and Pogosyan (2000) have shown that it is possible to disentangle these two contributions by studying the behavior of the H I power spectrum as the thickness of the frequency channel is varied. If the channel thickness Δv is greater than the velocity dispersion for a galaxy, the velocity fluctuations are averaged out and the intensity fluctuation power spectrum becomes a direct probe of the density fluctuation alone. We investigate the possible effect of the velocity fluctuation in the observed intensity fluctuation power spectrum by estimating $P_{HI}(U)$ increasing the channel thickness (Δv) beyond the velocity dispersion σ_v of the galaxy. We find the slope α of the power spectrum of the galaxies NGC 2403, NGC 3198,NGC 3621 and NGC 4736 increase as the channel thickness is varied beyond a value $\Delta v = v_c$. These galaxies are marked by an Astrix in the **Table 6.2**. We show the variation of α with the increasing channel thickness for these galaxies in **Figure 6.9**. It is interesting to note that for all four galaxies $v_c \sim 20$km s^{-1} and the change in slope is independent of the velocity dispersion σ_v of the galaxy in question. We interpret the value of α for the largest Δv to be the power law index of the density fluctuation power

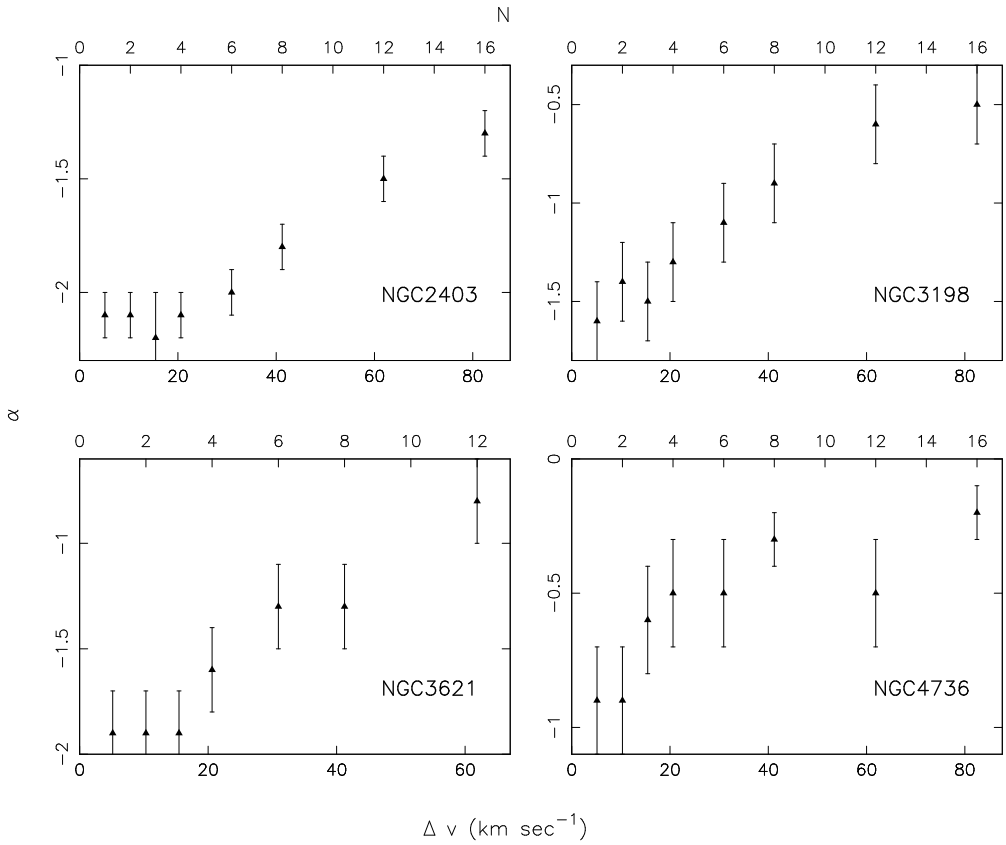

Figure 6.9: Change in the slope of the power law index α with velocity channel thickness is shown for the four galaxies NGC 2403, NGC 3198, NGC 3621 and NGC 4736. Levels at the bottom shows the width of the velocity channels whereas the top levels show the number of channels averaged together before evaluating the power spectrum.

spectrum (**Figure 6.9**). The slope of the power law is found to remain constant as the thickness of the channels is varied for the rest of the galaxies in the sample. Since for all the galaxies the thickest channel is considerably larger than the velocity dispersion, we conclude that for these galaxies, the H I power spectrum is purely due to density fluctuations and not the velocity fluctuations in the H I gas.

6.4 Summary and conclusion

This paper summarizes the power spectrum analysis of 18 spiral galaxies from the THINGS sample. The estimated power spectra can be well fitted with a power law, indicating the presence of turbulence in the ISM. This analysis is the first comprehensive study of turbulence in spiral galaxies with a moderate sample size. In this section we give a brief summary of the important findings from our power spectrum analysis.

- We find that the galaxies in our sample shows a power law power spectrum over length-scales ranging from $\sim$ 300 pc to $\sim$ 16 k pc with several galaxies having $R_{max} > 10$ kpc. Presently there is no known mechanism which can drive turbulence at such large length-scales.

- We have observed that for most of the galaxies in our sample, $\alpha \sim -1.6$ (**Figure 6.4**). This value of α is similar to that is found for 2D power spectrum of the galaxies in **Chapter 3**.

- In **Chapter 5** we have found no significant correlation between α and the SFR, dynamical mass, total H I mass of dwarf galaxies. Here we estimate the power spectrum of 18 external spiral galaxies which provide us a moderate sample size. However, our analysis also shows that the α has no correlation with the inclination angle, SFR, dynamical and total H I mass of these galaxies.

- For most of the galaxies in our sample the width of the frequency channel is found to have no effect on the power law index. The slope of the power spectrum remains the same as the channel-thickness becomes greater than the average velocity dispersion of the galaxies. This suggests that the intensity fluctuation power spectrum is a direct probe of the column-density fluctuations in the galaxy's disk. Interestingly, we notice that for four galaxies NGC 2403, NGC 3198, NGC 3621 and NGC 4736 the slope of the power spectrum decreases as the channel width Δv is increased, and beyond a certain value of $\Delta v \sim 20$ km s^{-1} it remains constant. However, the channel width where this transition occurs has no correlation with the velocity dispersion of the galaxy considered. We found this to be different from Lazarian and Pogosyan (2000) and presently do not have any physical understanding of the reason behind this.

7 Summary and Future Scopes

This thesis presents our effort of probing turbulence in the ISM of the external galaxies by estimating the power spectrum using radio-interferometric observations of H I 21-cm radiation. Here we summarize our main results and discuss the future scopes.

- We have estimated the power spectrum of 25 external galaxies including 5 nearby dwarf and 20 spirals. For every galaxy, the power spectrum is found to follow a power law over a wide range of length-scales which spans 60 pc to 16 kpc in total. This indicates that the ISM is turbulent at length-scale comparable to the radius of the galaxy's disk.

- We have observed a dichotomy in the estimated value of the power spectral index and have explained it in terms of 2D and 3D turbulence at large and small scales in the galaxy's disk respectively. Based on a break in the power spectrum of the galaxy NGC 1058 we have estimated its scale-height as 450 ± 60 pc. This is the first determination of the scale-height of any external spiral galaxy.

- We investigated whether the turbulence is related to the different dynamical parameters like dynamical and H I mass, star formation rate etc. of the galaxies. For the dwarf galaxies we found a weak correlation between surface density of star

formation rate and the power law index. There was no such correlation observed for the spiral galaxies.

- The observed power spectrum is found to have no effect of the velocity fluctuations for 21 of the 25 galaxies we have analyzed. For the rest of the galaxies we have observed power law index changes with the channel thickness indicating an effect of the velocity fluctuation.

- Our power spectrum analysis of the harassed galaxy NGC 4254 has shown that the galaxy harassment effects the ISM structures. The central part of such a galaxy exhibit different dynamics compared to that in the outer disk.

- Given a power law power spectrum, its estimator introduced in this thesis is sensitive to the slope but not to the amplitude of the power law. On the other hand, for smaller length scales in our galaxy, the amplitude and slope of the power spectrum is very well constrained. If one can carry out observations with more sensitivity with better uv-coverage at the larger baseline range, it would be possible to probe similar length scales in the external nearby galaxies with the existing radio interferometers like VLA or GMRT. This will provide a way of calibrating the amplitude of the estimator we have used and then a direct comparison between the large and small scale powers can be done. Also note that we have been restricted to the nearby galaxies because of the limited angular resolution and hence linear resolution in the disk of the galaxies that we can achieve with the present telescopes. For an even better uv-coverage and more dynamic range in the length scale within which the power spectrum can be estimated, upcoming radio telescopes like SKA will come be very useful.

The known energy sources of ISM turbulence include galaxy rotation, self gravity, supernovae etc., which are believed to drive turbulence at parsec scales. It is not clear if these are equally effective in explaining the large scale turbulence observations reported in this thesis. A detailed physical modeling is required to have better understanding of ISM dynamics. It may be possible to estimate the ISM velocity fluctuation power spectrum, which can independently test the existence and nature of turbulence in the ISM. We wish to perform numerical simulation to understand the effect of velocity fluctuations etc. in our power spectrum estimation. Finally, it will also be interesting to study the ISM turbulence in a sample of galaxies residing in the cluster environment.

References

Ali, S.S., Bharadwaj, S., and Chengalur, J.N. (2008). Foregrounds for redshifted 21-cm studies of reionization: Giant Meter Wave Radio Telescope 153-MHz observations. *Monthly Notices of Royal Astronomical Society*, 385, 2166–2174. doi: 10.1111/j.1365-2966.2008.12984.x.

Bania, T.M. and Lyon, J.G. (1980). OB stars and the structure of the interstellar medium - Cloud formation and effects of different equations of state. *Astrophysical Journal*, 239, 173–192. doi:10.1086/158099.

Bazell, D. and Desert, F.X. (1988). Fractal structure of interstellar cirrus. *Astrophysical Journal*, 333, 353–358. doi:10.1086/166751.

Begum, A. (2006). *A study of faint dwarf galaxies with the GMRT*. Tata Institute of Fundamental Rrsearch: deemed University.

Begum, A. and Chengalur, J.N. (2003). Kinematics of the dwarf irregular galaxy GR8. *Astronomy and Astrophysics*, 409, 879–886. doi:10.1051/0004-6361:20031163.

Begum, A. and Chengalur, J.N. (2004). Kinematics of the faintest gas-rich galaxy in the Local Group: DDO210. *Astronomy and Astrophysics*, 413, 525–534. doi: 10.1051/0004-6361:20031549.

Begum, A., Chengalur, J.N., and Bhardwaj, S. (2006a). Power spectrum of HI intensity fluctuations in DDO 210. *Monthly Notices of Royal Astronomical Society*, 372, L33–L37. doi:10.1111/j.1745-3933.2006.00220.x.

Begum, A., Chengalur, J.N., and Karachentsev, I.D. (2005). A dwarf galaxy with a giant HI disk. *Astronomy and Astrophysics*, 433, L1–L4. doi:10.1051/0004-6361:200500026.

Begum, A., Chengalur, J.N., Karachentsev, I.D., Kaisin, S.S., and Sharina, M.E. (2006b). Gas distribution, kinematics and star formation in faint dwarf galaxies. *Monthly Notices of Royal Astronomical Society*, 365, 1220–1234. doi:10.1111/j.1365-2966.2005.09817.x.

Begum, A., Chengalur, J.N., Karachentsev, I.D., Sharina, M.E., and Kaisin, S.S. (2008a). FIGGS: Faint Irregular Galaxies GMRT Survey - overview, observations and first results. *Monthly Notices of Royal Astronomical Society*, 386, 1667–1682. doi:10.1111/j.1365-2966.2008.13150.x.

Begum, A., Chengalur, J.N., Kennicutt, R.C., Karachentsev, I.D., and Lee, J.C. (2008b). Life in the last lane: star formation and chemical evolution in an extremely gas rich dwarf. *Monthly Notices of Royal Astronomical Society*, 383, 809–816. doi:10.1111/j.1365-2966.2007.12592.x.

Bharadwaj, S. and Ali, S.S. (2005). On using visibility correlations to probe the HI distribution from the dark ages to the present epoch - I. Formalism and the expected signal. *Monthly Notices of Royal Astronomical Society*, 356, 1519–1528. doi:10.1111/j.1365-2966.2004.08604.x.

Bigiel, F., Leroy, A., Walter, F., Brinks, E., de Blok, W.J.G., Madore, B., and Thornley, M.D. (2008). The Star Formation Law in Nearby Galaxies on Sub-Kpc Scales. *Astronomical Journal*, 136, 2846–2871. doi:10.1088/0004-6256/136/6/2846.

Binney, J. and Merrifield, M. (1998). *Galactic astronomy*.

Boldyrev, S., Nordlund, and Padoan, P. (2002). Supersonic Turbulence and Structure of Interstellar Molecular Clouds. *Physical Review Letters*, 89(3), 031102–+. doi:10.1103/PhysRevLett.89.031102.

Boroson, T. (1981). The distribution of luminosity in spiral galaxies. *Astrophysical Journal Supplement Series*, 46, 177–209. doi:10.1086/190742.

Bottinelli, L. and Gouguenheim, L. (1973). A neutral hydrogen study of the galaxy NGC 5236. *Astronomy and Astrophysics*, 29, 425–429.

Braun, R. and Kanekar, N. (2005). Tiny H I clouds in the local ISM. *Astronomy and Astrophysics*, 436, L53–L56. doi:10.1051/0004-6361:200500122.

Briggs, F.H., Wolfe, A.M., Krumm, N., and Salpeter, E.E. (1980). First results of a sensitive search for H I envelopes in a complete sample of spiral galaxies - Extensive H I near the isolated SC I NGC 628. *Astrophysical Journal*, 238, 510–523. doi:10.1086/158007.

Burkhart, B., Stanimirović, S., Lazarian, A., and Kowal, G. (2010). Characterizing Magnetohydrodynamic Turbulence in the Small Magellanic Cloud. *Astrophysical Journal*, 708, 1204–1220. doi:10.1088/0004-637X/708/2/1204.

Chandrasekhar, S. and Münch, G. (1952). The Theory of the Fluctuations in Brightness of the Milky way. V. *Astrophysical Journal*, 115, 103–+. doi:10.1086/145518.

Chappell, D. and Scalo, J. (2001). Multifractal Scaling, Geometrical Diversity, and Hierarchical Structure in the Cool Interstellar Medium. *Astrophysical Journal*, 551, 712–729. doi:10.1086/320242.

Chengalur, J.N., Gupta, Y., and Dwarakanath, K.S. (eds.) (2007). *Low Frequency Radio Astronomy*. NCRA, Tata Institute of Fundamental Research.

Crovisier, J. and Dickey, J.M. (1983). The spatial power spectrum of galactic neutral hydrogen from observations of the 21-cm emission line. *Astronomy and Astrophysics*, 122, 282–296.

de Blok, W.J.G., Walter, F., Brinks, E., Trachternach, C., Oh, S., and Kennicutt, R.C. (2008). High-Resolution Rotation Curves and Galaxy Mass Models from THINGS. *Astronomical Journal*, 136, 2648–2719. doi:10.1088/0004-6256/136/6/2648.

de Vaucouleurs, G., de Vaucouleurs, A., Corwin, Jr., H.G., Buta, R.J., Paturel, G., and Fouque, P. (1991). Book-Review - Third Reference Catalogue of Bright Galaxies. *Sky and Telescope*, 82, 621–+.

Deshpande, A.A., Dwarakanath, K.S., and Goss, W.M. (2000). Power Spectrum of the Density of Cold Atomic Gas in the Galaxy toward Cassiopeia A and Cygnus A. *Astrophysical Journal*, 543, 227–234. doi:10.1086/317104.

Dutta, P., Begum, A., Bharadwaj, S., and Chengalur, J.N. (2008). HI power spectrum of the spiral galaxy NGC628. *Monthly Notices of Royal Astronomical Society*, 384, L34–L37. doi:10.1111/j.1745-3933.2007.00417.x.

Dutta, P., Begum, A., Bharadwaj, S., and Chengalur, J.N. (2009a). A study of interstellar medium of dwarf galaxies using HI power spectrum analysis. *Monthly Notices of Royal Astronomical Society*, 398, 887–897. doi:10.1111/j.1365-2966.2009.15105.x.

Dutta, P., Begum, A., Bharadwaj, S., and Chengalur, J.N. (2009b). The scaleheight of NGC 1058 measured from its HI power spectrum. *Monthly Notices of Royal Astronomical Society*, 397, L60–L63. doi:10.1111/j.1745-3933.2009.00684.x.

Dutta, P., Begum, A., Bharadwaj, S., and Chengalur, J.N. (2010a). Turbulence in the harassed galaxy NGC4254. *Monthly Notices of Royal Astronomical Society*, 405, L102–L106. doi:10.1111/j.1745-3933.2010.00869.x.

Dutta, P., Guha Sarkar, T., and Khastgir, S.P. (2010b). The effect of the w-term on the visibility correlation and power spectrum estimation. *Monthly Notices of Royal Astronomical Society*, 406, L30–L34. doi:10.1111/j.1745-3933.2010.00875.x.

Elmegreen, B.G., Elmegreen, D.M., Chandar, R., Whitmore, B., and Regan, M. (2006). Hierarchical Star Formation in the Spiral Galaxy NGC 628. *Astrophysical Journal*, 644, 879–889. doi:10.1086/503797.

Elmegreen, B.G., Elmegreen, D.M., and Leitner, S.N. (2003). A Turbulent Origin for Flocculent Spiral Structure in Galaxies. *Astrophysical Journal*, 590, 271–283. doi:10.1086/374860.

Elmegreen, B.G., Kim, S., and Staveley-Smith, L. (2001). A Fractal Analysis of the H I Emission from the Large Magellanic Cloud. *Astrophysical Journal*, 548, 749–769. doi:10.1086/319021.

Elmegreen, B.G. and Scalo, J. (2004). Interstellar Turbulence I: Observations and Processes. *Annual Review of Astronomy & Astrophysics*, 42, 211–273. doi:10.1146/annurev.astro.41.011802.094859.

Faison, M.D. and Goss, W.M. (2001). The Structure of the Cold Neutral Interstellar Medium on 10-100 AU Scales. *Astronomical Journal*, 121, 2706–2722. doi:10.1086/320369.

Falgarone, E., Phillips, T.G., and Walker, C.K. (1991). The edges of molecular clouds - Fractal boundaries and density structure. *Astrophysical Journal*, 378, 186–201. doi:10.1086/170419.

Ferguson, A.M.N., Gallagher, J.S., and Wyse, R.F.G. (2000). On the Nature of Andromeda IV. *Astronomical Journal*, 120, 821–832. doi:10.1086/301485.

Ferriere, K.M., Zweibel, E.G., and Shull, J.M. (1988). Hydromagnetic wave heating of the low-density interstellar medium. *Astrophysical Journal*, 332, 984–994. doi:10.1086/166706.

Fuchs, B. and von Linden, S. (1998). Dynamical stability and evolution of the discs of SC galaxies. *Monthly Notices of Royal Astronomical Society*, 294, 513–+. doi:10.1046/j.1365-8711.1998.01024.x.

Gentile, G., Salucci, P., Klein, U., and Granato, G.L. (2007). NGC 3741: the dark halo profile from the most extended rotation curve. *Monthly Notices of Royal Astronomical Society*, 375, 199–212. doi:10.1111/j.1365-2966.2006.11283.x.

Gill, A.G. and Henriksen, R.N. (1990). A first use of wavelet analysis for molecular clouds. *Astrophysical Journal Letters*, 365, L27–L30. doi:10.1086/185880.

Green, D.A. (1993). A power spectrum analysis of the angular scale of Galactic neutral hydrogen emission towards L = 140 deg, B = 0 deg. *Monthly Notices of Royal Astronomical Society*, 262, 327–342.

Hall, A.N. (1980). On the origin of long time-scale pulsar scintillations. I - Cosmic ray streaming or the mirror instability. II - Growth of the mirror instability, and non-linear amplitude limitation. III - The density fluctuations in our Galaxy. *Monthly Notices of Royal Astronomical Society*, 190, 353–369.

Haynes, M.P., Giovanelli, R., and Kent, B.R. (2007). NGC 4254: An Act of Harassment Uncovered by the Arecibo Legacy Fast ALFA Survey. *Astrophysical Journal Letters*, 665, L19–L22. doi:10.1086/521188.

Hobson, M.P. (1992). High-resolution HCO(+) and HCN observations of M17SW - Clumps, turbulence and cloud support. *Monthly Notices of Royal Astronomical Society*, 256, 457–476.

Hobson, M.P. and Maisinger, K. (2002). Maximum-likelihood estimation of the cosmic microwave background power spectrum from interferometer observations. *Monthly Notices of Royal Astronomical Society*, 334, 569–588. doi:10.1046/j.1365-8711.2002.05524.x.

Hodge, P.W. (1967). The Nature of the Remarkable Galaxy G. R. *Astrophysical Journal*, 148, 719–+. doi:10.1086/149197.

Huber, D. and Pfenniger, D. (2002). Long-range correlations in self-gravitating N-body systems. *Astronomy and Astrophysics*, 386, 359–378. doi:10.1051/0004-6361:20020232.

Huchtmeier, W.K. and Seiradakis, J.H. (1985). H I observations of galaxies in nearby groups. *Astronomy and Astrophysics*, 143, 216–225.

Huchtmeier, W.K. and Witzel, A. (1979). Extended envelope of neutral hydrogen around M 101. *Astronomy and Astrophysics*, 74, 138–145.

Ikeuchi, S. and Spitzer, Jr., L. (1984). Scattering of shock waves by a spherical cloud. *Astrophysical Journal*, 283, 825–832. doi:10.1086/162368.

Kamphuis, J. and Briggs, F. (1992). Kinematics of the extended H I disk of NGC 628 - High velocity gas and deviations from circular rotation. *Astronomy and Astrophysics*, 253, 335–348.

Kaneda, Y., Ishihara, T., Yokokawa, M., Itakura, K., and Uno, A. (2003). Energy dissipation rate and energy spectrum in high resolution direct numerical simulations of turbulence in a periodic box. *Physics of Fluids*, 15, L21–L24. doi:10.1063/1.1539855.

Karachentsev, I.D. and Kaisin, S.S. (2007). A View of the M81 Galaxy Group via the Hα Window. *Astronomical Journal*, 133, 1883–1902. doi:10.1086/512127.

Karachentsev, I.D., Karachentseva, V.E., Huchtmeier, W.K., and Makarov, D.I. (2004). A Catalog of Neighboring Galaxies. *Astronomical Journal*, 127, 2031–2068. doi:10.1086/382905.

Kim, W., Ostriker, E.C., and Stone, J.M. (2003). Magnetorotationally Driven Galactic Turbulence and the Formation of Giant Molecular Clouds. *Astrophysical Journal*, 599, 1157–1172. doi:10.1086/379367.

Kregel, M., van der Kruit, P.C., and de Blok, W.J.G. (2004). Structure and kinematics of edge-on galaxy discs - II. Observations of the neutral hydrogen. *Monthly Notices of Royal Astronomical Society*, 352, 768–786. doi:10.1111/j.1365-2966.2004.07990.x.

Kunth, D. and Östlin, G. (2000). The most metal-poor galaxies. *Astronomy and Astrophysics Review*, 10, 1–79. doi:10.1007/s001590000005.

Lazarian, A. (1995). Study of turbulence in HI using radiointerferometers. *Astronomy and Astrophysics*, 293, 507–520.

Lazarian, A. and Pogosyan, D. (2000). Velocity Modification of H I Power Spectrum. *Astrophysical Journal*, 537, 720–748. doi:10.1086/309040.

Lazarian, A., Vishniac, E.T., and Cho, J. (2004). Magnetic Field Structure and Stochastic Reconnection in a Partially Ionized Gas. *Astrophysical Journal*, 603, 180–197. doi:10.1086/381383.

Lee, J.C., Kennicutt, R.C., Funes, José G., S.J., Sakai, S., and Akiyama, S. (2007). The Star Formation Demographics of Galaxies in the Local Volume. *Astrophysical Journal Letters*, 671, L113–L116. doi:10.1086/526341.

Lee, M.G., Aparicio, A., Tikonov, N., Byun, Y., and Kim, E. (1999). Stellar Populations and the Local Group Membership of the Dwarf Galaxy DDO 210. *Astronomical Journal*, 118, 853–861. doi:10.1086/300988.

Leorat, J., Passot, T., and Pouquet, A. (1990). Influence of supersonic turbulence on self-gravitating flows. *Monthly Notices of Royal Astronomical Society*, 243, 293–311.

Leroy, A.K., Walter, F., Brinks, E., Bigiel, F., de Blok, W.J.G., Madore, B., and Thornley, M.D. (2008). The Star Formation Efficiency in Nearby Galaxies: Measuring Where Gas Forms Stars Effectively. *Astronomical Journal*, 136, 2782–2845. doi: 10.1088/0004-6256/136/6/2782.

Li, Y., Klessen, R.S., and Mac Low, M. (2003). The Formation of Stellar Clusters in Turbulent Molecular Clouds: Effects of the Equation of State. *Astrophysical Journal*, 592, 975–985. doi:10.1086/375780.

Little, L.T. and Matheson, D.N. (1973). Radio scintillations due to plasma irregularitieswith power law spectra: the interstellar medium. *Monthly Notices of Royal Astronomical Society*, 162, 329–+.

Lockman, F.J., Hobbs, L.M., and Shull, J.M. (1984). The Thickness of the Galactic HI Layer. In *Bulletin of the American Astronomical Society*, volume 16 of *Bulletin of the American Astronomical Society*, 981–+.

Mei, S., Blakeslee, J.P., Côté, P., Tonry, J.L., West, M.J., Ferrarese, L., Jordán, A., Peng, E.W., Anthony, A., and Merritt, D. (2007). The ACS Virgo Cluster Survey. XIII. SBF Distance Catalog and the Three-dimensional Structure of the Virgo Cluster. *Astrophysical Journal*, 655, 144–162. doi:10.1086/509598.

Merrett, H.R., Merrifield, M.R., Douglas, N.G., Kuijken, K., Romanowsky, A.J., Napolitano, N.R., Arnaboldi, M., Capaccioli, M., Freeman, K.C., Gerhard, O., Coccato, L., Carter, D., Evans, N.W., Wilkinson, M.I., Halliday, C., and Bridges, T.J. (2006).

A deep kinematic survey of planetary nebulae in the Andromeda galaxy using the Planetary Nebula Spectrograph. *Monthly Notices of Royal Astronomical Society*, 369, 120–142. doi:10.1111/j.1365-2966.2006.10268.x.

Miesch, M.S. and Zweibel, E.G. (1994). Shock propagation and the generation of magnetohydrodynamic wave fields in inhomogeneous molecular clouds. *Astrophysical Journal*, 432, 622–640. doi:10.1086/174601.

Minchin, R., Davies, J., Disney, M., Boyce, P., Garcia, D., Jordan, C., Kilborn, V., Lang, R., Roberts, S., Sabatini, S., and van Driel, W. (2005). A Dark Hydrogen Cloud in the Virgo Cluster. *Astrophysical Journal Letters*, 622, L21–L24. doi:10.1086/429538.

Moore, B., Katz, N., and Lake, G. (1996). On the Destruction and Overmerging of Dark Halos in Dissipationless N-Body Simulations. *Astrophysical Journal*, 457, 455–+. doi:10.1086/176745.

Narayan, C.A. and Jog, C.J. (2002). Origin of radially increasing stellar scaleheight in a galactic disk. *Astronomy and Astrophysics*, 390, L35–L38. doi:10.1051/0004-6361:20020961.

Norman, C.A. and Ferrara, A. (1996). The Turbulent Interstellar Medium: Generalizing to a Scale-dependent Phase Continuum. *Astrophysical Journal*, 467, 280–+. doi:10.1086/177603.

Ossenkopf, V., Klessen, R.S., and Heitsch, F. (2001). On the structure of self-gravitating molecular clouds. *Astronomy and Astrophysics*, 379, 1005–1016. doi:10.1051/0004-6361:20011324.

Ossenkopf, V. and Mac Low, M. (2002). Turbulent velocity structure in molecular clouds. *Astronomy and Astrophysics*, 390, 307–326. doi:10.1051/0004-6361:20020629.

Padoan, P., Boldyrev, S., Langer, W., and Nordlund, A. (2003). Structure Function Scaling in the Taurus and Perseus Molecular Cloud Complexes. *Astrophysical Journal*, 583, 308–313. doi:10.1086/345351.

Padoan, P., Cambrésy, L., and Langer, W. (2002). Structure Function Scaling of a 2MASS Extinction Map of Taurus. *Astrophysical Journal Letters*, 580, L57–L60. doi:10.1086/345403.

Padoan, P., Kim, S., Goodman, A., and Staveley-Smith, L. (2001). A New Method to Measure and Map the Gas Scale Height of Disk Galaxies. *Astrophysical Journal Letters*, 555, L33–L36. doi:10.1086/321735.

Perley, R.A., Schwab, F.R., and Bridle, A.H. (eds.) (1989). *Synthesis imaging in radio astronomy*, volume 6 of *Astronomical Society of the Pacific Conference Series*.

Persic, M. and Rephaeli, Y. (2007). Galactic star formation rates gauged by stellar end-products. *Astronomy and Astrophysics*, 463, 481–492. doi:10.1051/0004-6361:20054146.

Petric, A.O. and Rupen, M.P. (2007). H I Velocity Dispersion in NGC 1058. *Astronomical Journal*, 134, 1952–1962. doi:10.1086/518558.

Phookun, B., Vogel, S.N., and Mundy, L.G. (1993). NGC 4254: A Spiral Galaxy with an M = 1 Mode and Infalling Gas. *Astrophysical Journal*, 418, 113–+. doi:10.1086/173375.

Piontek, R.A. and Ostriker, E.C. (2004). Thermal and Magnetorotational Instability in the Interstellar Medium: Two-dimensional Numerical Simulations. *Astrophysical Journal*, 601, 905–920. doi:10.1086/380785.

Porter, D., Pouquet, A., Sytine, I., and Woodward, P. (1999). Turbulence in compressible flows. *Physica A Statistical Mechanics and its Applications*, 263, 263–270. doi:10.1016/S0378-4371(98)00525-1.

Porter, D., Pouquet, A., and Woodward, P. (2002). Measures of intermittency in driven supersonic flows. *Physical Review E*, 66(2), 026301–+. doi:10.1103/PhysRevE.66.026301.

Roberts, W.W. (1969). Large-Scale Shock Formation in Spiral Galaxies and its Implications on Star Formation. *Astrophysical Journal*, 158, 123–+. doi:10.1086/150177.

Rosolowsky, E.W., Goodman, A.A., Wilner, D.J., and Williams, J.P. (1999). The Spectral Correlation Function: A New Tool for Analyzing Spectral Line Maps. *Astrophysical Journal*, 524, 887–894. doi:10.1086/307863.

Roy, N., Bharadwaj, S., Dutta, P., and Chengalur, J.N. (2009). Magnetohydrodynamic turbulence in supernova remnants. *Monthly Notices of Royal Astronomical Society*, 393, L26–L30. doi:10.1111/j.1745-3933.2008.00591.x.

Roy, N., Chengalur, J.N., Dutta, P., and Bharadwaj, S. (2010). H I 21 cm opacity fluctuations power spectra towards Cassiopeia A. *Monthly Notices of Royal Astronomical Society*, 404, L45–L49. doi:10.1111/j.1745-3933.2010.00831.x.

Sandage, A. and Tammann, G.A. (1974). Steps toward the Hubble constant. IV - Distances to 39 galaxies in the general field leading to a calibration of the galaxy luminosity classes and a first hint of the value of H sub 0. *Astrophysical Journal*, 194, 559–568. doi:10.1086/153275.

Scalo, J. and Elmegreen, B.G. (2004). Interstellar Turbulence II: Implications and Effects. *Annual Review of Astronomy & Astrophysics*, 42, 275–316. doi:10.1146/annurev.astro.42.120403.143327.

Sellwood, J.A. and Balbus, S.A. (1999). Differential Rotation and Turbulence in Extended H I Disks. *Astrophysical Journal*, 511, 660–665. doi:10.1086/306728.

Semelin, B., de Vega, H.J., Sánchez, N., and Combes, F. (1999). Renormalization group flow and fragmentation in the self-gravitating thermal gas. *Physical Review D*, 59(12), 125021–+. doi:10.1103/PhysRevD.59.125021.

Sharina, M.E., Karachentsev, I.D., Dolphin, A.E., Karachentseva, V.E., Tully, R.B., Karataeva, G.M., Makarov, D.I., Makarova, L.N., Sakai, S., Shaya, E.J., Nikolaev, E.Y., and Kuznetsov, A.N. (2008). Photometric properties of the Local Volume dwarf galaxies. *Monthly Notices of Royal Astronomical Society*, 384, 1544–1562. doi:10.1111/j.1365-2966.2007.12814.x.

Sharina, M.E., Karachentsev, I.D., and Tikhonov, N.A. (1996). Photometric distances to NGC 628 and its four companions. *Astronomy and Astrophysics Suppliment*, 119, 499–507.

She, Z.S. and Leveque, E. (1994). Universal scaling laws in fully developed turbulence. *Phys. Rev. Lett.*, 72(3), 336–339. doi:10.1103/PhysRevLett.72.336.

Shostak, G.S. and van der Kruit, P.C. (1984). Studies of nearly face-on spiral galaxies. II - H I synthesis observations and optical surface photometry of NGC 628. *Astronomy and Astrophysics*, 132, 20–32.

Sofue, Y. (1996). The Most Completely Sampled Rotation Curves for Galaxies. *Astrophysical Journal*, 458, 120–+. doi:10.1086/176796.

Sohn, Y. and Davidge, T.J. (1996). Multicolor CCD Photometry of Supergiants in the Disk of NGC 628. *Astronomical Journal*, 111, 2280–+. doi:10.1086/117962.

Sreenivasan, K.R. (1991). Fractals and multifractals in fluid turbulence. *Annual Review of Fluid Mechanics*, 23, 539–600. doi:10.1146/annurev.fl.23.010191.002543.

Stanimirović, S. and Lazarian, A. (2001). Velocity and Density Spectra of the Small Magellanic Cloud. *Astrophysical Journal Letters*, 551, L53–L56. doi:10.1086/319837.

Stanimirovic, S., Staveley-Smith, L., Dickey, J.M., Sault, R.J., and Snowden, S.L. (1999). The large-scale HI structure of the Small Magellanic Cloud. *Monthly Notices of Royal Astronomical Society*, 302, 417–436. doi:10.1046/j.1365-8711.1999.02013.x.

Stutzki, J., Bensch, F., Heithausen, A., Ossenkopf, V., and Zielinsky, M. (1998). On the fractal structure of molecular clouds. *Astronomy and Astrophysics*, 336, 697–720.

Vázquez-Semadeni, E., Ballesteros-Paredes, J., and Klessen, R. (2003). The Origin of Molecular Cloud Turbulence and its Role on Determining the Star Formation Efficiency. In J. M. De Buizer & N. S. van der Bliek (ed.), *Galactic Star Formation*

Across the Stellar Mass Spectrum, volume 287 of *Astronomical Society of the Pacific Conference Series*, 81–86.

Vazquez-Semadeni, E., Passot, T., and Pouquet, A. (1995). A turbulent model for the interstellar medium. 1: Threshold star formation and self-gravity. *Astrophysical Journal*, 441, 702–725. doi:10.1086/175393.

Vazquez-Semadeni, E., Passot, T., and Pouquet, A. (1996). Influence of Cooling-induced Compressibility on the Structure of Turbulent Flows and Gravitational Collapse. *Astrophysical Journal*, 473, 881–+. doi:10.1086/178200.

Vinkó, J., Blake, R.M., Sárneczky, K., Csák, B., Furész, G., Csizmadia, S., Kiss, L.L., Szabó, G.M., Szabó, R., DeBond, H., De Robertis, M.M., Thomson, J.R., and Mochnacki, S.W. (2004). Distance of the hypernova SN 2002ap via the expanding photosphere method. *Astronomy and Astrophysics*, 427, 453–464. doi:10.1051/0004-6361:20040272.

Vollmer, B., Huchtmeier, W., and van Driel, W. (2005). NGC 4254: a spiral galaxy entering the Virgo cluster. *Astronomy and Astrophysics*, 439, 921–933. doi:10.1051/0004-6361:20041350.

von Hoerner, S. (1951). Eine Methode zur Untersuchung der Turbulenz der interstellaren Materie. Mit 10 Textabbildungen. *Zeitschrift fur Astrophysik*, 30, 17–+.

von Weizsäcker, C.F. (1951). The Evolution of Galaxies and Stars. *Astrophysical Journal*, 114, 165–+. doi:10.1086/145462.

Walter, F., Brinks, E., de Blok, W.J.G., Bigiel, F., Kennicutt, R.C., Thornley, M.D., and Leroy, A. (2008). THINGS: The H I Nearby Galaxy Survey. *Astronomical Journal*, 136, 2563–2647. doi:10.1088/0004-6256/136/6/2563.

Wentzel, D.G. (1968). Hydromagnetic Waves Excited by Slowly Streaming Cosmic Rays. *Astrophysical Journal*, 152, 987–+. doi:10.1086/149611.

Wentzel, D.G. (1969). Pulsar Scintillations due to Distant Streaming Cosmic Rays. *Astrophysical Journal Letters*, 156, L91+. doi:10.1086/180355.

Westpfahl, D.J., Coleman, P.H., Alexander, J., and Tongue, T. (1999). The Geometry of the H I of Several Members of the M81 Group: The H I Is Fractal. *Astronomical Journal*, 117, 868–880. doi:10.1086/300717.

Willett, K.W., Elmegreen, B.G., and Hunter, D.A. (2005). Power Spectra in V band and Hα of Nine Irregular Galaxies. *Astronomical Journal*, 129, 2186–2196. doi:10.1086/429678.

Wilson, O.C., Minich, G., Flather, E., and Coffeen, M.F. (1959). Internal Kinematics of the Orion Nebula. *Astrophysical Journal Supplement Series*, 4, 199–+. doi:10.1086/190048.

Wouterloot, J.G.A., Brand, J., Burton, W.B., and Kwee, K.K. (1990). IRAS sources beyond the solar circle. II - Distribution in the Galactic warp. *Astronomy and Astrophysics*, 230, 21–36.

Zhou, Y. (1993). Degrees of locality of energy transfer in the inertial range. *Physics of Fluids*, 5, 1092–1094. doi:10.1063/1.858593.

Appendix

A Incomplete uv coverage and correlated noise in the radio-interferometric observations

Noise in the visibility plane $\mathcal{N}(\boldsymbol{U})$ corresponds to $I^{(N)}(\boldsymbol{\theta})$ given by

$$I^{(N)}(\boldsymbol{\theta}) \;=\; \int d\boldsymbol{U}\; e^{i2\pi \boldsymbol{U}.\boldsymbol{\theta}} \mathcal{N}(\boldsymbol{U}) \tag{A1}$$

Fourier transform is a linear operation and in practice a discrete Fourier transform is used. We can write **Eqn. (A1)** as

$$I_j^{(N)} \;=\; \sum_k \mathrm{F}_{jk} N_k, \tag{A2}$$

where F_{jk} are the components of the transformation matrix $\mathrm{F}_{jk} = \exp(\frac{i2\pi jk}{N})$. In a typical radio-interferometric observation the uv plane is not completely sampled. The actual inverse-transformation from the measured visibility to the specific intensity is given by

$$I_j^{(N)} \;=\; \mathrm{F}_{jk} \Gamma_{kl} N_l \,, \tag{A3}$$

where $\Gamma_{kl} N_l$ gives the measured visibility points. We call this matrix Γ as the projection matrix. It is to note here, that Γ is an Identity matrix if all the points in the uv plane are sampled, otherwise it is a diagonal matrix with diagonal elements as 0 or 1. In the latter case the inverse of this matrix does not exist. Components of the noise covariance matrix (assumed to be diagonal) can be written as

$$\mathrm{N}_{ij} \;=\; \delta_{ij} \sigma_i^2 \tag{A4}$$

We calculate the auto-correlation function as

$$\begin{aligned} \xi_{ij}^{(N)} \;&=\; \langle I_i^{(N)}\, I_j^{(N)^\dagger} \rangle \\ &=\; \mathrm{F}_{ik}\, \Gamma_{kp}\, \sigma_p^2\, \Gamma_{pn}^\dagger\, \mathrm{F}_{nj}^\dagger. \end{aligned} \tag{A5}$$

In case of complete uv coverage, we have

$$\begin{aligned} \xi_{ij}^{(N)} &= \mathrm{F}_{ik}\ \delta_{kp}\ \sigma_p^2\ \delta_{pn}\ \mathrm{F}_{nj}^{\dagger} \\ &= \sigma_i^2\ \delta_{ij}, \end{aligned} \tag{A6}$$

since $\mathbf{F}$ is unitary. However for real observations with limited uv coverage Γ_{kp} is not a identity matrix. The noise power spectrum is given by,

$$\begin{aligned} P_{mj}^{(N)} &= \mathrm{F}_{mi}^{\dagger}\ \xi_{ij} \\ &= \Gamma_{mp}\, \sigma_p^2\ \Gamma_{pn}^{\dagger}\ \mathrm{F}_{nj}^{\dagger} \end{aligned} \tag{A7}$$

This clearly shows that for limited baseline coverage, there exists correlated noise in the image plane. Every attempt to estimate power spectrum from the Fourier transform estimators hence has to take care of this correlated noise effect.

B Validity of the 2D approximation.

In **Chapter 2** we have assumed the baseline $\boldsymbol{U}$ as a 2D vector. This is rather an approximation and in reality the vector $\boldsymbol{U}$ has three components. Here we discuss the validity of the 2D assumption.*

B1 2D and 3D visibility, the effect of w-term on the aperture

The direct observable in the radio-interferometric observations is the complex visibility $\mathcal{V}^{3D}(\boldsymbol{U},\nu)$. For a pair of antennae separated by $\boldsymbol{d}$, with each antenna pointing along the direction of the unit vector $\boldsymbol{k}$ (referred to as the phase center) we have

$$\mathcal{V}^{3D}(\boldsymbol{U},\nu) = e^{2\pi i w} \int d\Omega_{\boldsymbol{n}}\, e^{2\pi i \boldsymbol{U}\cdot(\boldsymbol{n}-\boldsymbol{k})} A(\boldsymbol{n}-\boldsymbol{k},\nu) I(\boldsymbol{n}-\boldsymbol{k},\nu) \tag{B1}$$

where $\boldsymbol{n}$ denotes the unit vector to different directions of the sky, baseline $\boldsymbol{U} = \boldsymbol{d}/\lambda$, $A(\boldsymbol{n}-\boldsymbol{k},\nu)$ denotes the primary beam and $I(\boldsymbol{n}-\boldsymbol{k},\nu)$ is the specific intensity. Writing $\boldsymbol{U} = \boldsymbol{U}_\perp + w\boldsymbol{k}$, where $\boldsymbol{U}_\perp$ is a 2D vector, and defining $\boldsymbol{n}-\boldsymbol{k} = \boldsymbol{\theta}$, we have, for $\mid \boldsymbol{\theta} \mid \ll 1$, $\boldsymbol{\theta}\cdot\boldsymbol{k} \approx 0$, implying that $\boldsymbol{\theta}$ is a $2D$ vector. In this limit $\boldsymbol{\theta}$ gives the position of any point on the sky with respect to the phase centre in a 2D tangent plane. This is known as the flat-sky approximation. The term $w\boldsymbol{k}$ quantifies deviation from this. In the $2D$ approximation we have

$$\mathcal{V}^{2D}(\boldsymbol{U}_\perp,\nu) = \int d\boldsymbol{\theta}\; e^{2\pi i \boldsymbol{U}_\perp\cdot\boldsymbol{\theta}}\; A(\boldsymbol{\theta},\nu)\; I(\boldsymbol{\theta},\nu) \tag{B2}$$

Writing the specific intensity $I(\boldsymbol{\theta},\nu)$ as $I(\boldsymbol{\theta},\nu) = \bar{I}_\nu + \delta I(\boldsymbol{\theta},\nu)$, where the first term is a constant background and the second term is a fluctuation, we have

$$\mathcal{V}^{2D}(\boldsymbol{U}_\perp,\nu) = \bar{I}_\nu \tilde{A}(\boldsymbol{U}_\perp,\nu) + \tilde{A}(\boldsymbol{U}_\perp,\nu) \otimes \tilde{\delta I}(\boldsymbol{U}_\perp,\nu) \tag{B3}$$

where tilde represents a Fourier transform and $\otimes$ denotes a convolution.

The aperture function $\tilde{A}(\boldsymbol{U}_\perp,\nu)$, peaks at $\boldsymbol{U}_\perp = 0$ and has a finite width. Hence, we shall retain the second term in all subsequent discussions.

*The Appendix is adopted from the originally published in the paper titled "The Effect of w-term on Visibility Correlation and Power Spectrum Estimation" by Dutta et al. (2010b). Note that we have used different symbols here compared to what is defined in rest of the thesis for reasons given in the text.

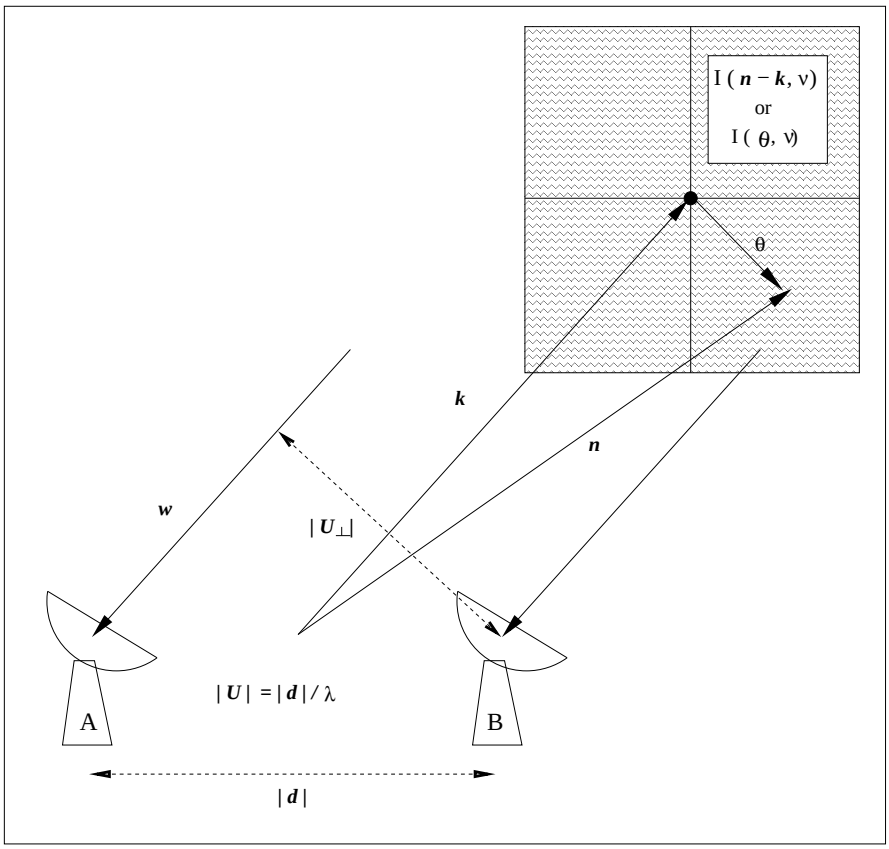

Figure B1: Schematic representation of a particular visibility measurement with a pair of antenna A and B separated by a distance $|\ \boldsymbol{d}\ |$. The square box at the top right corner represents the portion of sky observed or the field of view (FOV). The black dot at the centre of the FOV corresponds to the direction to the phase centre $\boldsymbol{k}$. Intensity fluctuations at a given direction $\boldsymbol{n}$ to the sky is denoted as $I(\boldsymbol{n}-\boldsymbol{k},\nu)$ or $I(\boldsymbol{\theta},\nu)$. Note that $\boldsymbol{\theta}$ is a 2D vector in the plane of the sky.

We note that, ignoring the w-term leads to a simplification of the expression for visibility and in the 2D approximation, $\mathcal{V}^{2D}(\boldsymbol{U}_\perp, \nu)$ is the Fourier transform of $A(\boldsymbol{\theta}, \nu)\delta I(\boldsymbol{\theta}, \nu)$. Hence, we have,

$$A(\boldsymbol{\theta}, \nu)\ \delta I(\boldsymbol{\theta}, \nu) = \int d\boldsymbol{U}'_\perp\ \mathcal{V}^{2D}(\boldsymbol{U}'_\perp, \nu)\ e^{-2\pi i \boldsymbol{U}'_\perp \cdot \boldsymbol{\theta}} \tag{B4}$$

Substituting in **Eqn. (B1)** we obtain

$$\mathcal{V}^{3D}(\boldsymbol{U}, \nu) = \int d\boldsymbol{U}'_\perp\ K(\boldsymbol{U}, \boldsymbol{U}'_\perp, \nu)\ \mathcal{V}^{2D}(\boldsymbol{U}'_\perp, \nu) \tag{B5}$$

Where the kernel $K(\boldsymbol{U}, \boldsymbol{U}'_\perp, \nu)$ is given as

$$\begin{aligned} K(\boldsymbol{U}, \boldsymbol{U}'_\perp, \nu) &= e^{-2\pi i w} \int d\Omega_{\boldsymbol{n}}\ e^{-2\pi i\ (\boldsymbol{U}'_\perp - \boldsymbol{U})\cdot(\boldsymbol{n}-\boldsymbol{k})} \\ &= 4\pi j_0\left(2\pi \mid \boldsymbol{U}'_\perp - \boldsymbol{U} \mid\right), \end{aligned} \tag{B6}$$

with j_0 denoting the Spherical Bessel function.

Defining a quantity $\tilde{\mathcal{A}}(\boldsymbol{U}, \nu)$ as

$$\tilde{\mathcal{A}}(\boldsymbol{U}, \nu) = 4\pi \int d\boldsymbol{U}'_\perp\ j_0\left(2\pi \mid \boldsymbol{U}'_\perp - \boldsymbol{U} \mid\right) \tilde{A}(\boldsymbol{U}'_\perp, \nu). \tag{B7}$$

The scalar 3D visibility takes the form

$$\mathcal{V}^{3D}(\boldsymbol{U}, \nu) = \int d\boldsymbol{U}'_\perp\ \tilde{\mathcal{A}}(\boldsymbol{U} - \boldsymbol{U}'_\perp, \nu)\ \delta\tilde{I}(\boldsymbol{U}'_\perp) \tag{B8}$$

It is to be noted that the 'w' dependence of $\mathcal{V}^{3D}(\boldsymbol{U}, \nu)$ is translated to the function $\tilde{\mathcal{A}}(\boldsymbol{U} - \boldsymbol{U}_\perp, \nu)$. This can be regarded as a modified aperture function. Note that this function is a real valued function, unlike the complex Gaussian as discussed in Hobson and Maisinger (2002). We investigate the nature of the modified aperture $\tilde{\mathcal{A}}(\boldsymbol{U}, \nu)$ as a function of $U_\perp$ for different values of w. We have assumed the primary aperture $\tilde{A}(\boldsymbol{U}_\perp, \nu)$ to be a Gaussian, $\exp\left[-\frac{U_\perp^2}{2U_0^2}\right]$, of width U_0, and evaluated the integral in **Eqn. (B7)** numerically. We shall not explicitly write the ν dependence of $\mathcal{A}$ and $\tilde{\mathcal{A}}$ henceforth. It can be shown that the modified aperture preserves the circular symmetry of the primary aperture. The implicit ν dependence is present in these functions through U_0. For an antenna of diameter D, U_0 can be approximately written as $U_0 \sim D/\lambda$ for

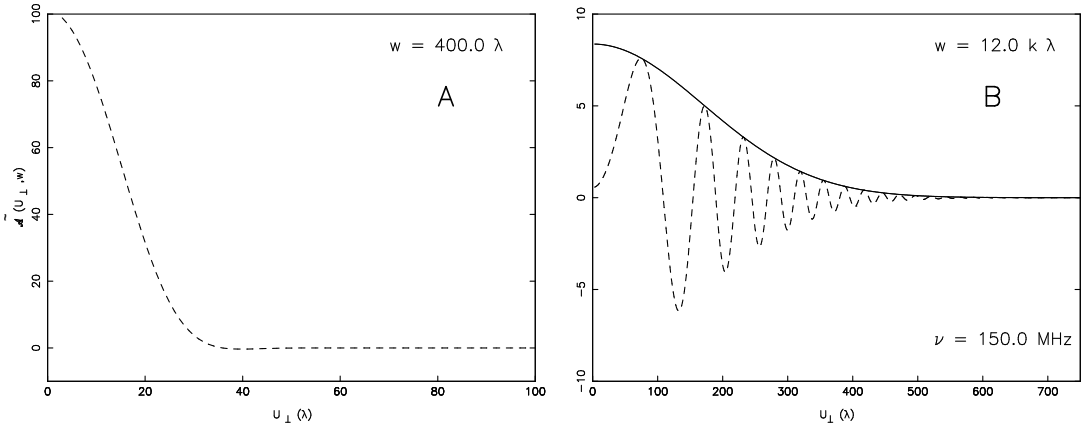

Figure B2: Modified aperture $\tilde{\mathcal{A}}(\boldsymbol{U}_\perp, w)$ plotted as a function of $\boldsymbol{U}_\perp$ for two different values of w, (A) $w = 400.\lambda$ and (B) $w = 12.$ kλ at $\nu = 150$ MHz. Solid line in B shows the Gaussian envelope.

observing wavelength λ. We use $U_0 = D/\lambda$ with $D = 45$ m (specifications of the GMRT) for the subsequent discussion. This corresponds to a FOV of 4° at 150 MHz. We shall discuss the effect of larger FOV later.

Figure B2 shows the numerically evaluated modified aperture $\tilde{\mathcal{A}}(\boldsymbol{U}_\perp, w)$ as a function of $U_\perp$ for two representative values of w (A: $w = 400$ λ, B: $w = 12$ kλ) at frequency $\nu = 150$ MHz.

For $w = 0$ one reproduces the primary Gaussian aperture trivially. We also note that for $w \ll U_\perp$ the Gaussian profile is still maintained (**Figure B2:A**). However for large values of w the aperture function manifests oscillations (**Figure B2:B**). The period of these oscillations is found to be sensitive to w (decreasing as w increases). The envelope of the modified aperture is maximum at $U_\perp = 0$ and falls of gradually as $U_\perp$ increases. We found that a Gaussian, $C \exp\left[-\frac{U^2}{2U_w^2}\right]$, provides a good fit to the envelope. Ignoring the effect of oscillations in $\tilde{\mathcal{A}}$, we note that the 3D formalism can be recast in the same form as its 2D counterpart with U_w taking the role of U_0. Hobson and Maisinger (2002) have obtained a similar result assuming small FOV, where, they have shown that the effect of w-distortion can be considered as turning the primary beam into a complex Gaussian.

We next investigate the dependence of U_w on w and frequency. For a given frequency at large w, U_w is found to increase linearly with w, i.e, $U_w \sim m(\nu)w$. This implies that the w-term effectively broadens the aperture of the instrument. **Figure B3** shows

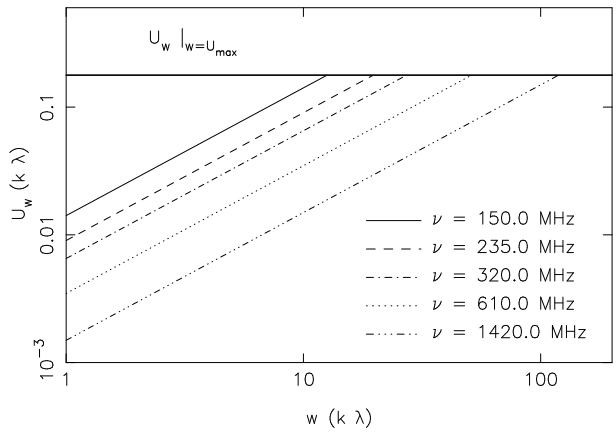

Figure B3: U_w is plotted as a function of w for different central frequencies of GMRT. Horizontal solid line corresponds to the maximum possible baseline.

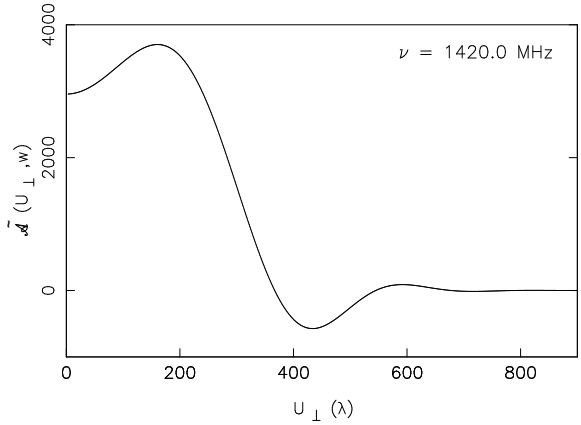

Figure B4: Modified aperture $\tilde{\mathcal{A}}(\boldsymbol{U}_\perp, w)$ plotted as a function of $\boldsymbol{U}_\perp$ for $w = 120.$ k λ at $\nu = 1420.$ MHz.

the variation of U_w with w for different frequencies in log-log scale. We note that, the slope $m(\nu)$ (as represented by the y-intercept in the **Figure B3**) determines the effect of w-term for increasing values of w. A small value of $m(\nu)$ implies a slow increase of U_w with w and the effect of the w-term is less. $m(\nu)$ is found to fall off as $\sim 1/\nu$ with frequency. This indicates that the departure from the flat-sky approximation is more pronounced at the lower frequencies. Redshifted 21-cm line observed at frequency ν probes the redshift $z = \left[\frac{1420(\mathrm{MHz})}{\nu} - 1\right]$. Hence, one may expect the w-term to have a greater effect while probing higher red-shifts.

In this thesis we use 21-cm line to study the ISM dynamics of the nearby galaxies ($z \sim 0$). **Figure B4** shows the modified aperture function for frequency 1420 MHz and $w = 120$ kλ (this being the maximum U for GMRT like arrays). At this frequency, for GMRT, $U_0 = 0.1$kλ, whereas $U_w \mid_{w=U_{max}} = 0.18k\lambda$. It follows that the flat-sky approximation can be safely used if the largest length scale probed, corresponds to a $U_\perp \gg U_w \mid_{w=U_{max}}$.

Till now, we have investigated the effect of w-term using $D = 45$ m, which corresponds to an FOV of 4° at 150 MHz. We estimated $U_w \mid_{w=U_{max}}$ assuming $D = 4$ m to $D = 45$ m at $\nu = 150$ MHz. At $D = 4$ m, (which corresponds to the largest proposed FOV, 45°, of SKA), $U_w \mid_{w=U_{max}} = 4$ kλ for $U_{max} = 120$ kλ. For all the cases mentioned above, a Gaussian of the form $C \exp\left[-\frac{U^2}{2U_w^2}\right]$ provides a good fit to the envelope of the modified aperture function and we could set a value for U_w. Further, we also observe that for these cases $U_w \mid_{w=U_{max}} \simeq \frac{d_{max}}{\pi D}$, where d_{max} is the largest baseline of the telescope array. This implies that $U_w \mid_{w=U_{max}}$ depends only on the geometry of the array configuration.

B2 Visibility correlation and power spectrum estimation

For 3D visibilities, power spectrum $P(U_\perp)$ can be estimated by performing the visibility correlation as

$$V_2^{3D}(\boldsymbol{U}) = \langle V^{3D}(\boldsymbol{U}) V^{3D}(\boldsymbol{U})^* \rangle = \int d^2\boldsymbol{U}'_\perp \, |\tilde{\mathcal{A}}(\boldsymbol{U} - \boldsymbol{U}'_\perp)|^2 \, P(U'_\perp) \tag{B9}$$

Noting that the effect of the w-term is contained in the modified aperture $\tilde{\mathcal{A}}$. We can retrieve the 2D estimator V_2^{2D} defined in **Section 2.2** (consider same baseline correlation)

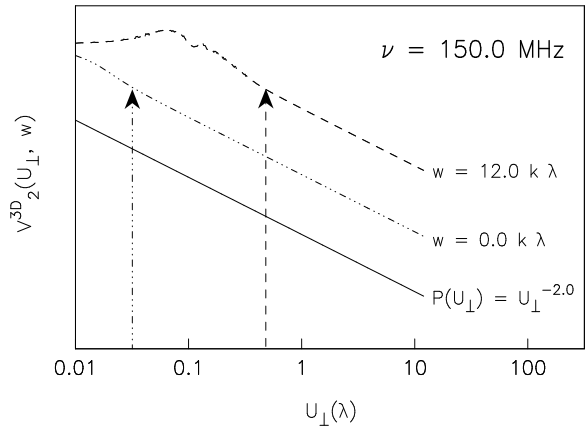

Figure B5: V_2^{3D} as a function of $U_\perp$ for $w = 0$ (dot-dash) and $w = U_{max}$ (dash) at $\nu = 150$ MHz, assuming $P(U_\perp) = {U_\perp}^{-2}$. We also plot $P(U_\perp) = {U_\perp}^{-2}$ (solid line) for reference. The vertical arrows show the $U_\perp$ value above which the power law is recovered at 1%. Note that the plots are given arbitrary offset for clarity.

by replacing $\tilde{\mathcal{A}}$ with $\tilde{A}$. Hence,

$$V_2^{2D}(\boldsymbol{U}_\perp) = \int d^2\boldsymbol{U}'_\perp \; |\tilde{A}(\boldsymbol{U}_\perp - \boldsymbol{U}'_\perp)|^2 \; P(U'_\perp). \tag{B10}$$

We note that $V_2^{3D}(\boldsymbol{U})$ and $V_2^{2D}(\boldsymbol{U}_\perp)$ become $V_2^{3D}(U)$ and $V_2^{2D}(U_\perp)$ for circularly symmetric primary aperture. We shall now discuss the effect of the w-term on the estimator defined in **Eqn. (B9)**.

Figure B5 shows V_2^{3D} plotted as a function of $U_\perp$ for two values of w, ($w = 0$ and $w = U_{max}$) at $\nu = 150$ MHz, assuming $P(U_\perp) = {U_\perp}^{-2}$. We have chosen $U_{max} = 12k\lambda$ (this being the largest baseline for the GMRT at 150 MHz). We have shown the power spectrum $P(U_\perp) = {U_\perp}^{-2}$ for comparison. For large values of w, V_2^{3D} show oscillations for $U_\perp < U_w$, which arises due to the oscillatory nature of $|\tilde{\mathcal{A}}(U)|^2$.

We find that V_2^{3D} faithfully recovers the power law ${U_\perp}^{-2}$ (at 1%) for $U_\perp$ greater than a certain value. This value is found to be $3 \times (\sqrt{2}U_0)$ for $w = 0$ and $3 \times (\sqrt{2}U_w)$ at $w = 12$ kλ. Hence, a non-zero w-term changes the $U_\perp$ value beyond which the power spectrum estimation would be valid.

The quantity of interest in power spectrum estimation using the radio-interferometric

	$w = 0$	$w \sim U_{max}$
Aperture	$\tilde{A}(U_\perp)$	$\tilde{\mathcal{A}}(U_\perp, w)$
width	U_0	U_w
Visibility		
correlation	$V_2^{2D}(U_\perp)$	$V_2^{3D}(U_\perp, w)$

Table B1: The effect of w-term, comparison between various quantities.

	150 (M Hz)	1420 (M Hz)
U_0	0.01	0.1
U_{max}	12.0	120.0
$U_w \mid_{w=U_{max}}$	0.18	0.18

Table B2: Relevant $U_\perp$ (k λ) values at different frequencies.

observations used in this thesis is actually the quantity

$$\mathcal{E}(U_\perp) = \int_0^{U_{max}} dw\ \rho(w)\ V_2^{3D}(U_\perp, w), \tag{B11}$$

where, $\rho(w)$ is a normalized probability distribution of w. The function $\rho(w)$ is specific to an observation as well as to the array configuration of the interferometer. Hence, it is difficult to make a general quantitative statement regarding the effect of w-term in $\mathcal{E}$. Since, for a given w, the largest baseline above which $V_2^{3D}(U_\perp, w) \sim P(U_\perp)$ is U_w, we can qualitatively state that $\mathcal{E}$ gives a good estimation of the power spectrum for $U \geq 3\ U_w \mid_{w=U_{max}}$. It is important to note that, for a specific array configuration, $U_w \mid_{w=U_{max}}$ is independent of the frequency ν, whereas $U_{max} \propto \nu$ (**Table B1**). Hence, the $U_\perp$ range amenable for power spectrum estimation is larger for large observing frequencies and the use of the 2D visibility for the analysis presented in this thesis is justified.

C Error in the visibility correlation estimator

The real and imaginary parts of the estimator $\mathcal{P}(U)$ have uncertainties arising from (1.) the sample variance and (2.) the system noise. In this section we provide a method of estimating the error in the visibility correlation estimator.

C1 The noise covariance matrix

In radio astronomy the total power available at a radio telescope terminal is conveniently stated in terms of the system temperature $T^{sys} = (\text{Total power})/k_B$, where k_B is the Boltzmann's constant. The system temperature obtained for the antenna looking at a blank sky gives a measure of the total random noise in the system. This noise is assumed to be Gaussian random with zero mean and its variance for the j^{th} antenna can be given by $\sigma_j^2 = T_j^{sys}$.

It can be shown that for most practical purposes, a pair of baselines i and j observing a point source with flux density S, with an integration time of T, at a bandwidth of $\Delta\nu$ the noise covariance matrix is (Chengalur et al., 2007)

$$\sigma_{ij}^2 = \frac{T_i^{sys}\, T_j^{sys}}{2\, T\, \Delta\nu}. \tag{C1}$$

It is important to remember that usually the interferometers do not record the self correlations and hence all $i = j$ are not considered from the above expressions. Now if the antenna pairs $i - j$ corresponds to a baseline of $\boldsymbol{U}$, then variance of both the real and imaginary part of $\mathcal{N}(\boldsymbol{U}, \nu)$ is σ_{ij}. For a typical observation, the noise is also uncorrelated and constant across the frequency channels.

An important property of the noise is that at two baselines $\boldsymbol{U}_A$ and $\boldsymbol{U}_B$ the noise is uncorrelated, i.e,

$$\langle \mathcal{N}(\boldsymbol{U}_A)\mathcal{N}(\boldsymbol{U}_B)\rangle = \delta_{AB}\, \mathbf{N_2}(\boldsymbol{U}_A) \tag{C2}$$

where $\mathbf{N_2}(\boldsymbol{U}_A)$ is noise covariance matrix for a given baseline $\boldsymbol{U}_A$. Assuming Poisson system noise we can write,

$$\mathbf{N_2}(\boldsymbol{U}) = \frac{(T^{sys})^4}{4T^2(\Delta\nu)^2} = N_2, \tag{C3}$$

since $\mathbf{N_2}(\boldsymbol{U})$ is independent of $\boldsymbol{U}$.

C2 Variance in the real and imaginary part of $\mathcal{P}(U)$

We assume that the density fluctuations produced due to the ISM turbulence is homogeneous and isotropic. In such cases we can replace the ensemble average in the **Eqn. (2.12)** by an angular average. The real part of each multiplication of the visibilities $\mathcal{V}(\boldsymbol{U}_i)$ and $\mathcal{V}(\boldsymbol{U}_i + \Delta\boldsymbol{U})$ with $\Delta\boldsymbol{U} < 1/\pi\theta_0$, provide us an independent estimate,

$$\mathcal{P}(\boldsymbol{U}_i) = Re\ [\mathcal{V}(\boldsymbol{U}_i)\mathcal{V}^*(\boldsymbol{U}_i + \Delta\boldsymbol{U})] = \mathcal{P}_i. \tag{C4}$$

We consider annular regions in the uv plane as shown in **Figure C2** (the region between $\boldsymbol{U}_a$ and $\boldsymbol{U}_b$) and average over all the individual estimates $\mathcal{P}_i$ in the annulus to get

$$\mathcal{P} = \frac{1}{N_b}\sum_{i=1}^{N_b}\mathcal{P}_i, \tag{C5}$$

where, N_b is the number of individual estimates $\mathcal{P}_i$ in the given $\boldsymbol{U}$ bin. This value of $\mathcal{P}$ is then proportional to the power spectrum $P_{HI}(U)$ for $U = (U_a + U_b)/2$.

We will now calculate the variance of the power spectrum estimator we have just discussed. It is to be noted that, since visibilities at two different baselines $\boldsymbol{U}_i$ and $\boldsymbol{U}_i + \Delta\boldsymbol{U}$ remains correlated for $\Delta\boldsymbol{U} \leq 1/\pi\theta_0$, all the estimates $\mathcal{P}_i$ of **Eqn. (C5)** are not independent. **Figure C1** shows three different estimates of $\mathcal{P}$, namely $\mathcal{P}_1$, $\mathcal{P}_2$ and $\mathcal{P}_3$, among which $\mathcal{P}_1$, $\mathcal{P}_3$ and $\mathcal{P}_2$, $\mathcal{P}_3$ are mutually independent estimates, but, $\mathcal{P}_1$, $\mathcal{P}_2$ are not independent. This suggests that we can break the $\mathcal{P}_i$'s in say N_g groups such that, inside a group, the $\mathcal{P}_i$'s are not independent, however, the estimates from different groups are independent. Hence, we can write,

$$\mathcal{P} = \frac{1}{N_g}\sum_{i=1}^{N_g}\mathcal{P}_{N_i} \tag{C6}$$

where, N_i are the number of $\mathcal{P}$'s in the i^{th} group and

$$\mathcal{P}_{N_i} = \frac{1}{N_i}\sum_{j=1}^{N_i}\mathcal{P}_j \tag{C7}$$

with $\langle\mathcal{P}_{N_i}\mathcal{P}_{N_j}\rangle = 0$ for $i \neq j$ and $\sum_{i=1}^{N_g} N_i = N_b$.

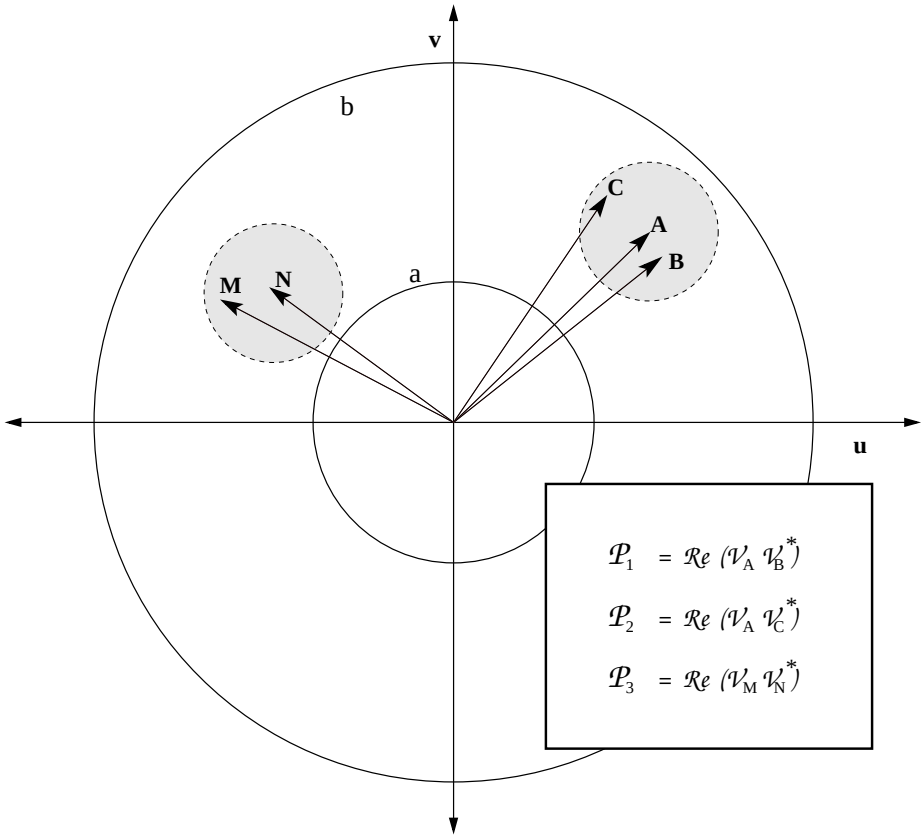

Figure C1: A particular annular region between U_A and U_B is shown. Note that the visibility $\mathcal{V}(\boldsymbol{U}_A)$ and $\mathcal{V}(\boldsymbol{U}_N)$ are correlated with all the visibilities in the corresponding shaded circular regions. The estimates $\mathcal{P}_1$ and $\mathcal{P}_2$ are not mutually independent estimates where as the estimates $\mathcal{P}_1$ and $\mathcal{P}_3$ or $\mathcal{P}_2$ and $\mathcal{P}_3$ are mutually independent estimates.

Variance of the estimator is defined as

$$\begin{aligned}\sigma^2_{\mathcal{P}} &= \langle \mathcal{P}^2 \rangle - \langle \mathcal{P} \rangle^2 \\ &= \frac{1}{N_g^2} \sum_{i=1}^{N_g} \sigma^2_{\mathcal{P}_{N_i}},\end{aligned} \tag{C8}$$

where $\sigma^2_{\mathcal{P}_{N_i}} = \langle \mathcal{P}^2_{N_i} \rangle - \langle \mathcal{P}_{N_i} \rangle^2$. Assuming $\mathcal{V}_2(\Delta U) = \langle \mathcal{V}(\boldsymbol{U}_i)\mathcal{V}(\boldsymbol{U}_i + \delta\boldsymbol{U}) \rangle$, we can write,

$$\sigma^2_{\mathcal{P}_{N_i}} = \frac{\mathcal{V}_2(\Delta U)^2 + \mathcal{V}_2(0)^2}{2} + \frac{N_2^2 + \mathcal{V}_2(0)N_2}{2N_i} \tag{C9}$$

Hence, using **Eqn. (C8)**, we get the variance of the estimator given by

$$\begin{aligned}\sigma^2_{\mathcal{P}} &= \langle \mathcal{P}^2 \rangle - \langle \mathcal{P} \rangle^2 \\ &= \frac{\mathcal{V}_2(\Delta \boldsymbol{U})^2 + \mathcal{V}_2(0)^2}{2N_g} + \frac{N_2^2 + 2\mathcal{V}_2(0)N_2}{2N_g^2} \sum_{i=1}^{N_g} \frac{1}{N_i}\end{aligned} \tag{C10}$$

In general, all N_i's are different. If we assume $N_1 = N_2 = \cdots = N_i$, then above **Eqn. (C10)** becomes

$$\sigma^2_{\mathcal{P}} = \frac{\mathcal{V}_2(\Delta \boldsymbol{U})^2 + \mathcal{V}_2(0)^2}{2N_g} + \frac{2\mathcal{V}_2(0)N_2 + N_2^2}{N_b} \tag{C11}$$

For an observation, when $N_2 \gg \mathcal{V}_2(0)$, we can approximate the above equation as

$$\sigma^2_{\mathcal{P}} = \frac{\mathcal{V}_2(\Delta \boldsymbol{U})^2 + \mathcal{V}_2(0)^2}{2N_g} + \frac{N_2^2}{2N_b} \tag{C12}$$

Since, we expect the value of the correlation $\mathcal{V}_2(\Delta \boldsymbol{U})$ at two different baselines separated by $\mid \delta \boldsymbol{U} \mid << \theta_0^{-1}$ is approximately same as the correlation $\mathcal{V}_2(0)$ at the same baselines, we can write,

$$\sigma^2_{\mathcal{P}} = \frac{\mathcal{P}^2}{N_g} + \frac{N_2^2}{2N_b} \tag{C13}$$

This expression is used by Ali et al. (2008) in calculating the variance in the power spectrum of the foreground signal in EOR (Epoch of Reionization) observation. We can identify the first term in **Eqn. (C13)** as a contribution from the sample variance and the second term arising due to the statistical fluctuation.

For the sake of completeness we mention here that the visibility correlation defined in

Eqn. (2.13) also have an imaginary part defined as

$$\mathcal{P}^I(\boldsymbol{U}_i) = Im\ [\mathcal{V}(\boldsymbol{U}_i)\mathcal{V}^*(\boldsymbol{U}_i + \Delta\boldsymbol{U})] = \mathcal{P}^I_i. \tag{C14}$$

However, when averaged over all the realizations, it can be shown that,

$$\langle \mathcal{P}^I \rangle = \langle \frac{1}{N_b} \sum_{i=1}^{N_b} \mathcal{P}^I_i \rangle = 0 \tag{C15}$$

with

$$\sigma^2_{\mathcal{P}^I} = \frac{\mathcal{V}_2(0)^2 - \mathcal{V}_2(\Delta\boldsymbol{U})^2}{2N_g} + \frac{N_2^2 + 2\mathcal{V}_2(0)N_2}{2N_g^2} \sum_{i=1}^{N_g} \frac{1}{N_i} \tag{C16}$$

Since, we expect the value of the correlation $\mathcal{V}_2(\Delta\boldsymbol{U})$ at two different baselines separated by $\mid \delta\boldsymbol{U} \mid << \theta_0^{-1}$ is approximately same as the correlation $\mathcal{V}_2(0)$ at the same baselines, we can safely neglect the first term compared to the second term. Further, if $N_1 = N_2 = \cdots = N_i$, and for $N_2 \gg \mathcal{S}_2(0)$, **Eqn. (C16)** becomes

$$\sigma^2_{\mathcal{P}^I} = \frac{N_2^2}{2N_g} \tag{C17}$$

Curriculum Vitae

Name :	Prasun Dutta
Affiliation :	Department of Physics and Meteorology, Indian Institute of Technology, Kharagpur Kharagpur 721302, India
Date of Birth :	1^{st} August, 1981
Email :	prasundutta151@gmail.com prasun@cts.iitkgp.ernet.in prasun@phy.iitkgp.ernet.in
Educational Qualifications :	**Master of Science, Physics,** May (2005) Indian Institute of Technology, Kharagpur. **Bachelor of Science, Physics (Hons.),** June (2003) University of Calcutta.
Research Interests :	Interstellar Medium Turbulence, Radio-interferometric observation techniques, Supernovae remnants.

List of Publications

In Journals :

- [†]**Dutta, P.**, Begum, A., Bharadwaj, S., and Chengalur, J.N. (2008).
  HI power spectrum of the spiral galaxy NGC 628.
  Monthly Notices of Royal Astronomical Society Letters, 384, L34L37.

- Roy, N., Bharadwaj, S., **Dutta, P.**, and Chengalur, J.N. (2009).
  Magnetohydrodynamic turbulence in supernova remnants.
  Monthly Notices of Royal Astronomical Society Letters, 393, L26L30.

- [†] **Dutta, P.**, Begum, A., Bharadwaj, S., and Chengalur, J.N. (2009).
  The scale-height of NGC 1058 measured from its HI power spectrum.
  Monthly Notices of Royal Astronomical Society Letters, 397, L60L63.

- [†] **Dutta, P.**, Begum, A., Bharadwaj, S., and Chengalur, J.N. (2009).
  A study of interstellar medium of dwarf galaxies using HI power spectrum analysis.
  Monthly Notices of Royal Astronomical Society, 398, 887897.

- Roy, N., Chengalur, J.N., **Dutta, P.**, and Bharadwaj, S. (2010).
  H I 21 cm opacity fluctuations power spectra towards Cassiopeia A.
  Monthly Notices of Royal Astronomical Society Letters, 404, L45L49.

- [†] **Dutta, P.**, Begum, A., Bharadwaj, S., and Chengalur, J.N. (2010).
  Turbulence in the harassed galaxy NGC 4254.
  Monthly Notices of Royal Astronomical Society Letters, 405, L102L106.

- [†] **Dutta, P.**, Guha Sarkar, T., and Khastgir, S.P. (2010).
  The effect of the w-term on the visibility correlation and power spectrum estimation.
  Monthly Notices of Royal Astronomical Society Letters, 406, L32-34.

- **Dutta, P.**, Khastgir, S.P., Roy, A. (2010).
  Steiner trees and spanning trees in six-pin soap films.
  American Journal of Physics, 78, 215-221.

[†] Used for the present thesis

In Proceedings :

- Roy, N., Bharadwaj, S., **Dutta P.**, and Chengalur, J. N. (2009)
  MHD turbulence in supernova remnants.
  Proceeding of the 27th Meeting of the ASI in BASI, 2009

- † **Dutta, P.**, Begum, A., Bharadwaj, S., and Chengalur, J.N. (2009).
  Probing Turbulence in the Interstellar Medium of Galaxies.
  Astronomical Society of the Pacific Conference Series, volume 407, 83

- Roy, N., Chengalur, J.N., Bharadwaj, S., and **Dutta, P.** (2009).
  Turbulence in Cold Neutral ISM and in Supernova Remnants.
  Astronomical Society of the Pacific Conference Series, volume 407, 272

In Preparation :

- † **Dutta, P.**, Begum, A., Bharadwaj, S., and Chengalur, J.N. (2009).
  Probing Interstellar Turbulence in Spiral Galaxies Using HI Power Spectrum Analysis.
  To be submitted to **Monthly Notices of Royal Astronomical Society**.

- **Dutta, P.**, Begum, A., Bharadwaj, S., and Chengalur, J.N. (2009).
  Simulating HI spectral observation from a turbulent ISM.
  To be submitted to **Monthly Notices of Royal Astronomical Society**.

† Used for the present thesis